β-Ray Angular Distribution from Aligned ^{12}B and ^{12}N

Yasuhiro Masuda

Department of Physics
Faculty of Science
Osaka University
Toyonaka, 560 Osaka

Abstract

The coefficients α_- and α_+ in the alignment terms, $A\alpha_{\mp}E$, in the β-ray angular distributions from aligned ^{12}B and ^{12}N were determined for a definite conclusion on the second class current, where A is the nuclear alignment and E is the β-ray energy. Polarized ^{12}B and ^{12}N were produced through $^{11}B(d,p)^{12}B$ and $^{10}B(^3He,n)^{12}N$. The polarizations were converted to alignments by use of NMR technique. Amounts of the nuclear alignments were $A(^{12}B) \simeq \pm 0.14$ and $A(^{12}N) \simeq \pm 0.29$, which were determined by use of the polarizations measured before and after the conversions. The productivity of ^{12}B and ^{12}N was increased using a rotating target system. Typical β-ray counting rates were ∿2000 cps and ∿50 cps for ^{12}B and ^{12}N, respectively. Spurious contributions to the values of $\alpha_{\mp}$ due to β-decay branches and unwanted scattered β rays were shown to be negligibly small in the measurement of the alignment terms. The signs of the alignments were determined from the measurements of the β-γ angular correlations in the aligned ^{12}B and ^{12}N. Thus the sign of α_+ was presently determined to be $\alpha_+ < 0$.

As the results the coefficients α_- and α_+ were determined as

$\alpha_- = +(0.006 \pm 0.018)$ %/MeV for ^{12}B,

$\alpha_+ = -(0.273 \pm 0.041)$ %/MeV for ^{12}N.

The difference, $(\alpha_- - \alpha_+)_{exp} = +(0.279 \pm 0.045)$%/MeV, agrees with the theoretical prediction, $(\alpha_- - \alpha_+)_{theory} = +(0.270 \pm 0.007)$%/MeV, without the second class induced tensor term. In comparison with the available data for CVC test, the present $(\alpha_- - \alpha_+)_{exp}$ is consistent with the CVC theory and with absence of the induced tensor term.

The sum, $(\alpha_- + \alpha_+)$, gives the time component of the axial vector current. The consistency of the experimental value, $(\alpha_- + \alpha_+)_{exp} = -(0.267 \pm 0.045)$ %/MeV, with the theoretical prediction, $(\alpha_- + \alpha_+)_{theory} = -(0.268 \pm 0.007)$ %/MeV, without the meson-exchange current, suggests that the effect due to the meson-exchange current is small in the axial vector current.

Contents

List of Figures

List of Tables

I. Introduction

The search for the second class current (SCC) in the nuclear β decay has been actively continued since the classification under G transformation was introduced by Weinberg[1]. The comparison of intrinsic decay rates (i.e., ft-value asymmetry) in several pairs of mirror Gamow-Teller(G-T) transitions attracted the first attention to the G-parity property of the weak interaction, because the systematic trend of the data at first appeared to reveal a SCC effect comparable with the effect due to the weak magnetism (WM)[2]. However, it is now known to be very difficult to extract a clear SCC signal from the ft-value asymmetry owing to the isospin-symmetry breaking caused by the Coulomb interaction.

Less ambiguous tests, correlation-type experiments, were proposed by Morita[3),4)], Holstein and Treiman[5)], and Kim[6)]. In this type of experiments, SCC and WM can be observed separately from the large G-T matrix element through which nuclear structure effects such as the isospin-symmetry breaking induced by the Coulomb interaction cause a large disturbance in extracting the SCC signal from the ft values. Recently the correlation-type experiments were performed: K. Sugimoto et al. performed measurements of polarization terms in the β-ray angular distributions of mirror transitions in mass-12 (A=12) system[7)]. E.P. Calaprice et al. also measured a polarization term in A=19[8)]. R.E. Tribble and G.T. Garvey measured β-α correlations in A=8[9)]. And N.D. Rolin et al. measured β-γ correlations in A=20[10),11)]. However a few serious problems still remained which had to be solved to draw a definite conclusion on SCC from the respective experiments.

The difference of β-ray angular distributions between mirror β decays from spin oriented unclei is caused by SCC and WM terms through interferences with the currents which have different G parities. The magnitude of these effects is of necleon-recoil order, E/M. Here E is β-ray energy and M is the nucleon mass. In the typical example of A=12 system, the effects come in the coefficients $\alpha_{\mp}$ which can be observed in the polarization and the alignment terms of β-ray angular distributions. The difference, $(\alpha_{-}-\alpha_{+})$, is composed of SCC and WM terms (recoil terms), and is insensitive to details of the nuclear structure. Therefore if the coefficients $\alpha_{\mp}$ are experimentally determined, we can extract a signal of SCC since the WM term has already been determined by the Columbia group[12] and recently by the Heidelberg group[13] for the verification of the conserved vector current (CVC) theory.

In the A=12 system, however, the leading allowed G-T terms are included in the polarization terms in the β-ray angular distributions. Thus small amounts of β-ray scatterings and different β-decay branches from the mirror decays might cause spurious effects in the measurement of the polarization terms[7]. It was difficult to correct the disturbing effects accurately, and to draw a definite conclusion on SCC from these measurements[7]. So it was urged to perform again the correlation-type experiment in A=12 system with a reliable method which is independent of the measurements by use of the polarizations.

In order to perform the reliable correlation-type experiment in which the β-ray angular distributions from aligned ^{12}B and ^{12}N were measured, we developed a new experimental technique[14]

by which a nuclear polarization was converted to a sizable alighment with a negligibly small polarization. The present experiment using the alignments with negligibly small polarization was reliable for the search of SCC, since the effects due to the unavoidable β-ray scatterings and the β-decay branches were shown to be small. In addition to the above mentioned success in the production of aligned ^{12}B and ^{12}N, the nuclei were chosen for the present study since (a) a detectable effect was expected, if SCC ever exists, because of the high β-ray energy, (b) the nuclear structure and the β decay in A=12 system have been well known[4),7),12),15),16)], and (c) high productivity of ^{12}B and ^{12}N was possible by use of a rotating target system. As the result, reliable values of $\alpha_{\mp}$ were obtained to extract a conclusive result on SCC.

The coefficients $\alpha_{\mp}$ also give us information of the nuclear structure such as meson-exchange effect in the axial vector current. As the sum, $(\alpha_{-}+\alpha_{+})$, is composed only of the time component of the axial vector current, the sum provides us a suitable probe for the meson-exchange effect since this effect is enhanced in the time component[17), 18)].

In this paper we describe the present experimental procedure and the results on the coefficients in the alignment terms for ^{12}B and ^{12}N, and discuss SCC and meson-exchange effects in the axial vector current. In chapter II, we describe the review of experimental searches for SCC. A brief survey of the theory of the β decay is also given to explain the physical meaning of the present experiment. In chapter III, the formula of the β-ray angular distribution from aligned ^{12}B and ^{12}N is described.

In chapter IV, the experimental method of the dynamic conversion of the nuclear polarization to the alignment and the method of data analyses are explained. In chapter V, the experimental results and discussions on SCC and WM are described. Finally the summary of the present work is given in chapter VI.

II. Status of the second class current in the weak interaction

(1) The β-decay interaction

Here we describe the β-decay interaction briefly, in order to point out a physical meaning of SCC.

Theory of the β decay was originally constructed by Fermi in a way analogous to the theory of the electromagnetic interaction. The Hamiltonian density for the electromagnetic interaction $\mathcal{H}_{em}$ is

$$\mathcal{H}_{em} = ej_\mu A_\mu \ , \qquad (1)$$

where j_μ is the electromagnetic current and A_μ is the four vector potential describing the electromagnetic field. Fermi introduced the β-decay Hamiltonian density by replacing

a) the electric charge e by the vector-coupling constant C_V,

b) the electromagnetic current $j_\mu = i\,(\bar{\psi}_p \gamma_\mu \psi_p)$ by the weak current $i(\bar{\psi}_p \gamma_\mu \tau_+ \psi_n)$,

c) the four vector potential A_μ by the lepton current $i(\bar{\psi}_e \gamma_\mu \psi_\nu)$,

where ψ's are the fields of relevant particles and $\bar{\psi}$'s are their adjoints. As the result, we can obtain the Hamiltonian density $\mathcal{H}'_W$,

$$\mathcal{H}'_W = C_V(\bar{\psi}_p \gamma_\mu \tau_+ \psi_n)\,(\bar{\psi}_e \gamma_\mu \psi_\nu) \ . \qquad (2)$$

Generally there are five Lorentz covariant forms as the four fermion couplings for the β decay; they are scalar (S), vector (V), tensor (T), axial vector (A) and pseudoscalar (P) couplings. In the nuclear β decay we can employ the non-relativistic approximation for these couplings. In this approximation the contribution of P comes only from the small

component of the Dirac spinor and is proportional to $(k_n-k_p)/2Mc$ where k_p and k_n are proton and neutron momenta, respectively and M is the nucleon mass. The contribution disappears in the limit as $k_n-k_p \to 0$. The detailed study of the β-ray spectral shape to examine the Fierz interference term b/E showed that combination of either S or V, and either A or T was possible[19] where b is proportional to the cross term of S and V, and A and T. The e-ν angular correlation experiments in ^{35}A, ^{19}Ne, ^{6}He and ^{23}Ne showed that the combination of V and A was valid[19] and supported the V-A theory. Theoretically the V-A theory was introduced from the chirality-invariance requirement[20], the two-component formulation of Dirac spinors [21], and mass-reversal invariance[22].

In 1956, Lee and Yang proposed the parity nonconservation in weak interactions to solve the θ-τ puzzle and introduced a more general form for $\mathcal{H}_w$[23]. In 1957, Wu et al. found the evidence of the parity nonconservation from the β-ray angular distribution from polarized ^{60}Co[24].

From the above discussions, the β-decay Hamiltonian density can be described as

$$\mathcal{H}_w = \frac{1}{\sqrt{2}} [(V_\lambda + A_\lambda) (\bar{\psi}_e \gamma_\lambda (1+\gamma_5)\psi_\nu) + (V'_\lambda + A'_\lambda) (\bar{\psi}_\nu \gamma_\lambda (1+\gamma_5)\psi_e). \quad (3)$$

For the nucleon current, the explicit form can not be written down as the lepton current because of the presence of the strong interaction. General covariant form of vector and axial vector currents can be described as follows neglecting off-mass-shell effects and exchange current[15],

$$V_\lambda = \bar{\psi}_p (f_V \gamma_\lambda + f_W \sigma_{\lambda\rho} k_\rho + i f_S k_\lambda)\ \psi_n,$$

$$A_\lambda = \bar{\psi}_p\ \gamma_5\ (f_A \gamma_\lambda + f_T \sigma_{\lambda\rho} k_\rho + i f_p k_\lambda)\ \psi_n,$$

for the electron decay,

$$V_\lambda' = \bar{\psi}_n\ (f_V^*\ \gamma_\lambda + f_W^* \sigma_{\lambda\rho} k_\rho' - i f_S^* k_\lambda')\ \psi_p,$$

$$A_\lambda' = \bar{\psi}_n \gamma_5 (f_A^* \gamma_\lambda - f_T^* \sigma_{\lambda\rho} k_\rho' + i f_p^* k_\lambda')\ \psi_p, \qquad (4)$$

for the positron decay. Here,

$$\bar{\psi} = \psi^\dagger \gamma_4, \qquad k = k_p - k_n = -k' \quad \text{and} \quad \sigma_{\lambda\rho} = [\gamma_\lambda, \gamma_\rho]/2i$$

The coupling constants f's are generally dependent on k^2, and they are real if time-reversal inveriance holds. The coupling constant f_V was determined from the ft values in the $0^+ \to 0^+$ transitions, and f_A from the ft value of the neutron decay and the β-ray angular distribution from the polarized neutron as[19],

$$f_V = (3.001 \pm 0.002) \times 10^{-12} \hbar^3/m^2 c,$$

$$f_A = -(1.239 \pm 0.011) f_V.$$

The coupling constants f_W and f_S are obtained from the conserved vector current (CVC) theory. The weak magnetism f_W is given as $f_W = -(\mu_p - \mu_n) f_V/2M = -3.7\ f_V/2M$ from the isotriplet-vector-current hypothesis, where μ_p and μ_n are the anomalous magnetic moments of proton and neutron, respectively. The f_S term is zero from the zero divergence of the vector current neglecting the proton and neutron mass difference. f_P is predicted to be $f_P \simeq f_A/25$, by the partially conserved axial vector current (PCAC) theory, in which the divergence of A_λ is assumed to be proportional to the pion field. The f_T term is characterized by the transformation property of G operation as second class current.

G is defined by the product of the charge-conjugation operator C and the charge-symmetry operator U. Under the G operation J_μ transforms as $J_\mu = \pm G J_\mu G^{-1}$, where the G parity of J_μ is ± 1. The G parities of all the six terms are

+1 for the f_V and the f_W terms,

-1 for the f_S term,

in the vector current, and

-1 for the f_A and the f_P terms,

+1 for the f_T term,

in the axial vector current. The current which has opposite G parity to the leading term is classified as the second class current (SCC)[1]. As $f_S = 0$ from the CVC theory, only the induced tensor term is SCC.

If the structure of the current A_λ (or V_λ) is induced by strong interactions, the current should have a definite G parity, unless strong interactions are noninvariant under the G transformation. Indeed electromagnetic interactions cause the violation of the symmetry in G transformation, however, this effect is small. A possible explanation of the existence of SCC is the contribution from hitherto undetected kind of weak interactions with anomalous G-parity properties.

In the nuclear β decay, the relative sign of the f_T term to the leading term is different for the electron and the positron decays as shown in Eq.(4). Therefore, the second class current can be found in the interferences with the first class current by comparing the transition probabilities (i.e., transition rate, angular distribution, etc.) for the

mirror β decays from the members of the same isospin multiplet. This was firstly proposed by Weinberg[1], and many intensive studies have been performed in nuclear physics. They are composed of mainly two types of experiments, e.g., the measurements of ft-value asymmetries and the correlation-type experiments.

(2) Search for the second class current in nuclear β decay

a) ft-value asymmetry

The ft-value asymmetry in a pair of mirror β decays was firstly examined by Huffaker and Greuling[25], and Blin-Stoyle and Rosina[26] in the A=12 system. The ft-value asymmetry δ is defined as

$$\delta = (ft)^{+}/(ft)^{-} - 1 \qquad (5)$$

and is expressed using the coupling constants f's as

$$\delta = \left[1 - \frac{4}{3}\,(E_o^{+}+E_o^{-})\,\mathrm{Re}(f_T/f_A)\right]\left|\frac{(\int\sigma)^{-}}{(\int\sigma)^{+}}\right|^{2} - 1. \qquad (6)$$

Here plus and minus signs refer to positron and electron decays, respectively, and E_o is the end-point energy. In a crude approximation, $|(\int\sigma)_{-}/(\int\sigma)_{+}|^{2}\simeq 1$, for the mirror β decays, the ft-value asymmetry is

$$\delta_{scc} = -\frac{4}{3}\,(E_o^{+} + E_o^{-})\,\mathrm{Re}\,(f_T/f_A). \qquad (7)$$

However, the isospin-symmetry breaking due to the Coulomb interaction causes a difference between the transition-matrix elements for the mirror decays, and thus produce a ft asymmetry, δ_{nucl}. The order of δ_{nucl} was expected to be the same as the one of the SCC effect, δ_{scc}, if it ever exists. The ambiguity of δ_{nucl} is known to be the same order of δ_{nucl} itself because

of our imperfect knowledges of the nuclear structure.

Possible δ_{nucl}-independent searches were performed by Wilkinson and Alburger. A dependence of δ on $(E_o^+ + E_o^-)$ was examined using the available ft values[2]. The slope of this energy dependence suggested the same order of SCC with the order of WM. However, δ_{nucl} could not be removed from this slope. δ in the A=8 system was also measured as a function of Q-value for the β decay. The decay rates of ^8L_i and ^8B to ^8Be were determined as a function of excitation energy of ^8Be using the fact that the first excited state of ^8Be, to which the decay take place, is very broad[27]. The result revealed no slope in δ as a function of $(E_o^+ + E_o^-)$. Although this slope was thought to be independent of nuclear structure, it was recently shown that the decay rate for the G-T transition to the broad first excited state has the Q-value dependence, which is also sensitive to the nuclear structure[28].

In the extraction of the small SCC effect, the large amount of the leading term was subtracted from the ft values in the analyses of the above mentioned experiments. Thus the result is sensitive to the difference of the nuclear structure between the members of the same isospin multiplet. And thus, we can not draw a definite conclusion on SCC from here because of the imperfect knowledges of the nuclear structure.

b) Correlation-type experiment

If we perform measurements of e-ν, e-γ, e-α and e-I angular correlations as a function of the β-ray energy in a pair of mirror decays, we can extract WM and SCC in the way which is less sensitive to details of the nuclear structure[3),4),5),6)], where I is a nuclear spin.

Recently these correlation type experiments were performed in A=12[7], A=19[8], A=8[9] and A=20[10),11] systems. The results were as follows. The expression follows the Holstein's formalism[29] for a comparison of the various data.

The SCC signal is represented by d_{II}/Ac, where d_{II} is the second class form factor, c is the G-T term and A is the mass number. This can be related to the formula of impulse approximation as $d_{II}/Ac = 2M\ f_T/f_A$, if we neglect the off-mass-shell effect and the exchange current;

$d_{II}/Ac = -3.5\pm1$ for A=12,

$d_{II}/Ac = -8\pm3$ for A=19,

$d_{II}/Ac = 0.6\pm0.8$ for A=8,

$d_{II}/Ac = 1.4\pm1.5$ for A=20.

These values were compared with WM, $2Mf_W/f_V = -3.7$. As seen in this comparison, consistent results were not obtained from these experiments. Furthermore, the results of the former two experiments contradicted to the ones of the latter two. We cannot draw a clear conclusion on SCC from these experiments because of the reasons discussed below on A=12, A=19, A=8 and A=20 systems.

In the A=12 system, polarization terms in the angular distributions from polarized ^{12}B and ^{12}N were measured as a function of β-ray energy. The observed β-decay asymmetry due to the polarization was sensitive to β-ray scatterings and β-decay branches because of the existence of the leading G-T term in the polarization term.

In the A=19 system, the energy dependence of a polarization term was measured. The observed β-decay asymmetry in this

experiment was sensitive to β-ray scatterings and annihilation γ-rays.

In the A=8 system, β-α angular correlations were measured as a function of β-ray energy. In the correlations, the SCC signal appears in a ratio of WM and SCC terms to an allowed G-T term. These terms are dependent on the Q-value. The Q-value dependence of the analogue M1 transition is different from the one of the G-T transitions[30]. As the nuclear structure affects the Q-value dependence, the extraction of the SCC effect from the ratio depends on the details of the nuclear structure.

The data obtained from β-γ correlation in A=20 system have a significant quadratic nature due to the second forbidden term. This fact prevents us to obtain a definite conclusion.

c) KDR model

A possible theoretical explanation was proposed by Kubodera, Delorme and Rho[31] for the experimental data obtained by the correlation type experiments and the ft-value asymmetries.

An off-mass-shell effect on one-body currents and meson-exchange effects may play a role in nuclear weak processes, since these effects have nuclear structure dependence. The SCC signals from the ft-value asymmetry and the correlation-type experiment which are denoted by δ_{SCC} and κ, respectively, are expressed using one-body effective coupling ζ and two-body effective coupling λ as

$$\delta_{SCC} = 4\lambda J + \frac{4}{3}\left(\frac{1}{2}\lambda L - \zeta\right)\left(E_o^+ + E_o^-\right)/f_A, \qquad (8)$$

$$\kappa = \zeta + \lambda L. \qquad (9)$$

Here J and L are matrix elements of two-body-transition operators, which are dependent on nuclear structure. Kubodera, Delorme and Rho reexamined the experimental results of ft-value asymmetries and correlation-type experiments in order to resolve the inconsistensy of these experimental results using Eqs. (8) and (9). In the analysis they used δ_{SCC}'s which were shown to be independent of $(E_o^+ + E_o^-)$ by recent Wilkinson's analysis. However, they could not resolve the contradiction between the two results, e.g., the one was determined from the ft-value asymmetries and the correlations in A=8 and A=20 systems, and the other was determined from the ft-value asymmetries and correlations in A=12 and A=19 systems.

We summarize here the discussions in this section. From the ft-value asymmetry we can not extract a definite conclusion on SCC because of the limitation of our knowledges on details of the nuclear structure. The information obtained from the correlation-type experiments in A=8 and A=20 systems is also dependent on details of the nuclear structure. In A=19 and A=12 systems, experimentally unavoidable effects due to the background radiations (for A=19), β-ray scatterings and β-decay branches (for A=12) disturbed us to draw a definite conclusion from the measurements by use of the polarization, though they are theoretically less sensitive to details of the nuclear structure.

In this respect, the present experiment in the A=12 system which is independent of the previous experiment in which polarization terms were observed[7], is reliable for the search of SCC, since the alignment terms, $A\alpha_{\mp}E$, in the angular

distributions do not include the leading G-T terms. Thus the measurement of these terms is less sensitive to the unavoidable β-ray scatterings and β-decay branches. In the next chapter, we describe the β-ray angular distribution from aligned ^{12}B and ^{12}N in order to explain how the present experiment gives us reliable data in theoretical and experimental view points.

III. β-ray angular distribution from aligned ^{12}B and ^{12}N

We obtained information on SCC and the exchange current in the axial vector current from the measurement of the β-ray angular distribution from aligned ^{12}B and ^{12}N.

(1) β-ray angular distribution from aligned ^{12}B and ^{12}N

The decay scheme of ^{12}B and ^{12}N is shown in Fig. 1. The ground states of ^{12}B and ^{12}N are members of an isospin triplet together with the excited state at 15.11 MeV of ^{12}C. SCC affects the β-ray angular distribution from aligned nuclei and causes the difference between the distributions from ^{12}B and ^{12}N. The formula of the β-ray angular distribution of the Gamow-Teller transition (I^{π}, T, T_z; 1^+, 1, $\mp 1 \rightarrow 0^+$, 0, 0) was given by M. Morita et al[15] in the impulse approximation as follows.

$$W(\theta) = (\text{const})\ g_A^2\,|\int \sigma|^2\, pE(E_o-E)^2\, F(\pm Z,E)\,\{1+F(E,E_o)\}(1\pm\tfrac{8}{3}aE)$$
$$\times\{1\mp P(\tfrac{p}{E})(1+\alpha_{\mp}E)P_1(\cos\theta) + A\alpha_{\mp}EP_2(\cos\theta)\}. \qquad (10)$$

Here

E and p are the electron energy and momentum in natural unit,

E_o is the end-point energy,

$F(\pm Z,E)$ is Fermi function,

$F(E,E_o)$ is the radiative correction,

$P_n(\cos\theta)$ is Legendre polynomial,

θ is the angle between the electron momentum and the axis of the nuclear spin orientation

and

P and A are the nuclear polarization and the alignment, which are defined with magnetic substate population a_m as, $P = a_1 - a_{-1}$, $A = 1-3a_o$,

$$a_1 + a_o + a_{-1} = 1.$$

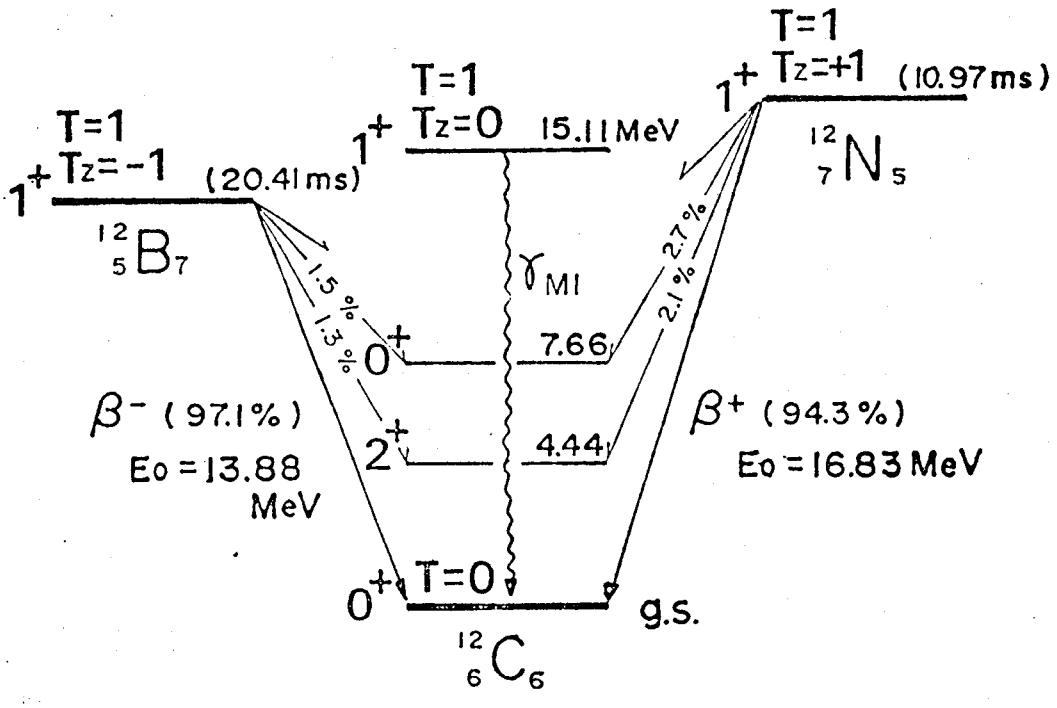

Fig. 1 Decays of the isospin triplet (T=1) to the ground state of ^{12}C in A = 12 system.

The difference between the two coefficients $\alpha_{\mp}$ in the angular distributions for electron and positron decays is caused by the interference terms between the second class and the first class currents and between the vector and the axial vector currents. The coefficients $\alpha_{\mp}$ are expressed by effective coupling constants g_A, g_W and g_T as

$$\alpha_{\mp} = \frac{2}{3}(a-b), \tag{11}$$

where

$$a = \mathrm{Re}\,(g_W/g_A), \quad b = \mathrm{Re}\,(g_T/g_A). \tag{12}$$

Here g's are real if time-reversal invariance holds, and they can be related to the form factors of a free nucleon as

$$g_A = f_A \bar{+} E_o f_T, \tag{13}$$

$$g_W = x[f_W-(f_V/2M)] = x[-(\mu_p-\mu_n)(f_V/2M)-(f_V/2M)], \tag{14}$$

$$g_T = f_T \pm y\,(f_A/2M), \tag{15}$$

where the nuclear parameters x and y are given by

$$x = 1 + \frac{1}{1+\mu_p-\mu_n}\,[\int \mathbf{r}\times\mathbf{p}/\int\sigma], \tag{16}$$

$$y = 1 + 2i\,[\int \mathbf{r}(\sigma\cdot\mathbf{p})/\int\sigma]. \tag{17}$$

Using the nuclear wave function of Cohen-Kuruth (8-16)2BME type[16], x = 0.98 and y = 3.6. We can rewrite the Eq. (11) as[17]

$$\alpha_{\mp} = \frac{2}{3}(\pm a \bar{+} b_T - b_y), \tag{18}$$

with

$$a = -x\left(\frac{1}{2M} + \frac{\mu_p-\mu_n}{2M}\right)(f_V/g_A), \tag{19}$$

$$b_T = f_T/g_A, \tag{20}$$

$$b_y = y/2M. \tag{21}$$

The same formula in the elementary particle treatment is obtained in a nuclear structure independent way[15),33),34)]. The coefficients $\alpha_{\mp}$ in the angular distributions are expressed by nuclear form factors which include the off-mass-shell effect and the exchange current as

$$\alpha_{\mp} = \frac{2}{3}\,[\pm(F_M - F_T^{(2)}) - F_T^{(1)}]/F_A^{(1)}, \tag{22}$$

where the superscripts (1) and (2) are referred to the first and second class form factors. For example the nucler form factor F_A consisted of the two parts as

$$F_A = F_A^{(1)} \pm F_A^{(2)} \quad \text{for } \beta\mp \tag{23}$$

Here we used the approximation,

$$|F_A^{(1)}| >> E_o|F_T|,\ E_o|F_M|, |F_A^{(2)}|. \tag{24}$$

Under the impulse approximation, these nuclear form factors can be related to the one-body operators[15),34)] as,

$$F_M^{(1)} = \frac{1}{2M}\,[(1+\mu_p-\mu_n)\int\sigma + \int\mathbf{r}\times\mathbf{p}], \tag{25}$$

$$F_M^{(2)} = 0, \tag{26}$$

$$F_A^{(1)} = -f_A\int\sigma, \tag{27}$$

$$F_T^{(1)} = -(f_A/2M)\,[\int\sigma + 2i\int\mathbf{r}(\sigma\cdot\mathbf{p}) + (E_oM/5)\{\int\sigma\mathbf{r}^2 - 3\int\mathbf{r}(\sigma\cdot\mathbf{r})\}], \tag{28}$$

$$F_T^{(2)} = -f_T[\int\sigma - (E_o^2/10)\{\int\sigma\mathbf{r}^2 - 3\int\mathbf{r}(\sigma\cdot\mathbf{r})\}]. \tag{29}$$

Thus the formula obtained in the impulse approximation is essentially the same with the one given in the elementary-particle treatment. Hereafter we use the formula obtained in the impulse approximation except for the case in which we discuss the nuclear model independence.

(2) Coefficients $\alpha_{\mp}$

From the two coefficients $\alpha_{\mp}$ we obtain information of SCC and the exchange current in the axial vector current.

The difference, $(\alpha_{-}-\alpha_{+})$, provides us the sum of weak magnetism term "a" and induced tensor term b_T as $\frac{4}{3}(a-b_T)$. The parameter "a" was experimentally determined from the spectral shape factor observed by Wu et al.[12] and recently by Kaina et al.[13] for the verification of the CVC theory. Using these experimental results, the second class induced tensor term is experimentally determined.

The sum, $(\alpha_{-}+\alpha_{+})$, gives us the b_y term which is dependent on the nuclear structure. The b_y term consists only of the time component of the leading axial vector current.

(3) Time component of the axial vector current and the meson-exchange effect

The nucleons in the nucleus interact each other. This fact introduces additional currents to the single particle current, which are called exchange currents. The best evidence for the exchange currents was found in the radiative thermal neutron capture by proton; $n+p \rightarrow d+\gamma$[35]. The experimental cross section for this electromagnetic process is ~10% larger than the predicted value from the single particle operator. Although the relevent wave function in this process was well determined, it was known that this discrepancy could not be removed within the frame work of the impulse approximation. One-pion-exchange current is known to explain the greater part of this anomaly.

For the axial vector current there have been no such experiments so far. In the axial vector current the order of a nonrelativistic one-body operator is O(p/M) and O(1) for the time and space components, respectively, where p is nucleon momentum in a nucleus and M is the nucleon mass.
For a low momentum transfer process, the order of the meson-exchange current is O(1) and O(p/M) for the time and space components, respectively. Thus the meson-exchange effect is enhanced in the time component for the axial vector current[36].

In the $0^- \leftrightarrow 0^+$ transitions[36),37)] the main contributions are the time component of the axial vector current and the small pseudoscalar term which is predicted from the PCAC theory. So this process is sensitive to the time component of the axial vector current.

The correlation-type experiments also give us useful information. For example, in the A=12 system, the sum, $(\alpha_- + \alpha_+)$, is composed only of the time component of the axial vector current. Threfore, the sum, $(\alpha_- + \alpha_+)$, is a suitable probe to search the meson-exchange effect.

(4) Comment on the angular distribution in an experimental view point

In an experimental view point, the determination of the coefficients $\alpha_{\mp}$ from the polarization terms, $P(p/E)(1+\alpha_{\mp}E)$, is sensitive to the mixing effect due to β-decay branches and β-ray scatterings. These disturbances produced relatively large spurious energy dependence of the β-decay asymmetry compared with the recoil terms, $\alpha_{\mp}E$, through the leading allowed G-T term. On the other hand, the determination from

the alignment terms, $A\alpha_{\pm}E$, is less sensitive to these spurious effects, because the terms include no such allowed terms. In order to obtain a reliable result, it is, therefore, essential to perform measurements with the large amount of alignment and the negligibly small polarization.

IV. Experiment

Our new experiment was composed of two parts. The first part was the measurement of the alignment terms $A\alpha_{\mp}E$, in which we observed β-ray-energy dependence of the angular distributions from aligned nuclei ^{12}B and ^{12}N. The other part was the sign determination of the nuclear alignment which was converted from the polarization by use of NMR technique. In other words, we obtained the absolute values of $\alpha_{\mp}$ in the former experiment, and obtained the sign of $\alpha_{\mp}$ in the latter experiment. The details of the two experiments are described in the following sections (1) and (2).

(1) Measurement of the alignment terms, $A\alpha_{\mp}E$

The production of polarized nuclei ^{12}B and ^{12}N through nuclear reaction was previously made possible by Sugimoto et al.[38]. They found large amount of nuclear polarization with small alignment in the experimental conditions to which present one is essentially similar. The NMR technique necessary for the spin-ensemble control has been established in our laboratory[14].

In the present experiment we produced a large amount of nuclear alignment by use of these techniques, and observed the alignment terms, $A\alpha_{\mp}E$, in the β-ray angular distributions from aligned ^{12}B and ^{12}N. The experimental procedure is summarized as follows;

a) production of polarized nuclei (see section (1)-a)),

b) dynamic conversion of the nuclear polarization to positive and negative alignments by use of the NMR technique (section (1)-b)),

c) detection of β-ray-energy spectra from aligned nuclei (section (1)-c)), and

d) comparison of energy spectra with positive and negative alignments to derive $\alpha_{\mp}$ values (section (3)).

a) Production of polarized nuclei

We employed $^{11}B(d,p)^{12}B$ and $^{10}B(^{3}He,n)^{12}N$ reactions to produce the polarized nuclei, ^{12}B and ^{12}N. The recoil nuclei ^{12}B and ^{12}N were implanted into a recoil stopper using the recoil energy. The nuclear polarization was expected to be perpendicular to the reaction plane which is formed by trajectories of incident particles and recoil nuclei (see Fig.2). We obtained the polarization of about 13% (25%) at the energy of incident particle of E_d=1.5 MeV ($E_{^3He}$ = 3.0 MeV) and at the recoil angle of θ= 40~75° (θ = 25~45°) for $^{12}B(^{12}N)$. The experimental condition of the reaction was optimized to obtain the maximum polarization and the productivity of $^{12}B(^{12}N)$ by using the previous data[39] of the polarization production. As the initial alignments produced through the nuclear reactions were small amounts of ~6% for the both cases, we converted the polarization to the alignment of sizable amount by use of NMR technique.

We utilized a rotating target system which is shown in Fig. 2 and 3, to improve the productivity of ^{12}B and ^{12}N. The backing of the target was a Ta ribbon on which the enriched ^{11}B or ^{10}B was deposited and the ribbon was attached in the groove of the target holer. The target holder was rotated with a period of 60 msec. The incident beam was pulsed to synchronize

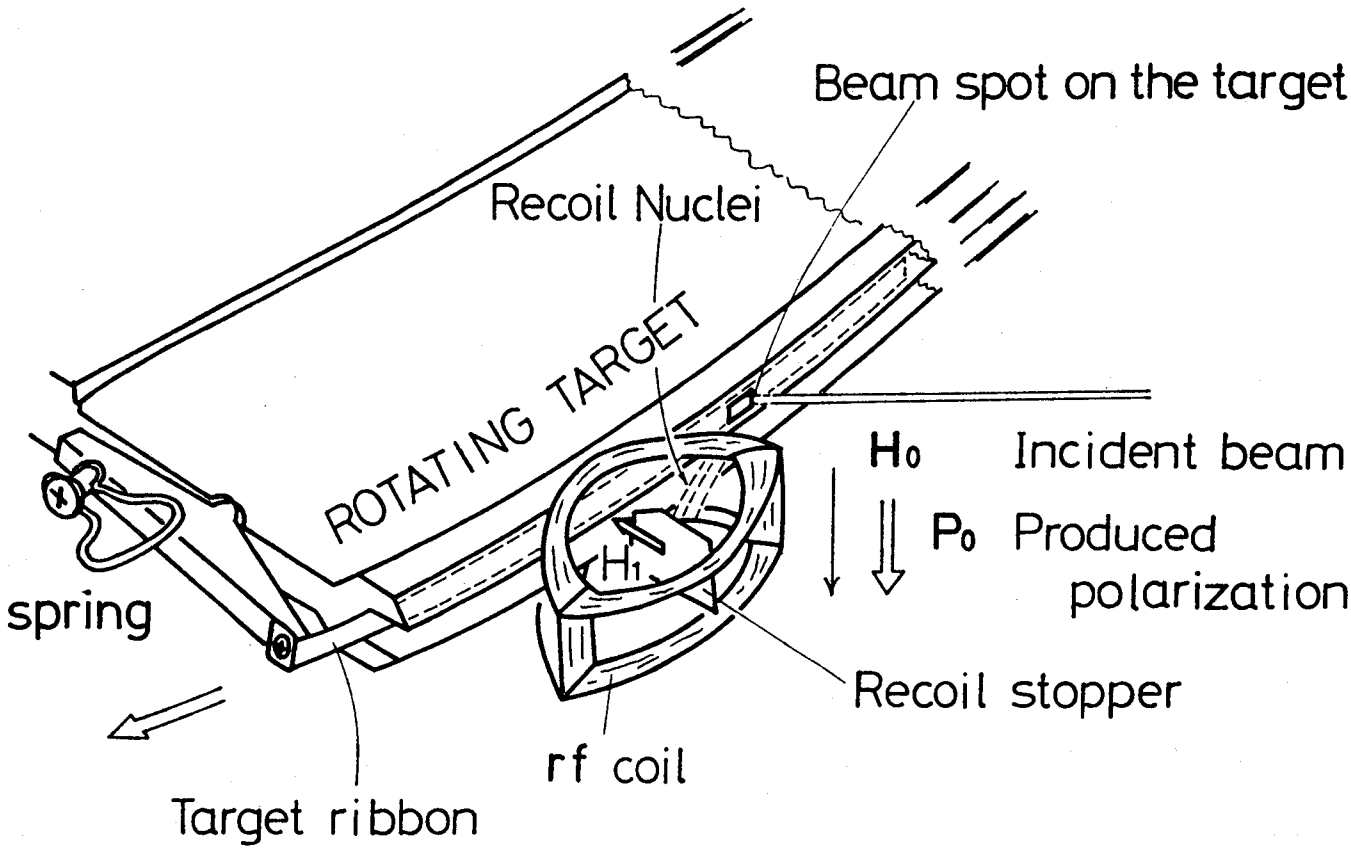

Fig. 2 Production of nuclear polarization. The ^{11}B or ^{10}B target was deposited on the tantalum ribbon. The ribbon was mounted in the groove of the target holder and was pulled by a spring so as to keep the target in contact with the groove tightly for good heat conduction. The recoil nuclei produced through the reactions $^{11}B(d,p)^{12}B$ and $^{12}B(^{3}He,n)^{12}N$ were implanted in a Mg recoil stopper which was in the center of the rf coil. The direction of the polarization is perpendicular to the reaction plane formed by the two trajectories of the incident beam and the recoil nuclei. The polarization was dynamically converted to the nuclear alignment by use of NMR technique.

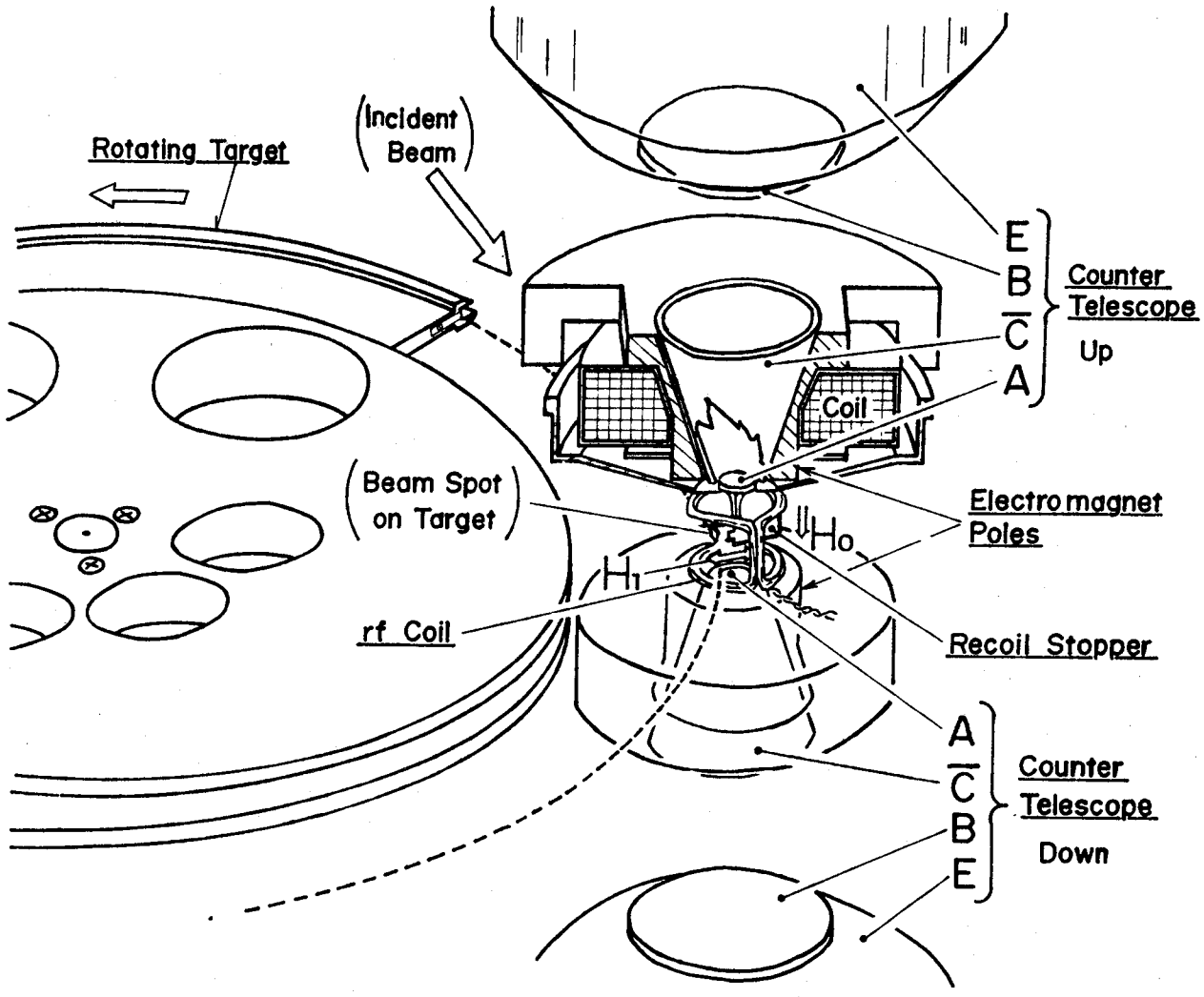

Fig. 3 Schematic view of the experimental setup. The target was rotated in a vacuum chamber with a period of 60 msec along the track shown by the bloken line. The nuclear polarization was preserved by the static holding magnetic field during the flight. It was converted to the alignment by the NMR technique. The β ray from the stopper was observed by the two sets of counter telescopes, one of which consisted of four plastic scintillators A,B,C and E ($A \cap B \cap \bar{C} \cap E$) at $\theta=0$ and $\theta=\pi$.

with the period of the rotation of the target. In every 60 msec the target crossed the beam line for 20 msec when the beam bombarded the target. The recoil stopper was set close to the beam spot on the target to make possible to implant the nuclei which recoiled from the target into a wide solid angle. The beam was stopped when the target left the beam line. After the target was hidden in the radiation-shielded part of the chamber together with unwanted activities, the β rays were started to be counted. The count was stopped before the target came back close to the stopper.

The polarization of the recoil nuclei in flight was preserved by applying a strong magnetic field (1~1.4 k Gauss) to decouple the perturbations due to the interaction with the atomic elections during the flight. The magnetic field was effective also to protect the polarization from the depolarization mechanisms due to the radiation damages which is active in the implantation material before the damages at the implantation were settled down.

The magnetic field was also necessary for the spin-ensemble control by use of the NMR technique. The homogeneity of the field in the effective area of the recoil stopper was better than 1%. The stability of the field was better than 0.1%/day.

b) Conversion of the nuclear polarization to a sizable alignment

The energy E_m of the magnetic sublevel m of ^{12}B and ^{12}N in the Mg single crystal the c-axis of which was set parallel and perpendicular to the magnetic field for ^{12}B and ^{12}N, respectively, can be expressed as,

$$E_m = -m\hbar\omega_L + \frac{1}{6}\hbar\omega_Q\,(3m^2 - 2) \qquad \text{for } {}^{12}B, \qquad (30)$$

$$E_m = -m\hbar\omega_L - \frac{1}{12}\hbar\omega_Q(3m^2 - 2) \qquad \text{for } {}^{12}N. \qquad (31)$$

Here Larmor frequency $\omega_L = \gamma H_O$ and $\omega_Q = \frac{3}{2}eqQ$ where γ is the gyromagnetic ratio, Q is the electric quadrupole moment and q is the electric field gradient in the crystal. The details are explained in Appendix I. The energy levels together with substate populations are schematically shown in Fig. 4 for the case of negative eqQ, positive initial alignment and parallel initial polarization to the magnetic field.

The conversion of the polarization to an alignment was performed by interchanging and equalizing the relevant substate populations by use of the NMR technique. Details of the NMR technique are explained in Appendix I. The processes of the conversion were the same for both experiments in ^{12}B and ^{12}N. For ^{12}B this conversion is schematically explained in Fig. 5.

Immediately after an on-beam period, an equalization rf field was applied to induce the transition between the magnetic sublevels $m = +1 \leftrightarrow 0$ (or $0 \leftrightarrow -1$), so $a'_{+1} \simeq a'_0 (a'_0 \simeq a'_{-1})$ was realized with a resultant polarization P_I. In the next step, the rf field which was swept in frequency over a resonance frequency ν_L (ν_H) and was simultaneously modulated in the amplitude as a function of time was applied for the adiabatic fast passage (AFP) between $m = 0 \leftrightarrow -1$ ($+1 \leftrightarrow 0$) in order to interchange the populations a'_0 and a_{-1} (a_{+1} and a'_0). The typical duration of rf was 2.5 msec and the effective rf magnetic field was $H_1 \sim 7$ Gauss for regular AFP and $H_1 \sim 20$ Gauss for double

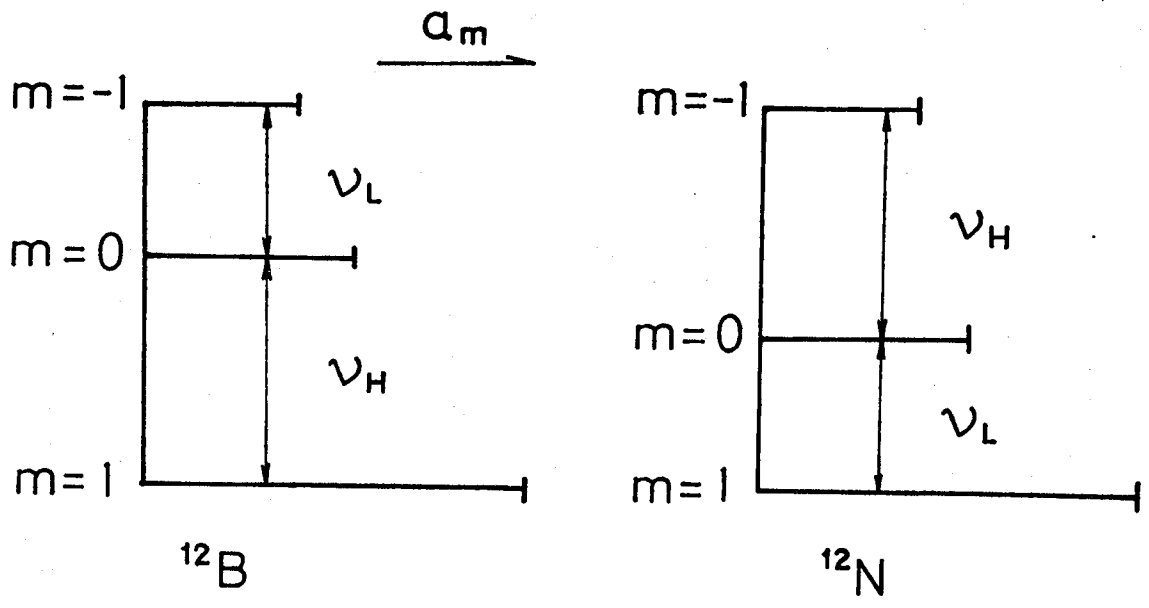

Fig. 4 Magnetic substate populations of ^{12}B and ^{12}N produced through the nuclear reactions, $^{11}B(d,p)^{12}B$ and $^{10}B(^3He,n)^{12}N$.

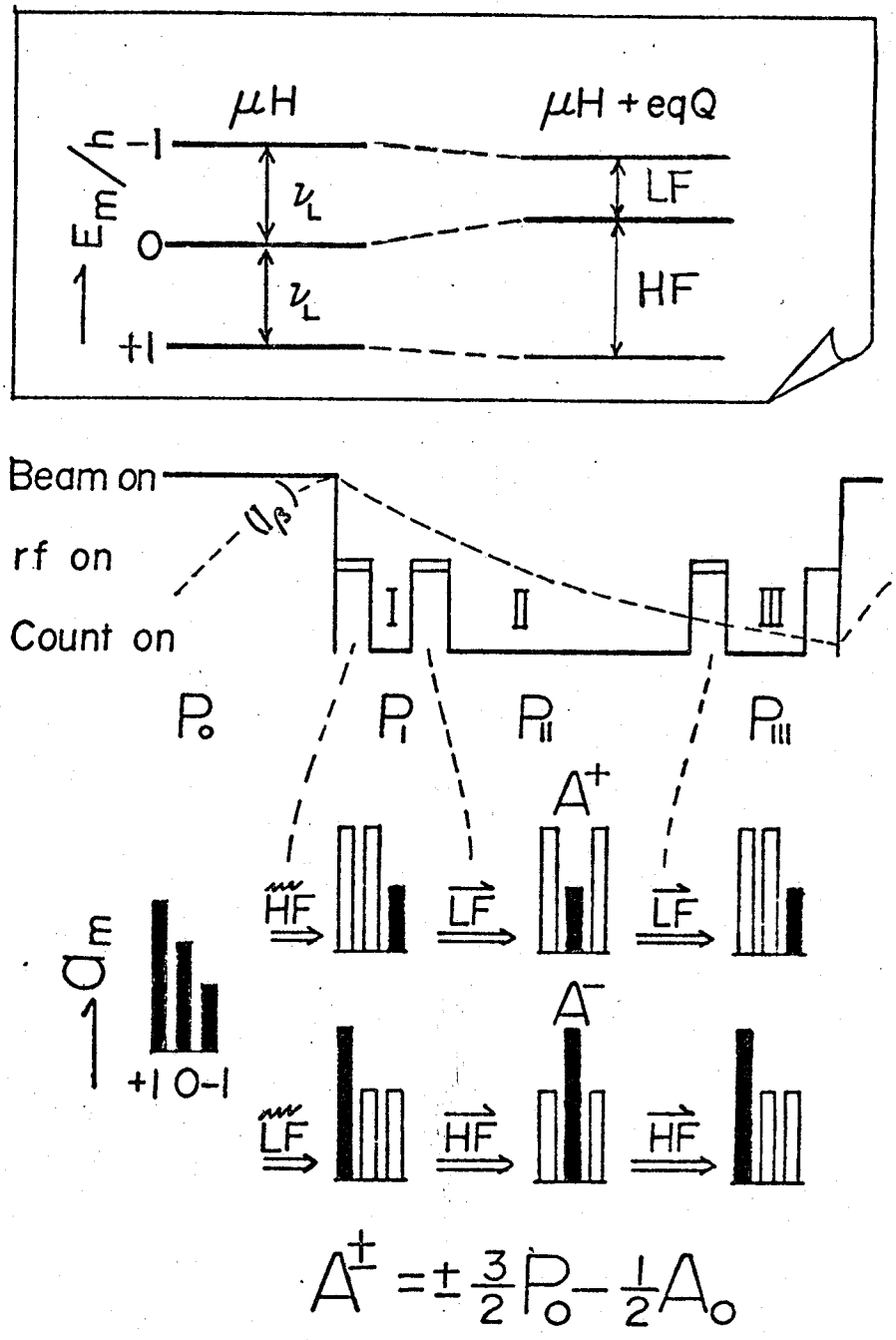

Fig. 5 Schematic diagram to explain the principle of the conversion of the initial polarization P_0 into a positive A^+ (or negative A^-) alignment by use of the NMR technique. Equalization processes are denoted by $\widetilde{\overrightarrow{HF}}$ and $\widetilde{\overrightarrow{LF}}$, and AFP by $\overrightarrow{HF}$ and $\overrightarrow{LF}$.

quantum transition (DQT) at the middle of the rf sweep. Thus a positive (negative) alignment A^+ (A^-) was produced with a small residual polarization P_{II}. The sign of the alignment was determined from β-γ angular correlation. The method is explained in the section IV-(2). The alignments $A^{\pm}$ can be related to the initial polarization P_o and alignment A_o with the perfect achievement of AFP and long spin-lattice relaxation time as $A^{\pm} = \pm 3/2\ P_o - 1/2\ A_o$. Simultaneously, with the perfect level equalization, the residual polarization $P_{II} = 0$ is achieved. Then we observed the β-ray-energy spectrum by two counter telescopes at $\theta=0$ (down) and $\theta=\pi$ (up). At the end of this observation, the alignment was reexamined by applying the AFP to the transition between $m = 0 \leftrightarrow -1$ $(+1 \leftrightarrow 0)$ and reproducing a polarization P_{III}. The data accumulation was continued by repeating a pair of $A^{\pm}$-production cycles in 20 times followed by two pairs of normalization cycles which consisted of the one without any NMR transition and the other with polarization inversion by adopting AFP on the DQT.
In the normalization cycles a geometrical asymmetry of counters at $\theta=0$ and $\theta=\pi$ was examined and also the variation of the initial polarization was measured as a function of time. A change of the spin ensemble controlled by the NMR technique was clearly observed in the resultant polarizations P_I, P_{II} and P_{III}. The polarization was determined from the up-down counting ratio $W(\theta=0)/W(\theta=\pi)$ and the up-down efficiency ratio $\varepsilon_0/\varepsilon_\pi$ determined from the normarization cycles. The details are described in Appendix II. They are shown in fig. 6, where the open

and closed circles are the polarizations observed in the positive and negative alignment-production cycles, respectively. The difference between the two values comes from the initial alignment A_o. The open squares are the polarizations observed in the normalization cycles.

The alignments $A^{\pm}$ in the main counting section II were obtained from the observed polarizations P_I, P_{II} and P_{III} by taking account of the attenuation due to the spin-lattice relaxation and the degree of the achievement for AFP processes. The polarizations $P_I^{\pm}$, $P_{II}^{\pm}$ and $P_{III}^{\pm}$ at the beginning (t_i) and the end (t_f) of the section II were deduced from the observed polarizations, P_I, P_{II} and P_{III} taking account of the relaxation time and the nuclear lifetime of ^{12}B (^{12}N), where the superscripts ($\pm$) refer to the positive and negative alignment-production cycles. The relaxation time for the polarization, T_1^P, was determined from the normalization cycle as

$$T_1^P \sim 100 \text{ msec} \qquad \text{for } ^{12}B,$$

$$T_1^P \sim 270 \text{ msec} \qquad \text{for } ^{12}N.$$

The value $(A^+ - A^-)$ was calculated at t_i and t_f from $P_I^{(\pm)}$ $P_{II}^{(\pm)}$, $P_{III}^{(\pm)}$ and η as,

$$[A^+ - A^-]_{t_i} = 2[P_I^{(+)}\eta^{(+)} + P_I^{(-)}\eta^{(-)}]_{t_i} - [P_{II}^{(+)} + P_{II}^{(-)}]_{t_i}, \qquad (32)$$

$$[A^+ - A^-]_{t_f} = 2[P_{III}^{(+)}/\eta^{(+)} + P_{III}^{(-)}/\eta^{(-)}]_{t_f} - [P_{II}^{(+)} + P_{II}^{(-)}]_{t_f}, \qquad (33)$$

where $\eta^{(+)}$ ($\eta^{(-)}$) is a degree of achievement of the AFP between $m = 0 \leftrightarrow -1$ ($+1 \leftrightarrow 0$). The details of the derivation of Eqs. (32)

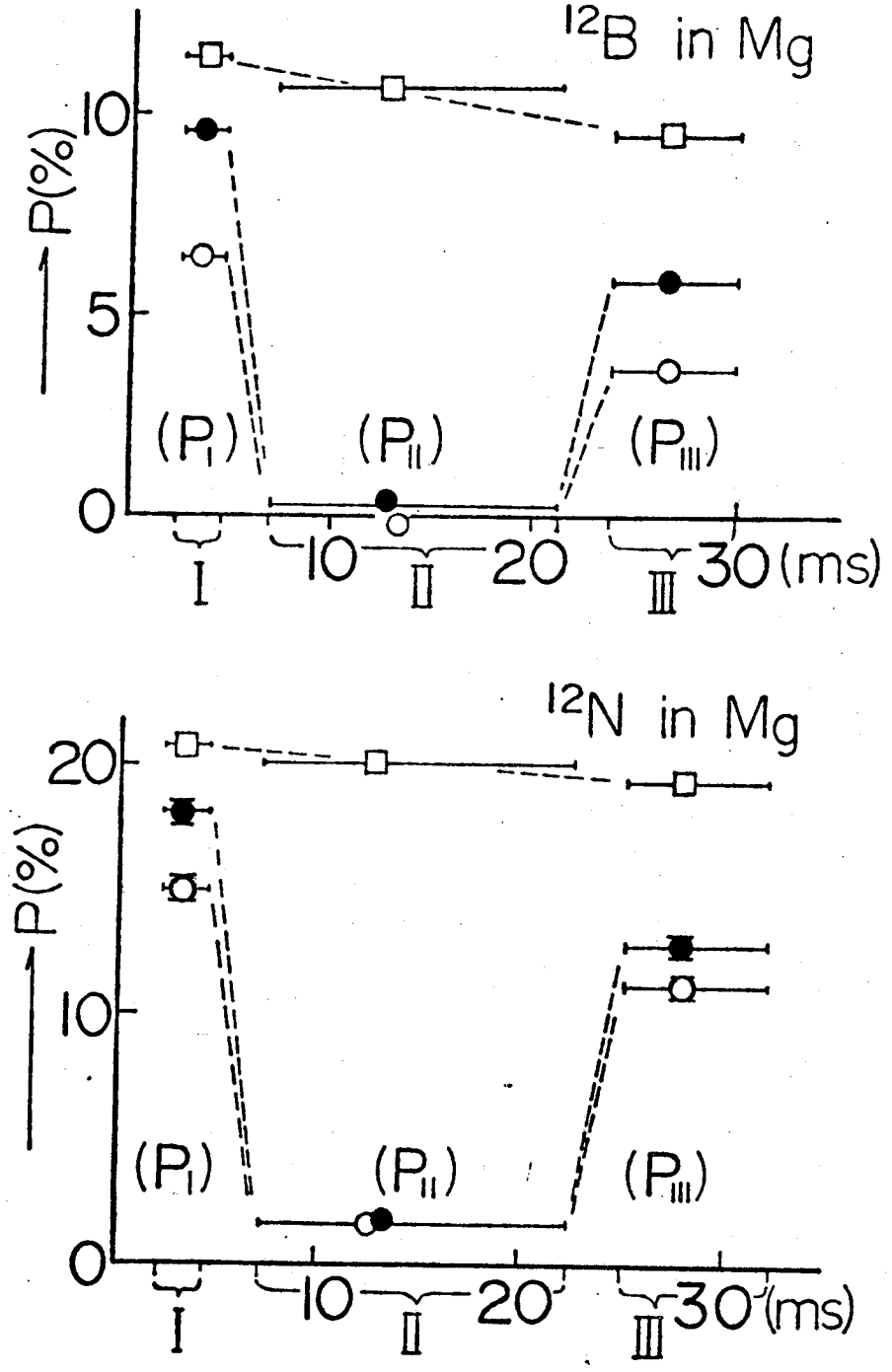

Fig. 6 Typical examples of the spin-ensemble control in the main routine. The open and closed circles are the polarizations observed in the A^+ and A^- -production cycles, respectively. The open squares are the polarizations observed in the normarization cycle.

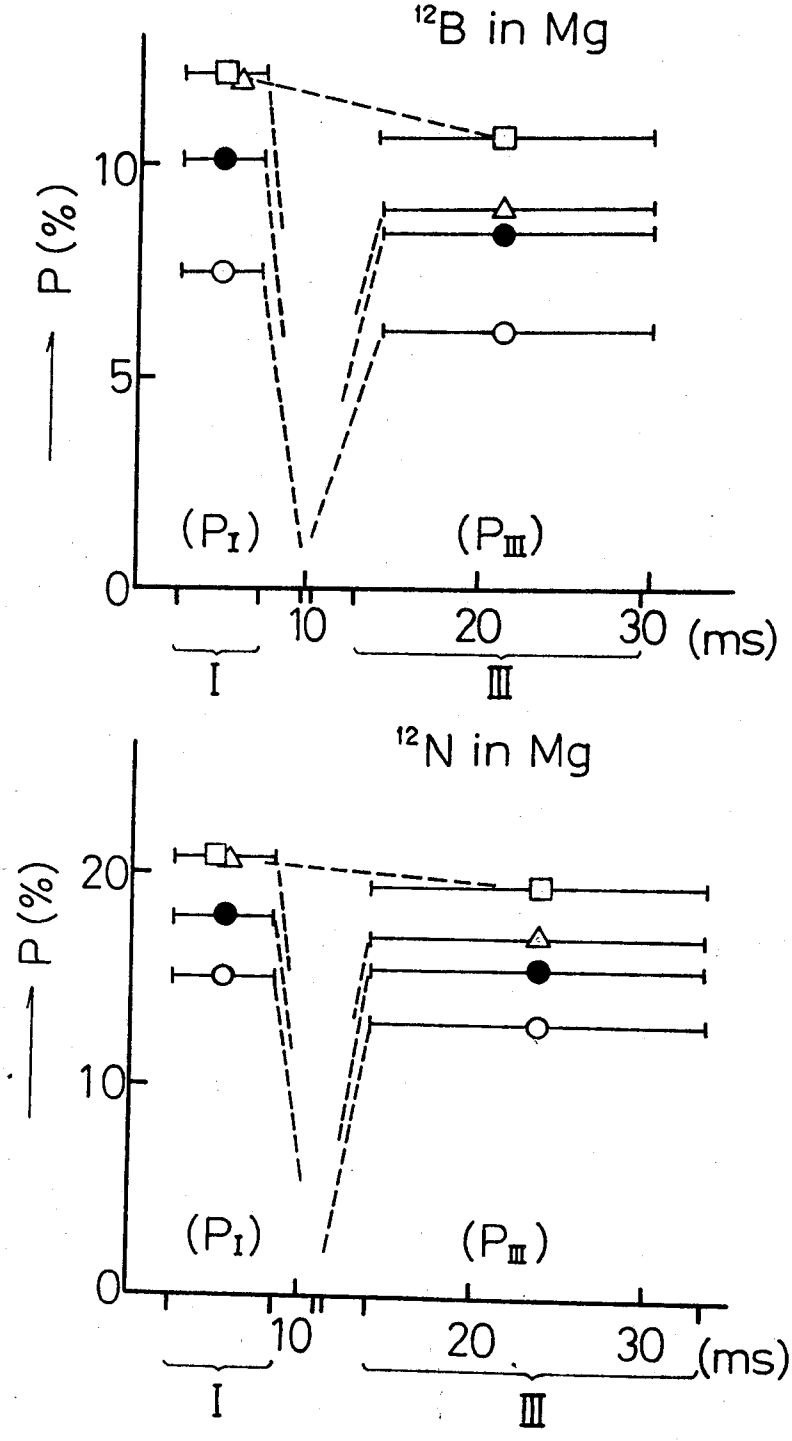

Fig. 7 Typical examples of the spin-ensemble control in the test routine. The triangles are the polarizations observed in the test routine for double-quantum transition. The meanings of the other marks are the same as in Fig. 6.

and (33) are described in Appendix II. The relaxation time of the nuclear alignment was determined from the two $(A^{+} - A^{-})$ values at t_i and t_f as

$T_1^A \sim 36$ msec for ^{12}B,

$T_1^A \sim 62$ msec for ^{12}N.

A proper value of the alignment for the counting section II was obtained by interpolating the two values at t_i and t_f taking account of the nuclear lifetime and the relaxation time. The factors $\eta^{(\pm)}$ were determined by comparing P_I and P_{III} observed in a separate test run with reduced counting section II ($t_f - t_i \to 0$) and $\eta > 0.9$ was required to continue the measurements. The averaged value of alignment observed at the section II was $|A^{+} - A^{-}| \simeq 0.27$ with $|P^{(+)} - P^{(-)}| < 0.01$ for ^{12}B and $|A^{+} - A^{-}| \simeq 0.58$ with $|P^{(+)} - P^{(-)}| < 0.01$ for ^{12}N.

c) β-ray-energy spectra from aligned nuclei

The β-ray-energy spectra with positive and negative alignments in the counting section II were observed by two sets of counter telescopes at $\theta = 0$ and $\theta = \pi$, which are shown in Fig. 3. The counters A and B, the thickness of which were 1mm and 5mm, respectively, determined the solid angle for the β-ray detection. The cone-shaped counter C, the thickness of which was 2 mm, was used to reject β rays scattered by the electromagnet. The 16cmϕ x 16cm plastic counter E is an energy detector by which β-ray-energy spectra were observed. The β-ray-energy singnal was accumulated with the condition that the signals from A, B, C and E counters satisfy $(A \cap B \cap \bar{C} \cap E)$. The gates of these

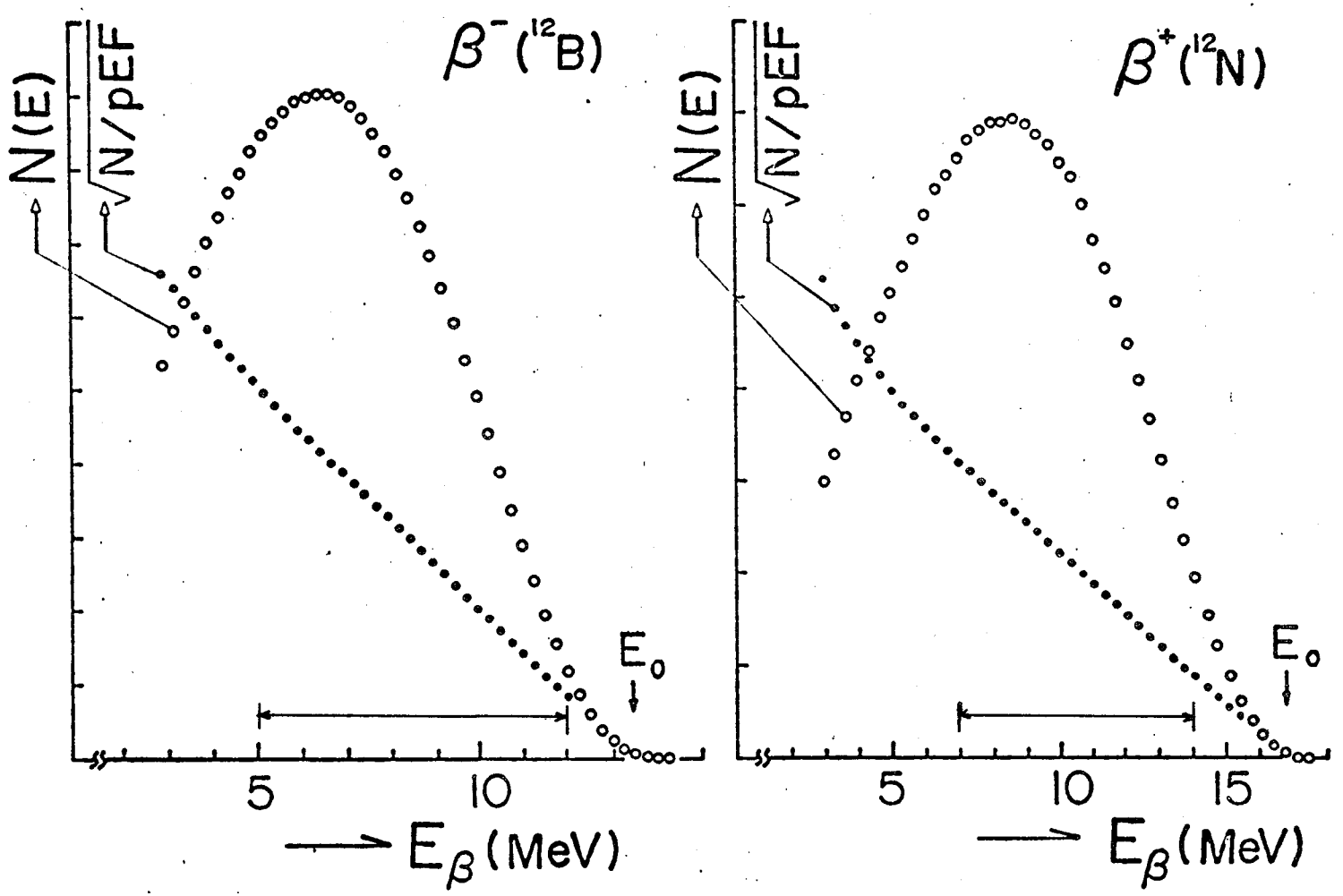

Fig. 8 Typical β-ray-energy spectra together with their Kurie plots. The arrows indicate the energy regions used for the R(E) analyses.

counters were closed during an on-beam period to avoid the disturbing effects due to the intense beam burst. In the case of the high counting rate, the pulse-height spectra were disturbed by the pile-up of the signals. A pile-up rejector was used for a telescope to remove the pile-up pulses from the energy signal. Details of these counting systems are described in Appendix III.

Typical examples of the β-ray-pulse-height spectra together with the Kurie plots for ^{12}B and ^{12}N are shown in Fig. 8. The energy scale was determined by the chi-squares fitting of theoretical spectral shape to the experimental pulse-height spectra. Details of this analysis are described in the section (3).

e) Time-sequence program of the $\alpha_{\mp}$ measurement

The experimental procedure was composed of two parts, the main routine and the test routine. The time-sequence program of these two routines are shown in Fig. 9 and 10. The whole experimental system was synchronized with the rotation of the target. The motion of the rotating target was monitored with the photo-coupler which picked up the position of the target. The signal from the photo-coupler in every period triggered the clock pulse which was used for the control of the experimental system. A mini-computer supervised the whole system referring to the signal from the photo-coupler and to the clock pulse. The first and second lines show the time-sequence for the beam

and rf control. The incident beam was swiched on during the time when the target was in the right position and was swiched off when the target left the beam line. During the beam off time rf was applied referring to the clock pulse. The third and fourth lines show the rf-frequency modulation for the $A^{\pm}$-production cycles and the normarization cycles. And finally, in the fifth line, the counting periods were shown.

From the test routine, the degrees of achievement for AFP's were determined for the single quantum transition (SQT) and the double quantum transition (DQT). The time-sequence program for the test routine was the same as the main routine except for the time duration of the counting sections I, II and III. Especially the period of the counting section II was reduced to nearly equal zero (see Fig. 10), in order to minimize a depolarization due to the spin-lattice relaxation for the alignment in the counting section II.

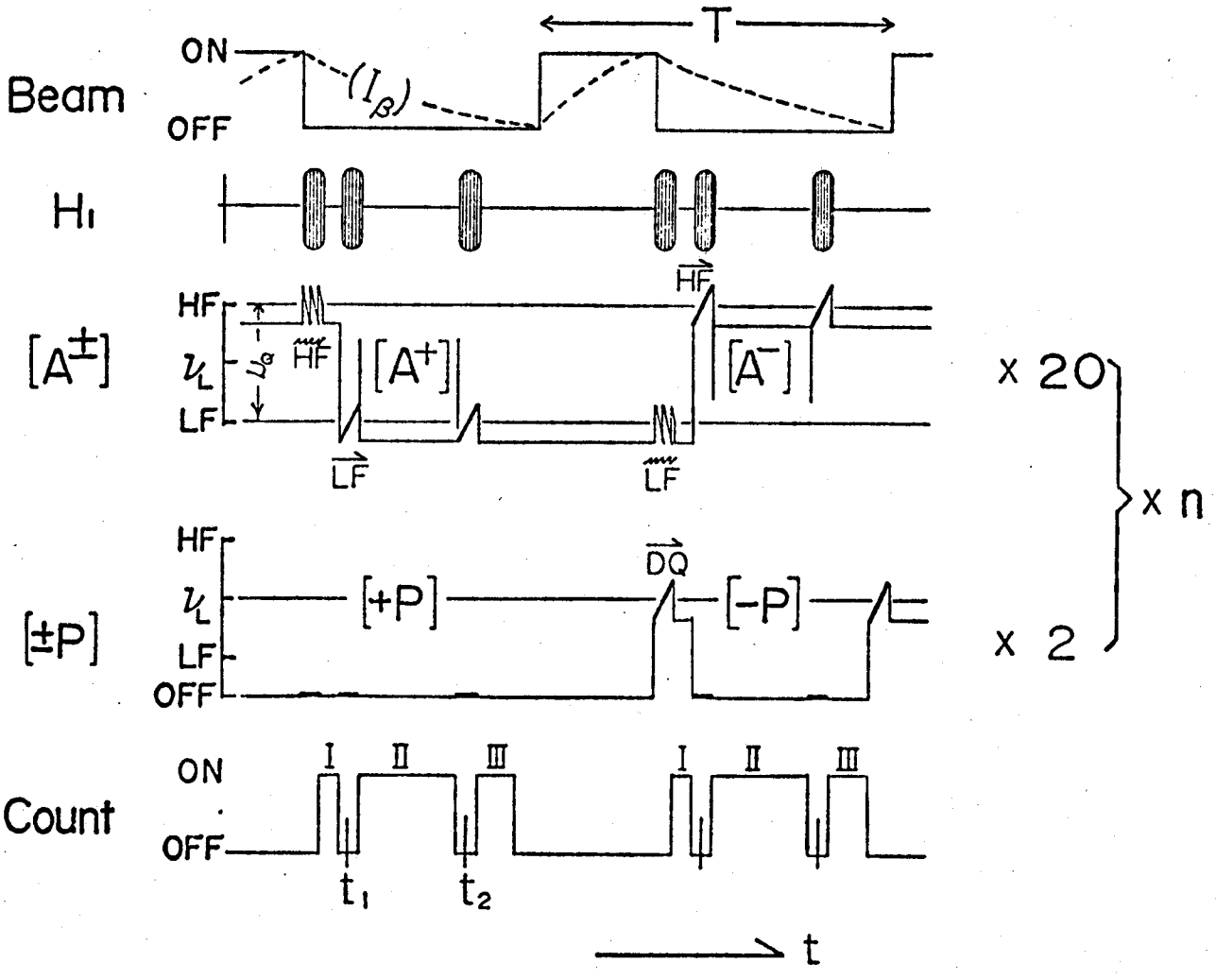

Fig. 9 Time-sequence program for the ^{12}B and ^{12}N production, the spin-ensemble control by NMR and the β-ray counting in the main routine. The repetition period T was 60 msec. The duration of the beam and rf-on time were 20 msec and 2.5 msec, respectively.

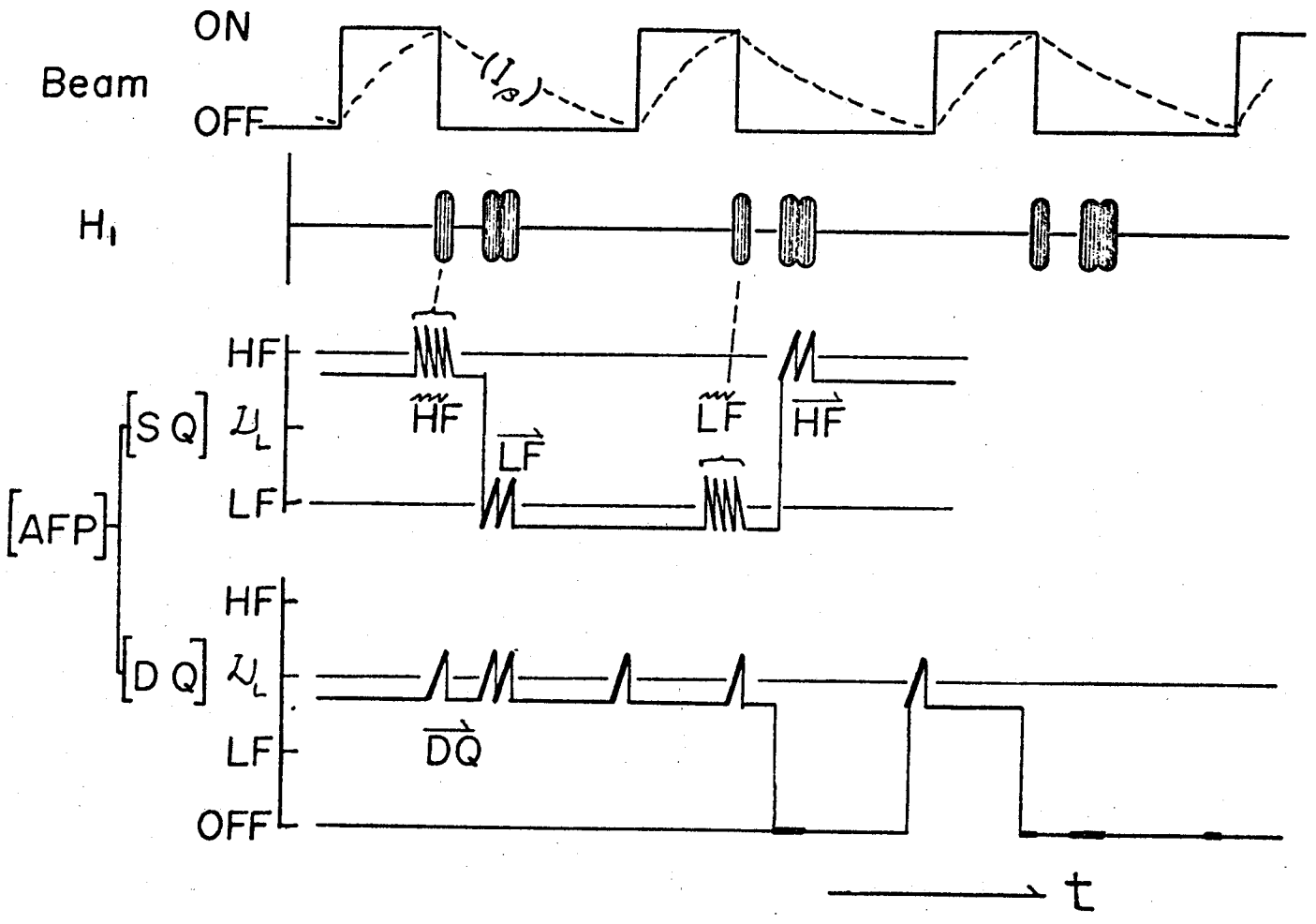

Fig. 10 Time-sequence program for the test routine.

(2) Sign determination of the nuclear alignment

Signs of the alignments which were converted from the polarization by use of NMR technique were determined from the β-γ angular correlation in aligned nuclei ^{12}B and ^{12}N.

Alignments were converted from the polarization by the method described in the section (1). Here we define A^L and A^H for the alignments which are converted by applying AFP to the lower and higher resonance frequencies, ν_L and ν_H, respectively. Signs of A^L and A^H were determined from the β-γ angular correlation as follows.

a) β-γ angular correlation in the oriented ^{12}B and ^{12}N

We can determine the degree of nuclear alignments of ^{12}B and ^{12}N by measuring the angular distributions of the 4.44-MeV γ rays emmitted from ^{12}C following the β decays to the first excited state ($I = 2^+$ at 4.44 MeV) of ^{12}C, since the alignments are transferred to the daughter state. In order to reject signals due to background radiations we observed the β rays in coincidence with the γ rays in the transition to the first excited state. In this experiment, enough counting statistics of the β-γ coincidence were not obtained to determine the accurate value of the alignment compared with the determination from the polarizations, because of the small β-decay branch to the state. The sign, however, could be determined reliably from the β-γ correlation measurement.

The β-γ angular correlation for the transition ($1^+ \xrightarrow{\beta} 2^+ \xrightarrow{\gamma} 0^+$) in aligned nuclei was given as[40],

$$W_{\beta\gamma} \propto [S(0) - \frac{1}{3}P_2(\cos\theta_{\beta\gamma})S(2)] + \frac{3}{4}P[\cos\theta_{\beta\gamma}\cos\theta_{\gamma} - \cos\theta_{\beta}]S(1)$$
$$+A[-\frac{1}{4}P_2(\cos\theta_{\gamma})S(0)$$
$$-\{\frac{1}{3}P_2(\cos\theta_{\gamma}) - \frac{3}{2}\cos\theta_{\beta\gamma}D + \frac{4}{3}P_2(\cos\theta_{\beta\gamma})$$
$$\times P_2(\cos\theta_{\gamma})\}\, S(2)], \qquad (34)$$

where the orientation axis was defined as z axis, then θ_{β} and θ_{γ} are the polar angles of the directions of a β-particle and a photon momentum, respectively, and $\theta_{\beta\gamma}$ is the angle between these directions. A and P are the alignment and the polarization of the parent nuclei, respectively. D is defined as $D = \cos\theta_{\beta}\cos\theta_{\gamma} - 1/3\cos\theta_{\beta\gamma}$. If we neglect higher order terms such as recoil-order term, then S(0), S(1) and S(2) are expressed as

$$S(0) = |f_A|^2, \qquad (35)$$

$$S(1) = \mp p/E\, |f_A|^2, \qquad (36)$$

$$S(2) = 0. \qquad (37)$$

In our experimental condition of $\theta_{\beta} = 0$, $\theta_{\gamma} = \theta_{\beta\gamma} = \theta$, $W_{\beta\gamma}$ is

$$W_{\beta\gamma} \propto 1 \mp \frac{3}{4}P(\frac{p}{E})(\cos^2\theta - 1) - \frac{1}{4}AP_2(\cos\theta), \qquad (38)$$

where the upper sign refers to ^{12}B and the lower sign refers to ^{12}N, and for $\theta = \pi$,

$$W_{\beta\gamma} \propto 1 - \frac{1}{4}A. \qquad (39)$$

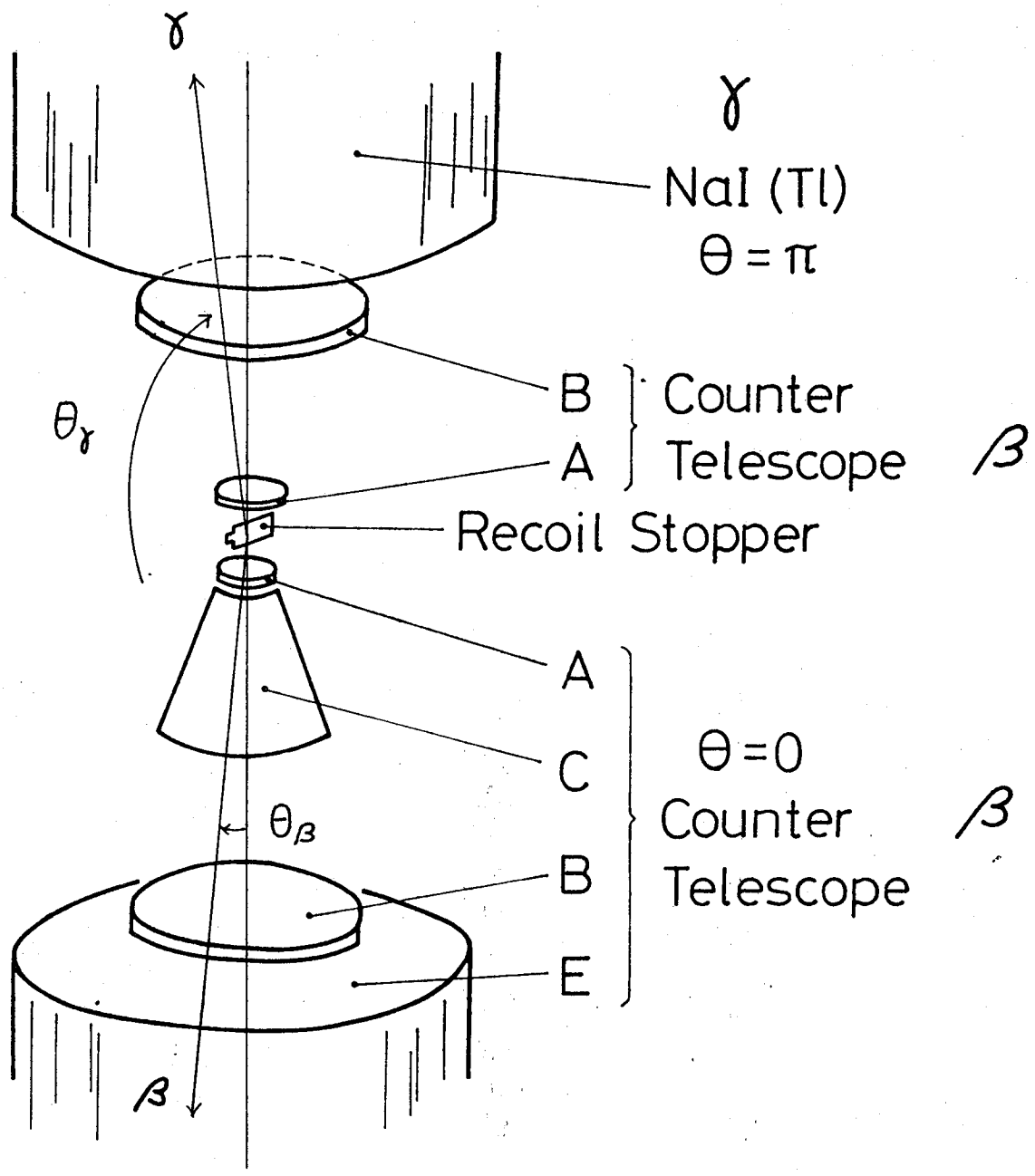

Fig. 11 Counter telescopes for β-γ correlation measurement. The same counter telescope at θ=0 as the one in the measurement of $\alpha_{\overset{-}{+}}$ was used for the detection of β rays. A 5"ϕ × 5" NaI(Tl) was set at θ=π to detect the 4.44 MeV γ-ray from the excited state of ^{12}C which was populated through the β-decay branch of ^{12}N (or ^{12}B). The amount of polarization was determined from the β ray counting ratio W(θ=0)/W(θ=π) detected by the two counter telescopes $(A \cap B \cap \bar{C} \cap E)$ at θ=0 and $(A \cap B)$ at θ=π.

b) Experimental procedure

Aligned ^{12}B and ^{12}N were produced by the same method used in the measurement of the alignment terms, $A\alpha_{\mp}E$. Counter telescopes for the observation of the β-γ angular correlation are shown in Fig. 11. The up-down counting rate asymmetry of β rays was observed by the counter telescopes; one $(A \cap B \cap \bar{C} \cap E)$ at $\theta=0$ and the other $(A \cap B)$ at $\theta=\pi$. The γ rays were observed by a 5"ϕ × 5" NaI(Tl) at $\theta=\pi$. True signals from the β-counter telescope and γ counter were successively accumulated for the two A^L and A^H cycles. In order to increase the counting statistics the equalization rf was not used, since β-γ angular correlation at $\theta=\pi$ is not dependent on the polarization. The spin-ensemble control is schematically shown in Fig. 12. The β-ray-energy spectra in the transition to the first excited state were simultaneously observed using the β-γ coincidence signals for the energy gate of the E counter. The production rates for A^L and A^H cycles were monitored by the β rays detected by the telescopes. This monitor was necessary in order to normalize production rates in A^L and A^H cycles. The detail of the electronics of the β and γ ray detection system is described in Appendix III. The observed β-ray-energy spectra are shown in Fig. 17.

c) Experimental results

Typical examples of the spin-ensemble control in a run of the sign determination of alignments are shown in Fig. 13 for ^{12}N. The open and closed circles are the polarizations of the A^L and A^H cycles, respectively.

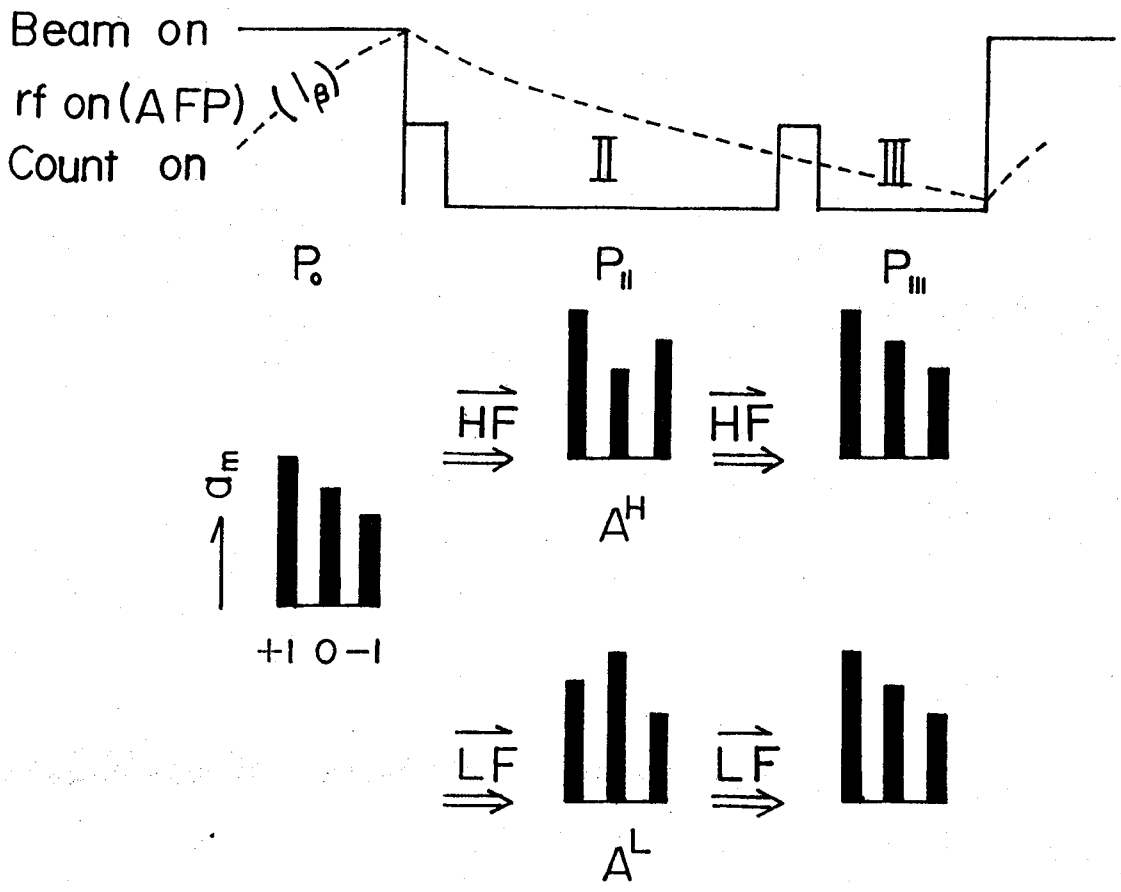

Fig. 12 A schematic diagram which explains the method of the conversion of the initial polarization into the alignments A^L and A^H in the sign determination of the alignments. For ^{12}N (^{12}B) the signs of the two alignments were $A^L < 0$ and $A^H > 0$ ($A^L > 0$ and $A^H < 0$).

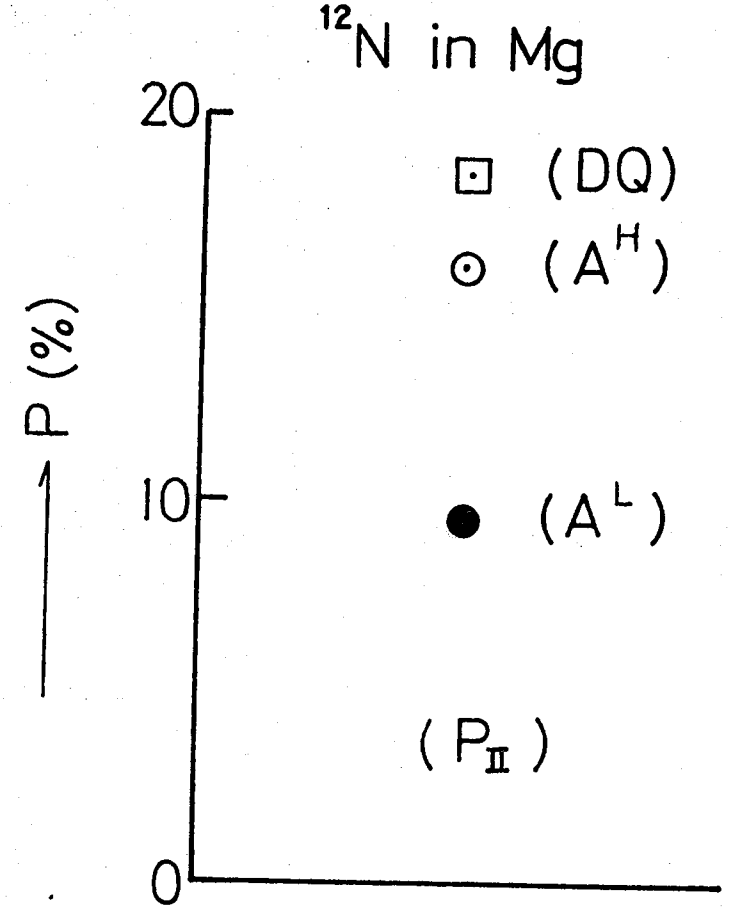

Fig. 13 Polarization P_{II} observed in the experiment of the sign determination of the alignment. The open and closed circles are the polarizations observed in the A^H and A^L cycles, respectively. The open square is the initial polarization.

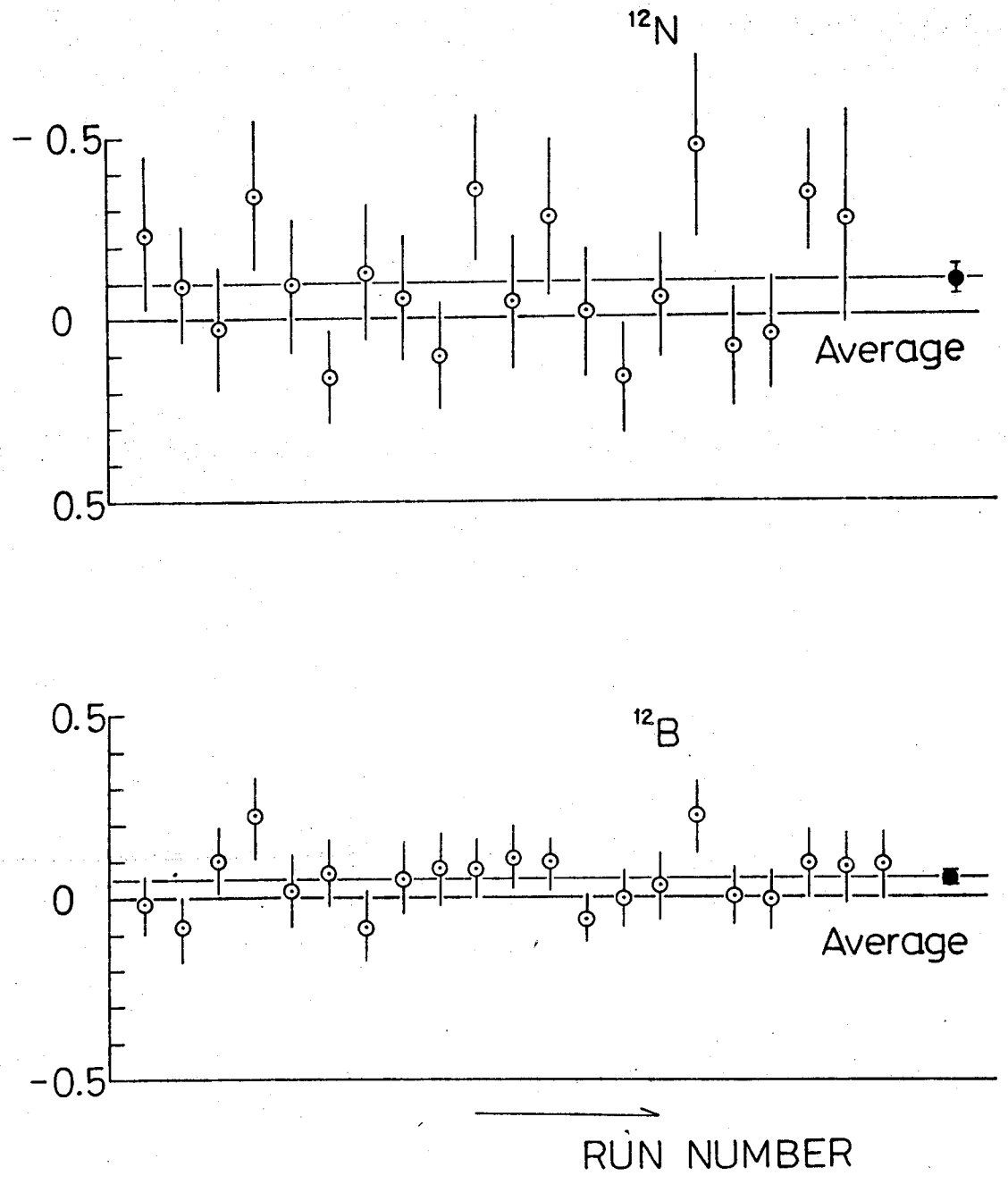

Fig. 14 Deviation $\Delta = 2\left\{\frac{W_{\beta\gamma}(\pi,A^{H}) - W_{\beta\gamma}(\pi,A^{L})}{W_{\beta\gamma}(\pi,A^{H}) + W_{\beta\gamma}(\pi,A^{L})}\right\}$.

The open circles are the results of individual runs and closed circles are the averaged values.

Typical examples of the experimental result for the deviation

$$\Delta = 2 \left\{ \frac{W_{\beta\gamma}(\pi, A^H) - W_{\beta\gamma}(\pi, A^L)}{W_{\beta\gamma}(\pi, A^H) + W_{\beta\gamma}(\pi, A^L)} \right\}$$ are shown in Fig. 14.

From these results the sign of the alignment was determined. The values of alignments were also obtained by the polarization measurement to examine the consistency of the β-γ correlation, since the alighment was related to Δ as,

$$\Delta = 2 \left\{ \frac{W_{\beta\gamma}(\pi, A^H) - W_{\beta\gamma}(\pi, A^L)}{W_{\beta\gamma}(\pi, A^H) + W_{\beta\gamma}(\pi, A^L)} \right\} = -\frac{1}{4} (A^H - A^L), \qquad (40)$$

which is derived from the equation (39). The results were

$$\Delta = -0.101 \pm 0.036 \quad \text{for } {}^{12}N,$$

$$\Delta = +0.048 \pm 0.019 \quad \text{for } {}^{12}B.$$

The value of Δ estimated from the initial polarization taking account of the degree of achievement and the relaxation time which were obtained in the preceding measurement was

$$|-I/4 (A^H - A^L)| = 0.12 \quad \text{for } {}^{12}N,$$

$$= 0.053 \quad \text{for } {}^{12}B.$$

The agreement between the experimental result and the predicted value is good in each case. Thus the signs of the alignments were determined as

$$A^H < 0, \quad A^L > 0 \quad \text{for } {}^{12}B,$$

$$A^H > 0, \quad A^L < o \quad \text{for } {}^{12}N.$$

The sign of the alignment converted by AFP with ν_L or ν_H from the polarization is related to the sign of the coupling constant, eqQ, of ${}^{12}N({}^{12}B)$ in a Mg crystal. The sign of A^L (or A^H) for ${}^{12}N$ can be predicted to be minus or plus for minus or plus eqQ, respectively, from the energy split of the magnetic sublevels and the level populations (see Fig. 4)

with the present condition that the polarization is parallel to the magnetic field and the sign of the magnetic moment is plus. The result of the alignment sign indicates that the sign of the coupling constant, eqQ, is negative for ^{12}N in Mg. The sign of the coupling constant is negative for ^{12}B in Mg from the same discussions with ^{12}N. The sign of initial alignment A_o was also determined from the decrease of polarization after the equalization by the rf field. The decrease shown in Fig. 6 reveals the sign of initial alignments as

$A_o > 0$ for ^{12}N,

$A_o > 0$ for ^{12}B.

The present results of the signs of A_o and eqQ for ^{12}B was consistent with the previous result[39].

(3) Data analyses

a) Comparison of the energy spectra with positive and negative alignments

We obtained the alignment terms $A\alpha_{\mp}E$, by comparing the β-ray-energy spectra with the positive and negative alignments observed by a counter telescope.

The β-ray angular distribution from aligned ^{12}B and ^{12}N is given as,

$$W(\theta,E,A)=C\cdot f(E)\{1\mp P(p/E)(1+\alpha_{\mp}E)P_1(\cos\theta)+A\alpha_{\mp}EP_2(\cos\theta)\}, \quad (41)$$

where

C = constant,

f(E) = theoretical β-ray-energy spectra emitted from unoriented nuclei.

When we compare the experimentally observed spectra, we need to normalize the spectra by the factor C. We used the total counts of β rays in the energy region used for the analyses in this normalization. Namely we normalized the integrated value of $W(\theta,E,A)$ over energy E to unity,

$$\int_{E_\ell}^{E_h} W(\theta,E,A)dE = 1 , \qquad (42)$$

where $(E_\ell \sim E_h)$ is the energy region used for this integration. Here we can rewrite the formula $W(\theta,E,A)$ at $\theta=0$ as

$$W(0,E,A)=C\cdot f(E)\ (1\mp P')\{1+\frac{A\mp P'}{1\mp P'}\alpha_\mp E\}, \qquad (43)$$

where P' is $P(p/E)$. In the following discussions we replace P' by P for simplicity. Then the integration was reduced to as follows,

$$\int_{E_\ell}^{E_h} W(0,E,A)dE=C\int_{E_\ell}^{E_h} f(E)dE\cdot(1\mp P)\{1+\tilde{A}\alpha_\mp \bar{E}\}, \qquad (44)$$

where

$$\bar{E} = \int_{E_\ell}^{E_h} E\cdot f(E)dE/\int_{E_\ell}^{E_h} f(E)dE, \qquad (45)$$

$$\tilde{A} = \frac{A\mp P}{1\mp P} . \qquad (46)$$

Finally the normalized spectrum $N(O,E,A)$ can be obtained from Eqs. (43),(44),(45) and (46) as

$$N(O,E,A) = \{(1+\tilde{A}\alpha_\mp E)/(1+\tilde{A}\alpha_\mp \bar{E})\}\,\tilde{f}(E), \qquad (47)$$

$$\tilde{f}(E) = f(E)/\int_{E_\ell}^{E_h} f(E)dE. \qquad (48)$$

The ratio $N(O,E,A^+)/N(O,E,A^-)$ which does not include the spectral shape function f(E), can be expressed for the down counter at $\theta=0$ as,

$$R_D(E) = \frac{1+\tilde{A}^+\alpha_\mp E}{1+\tilde{A}^+\alpha_\mp \bar{E}} \Big/ \frac{1+\tilde{A}^-\alpha_\mp E}{1+\tilde{A}^-\alpha_\mp \bar{E}} . \qquad (49)$$

If we neglect the higher order terms, $O(\alpha_{\mp}^{2})$, the R_D (E) is given by

$$R_D(E) = 1 + (A^+ - A^-)\alpha_{\mp}E \mp (P^+ - P^-)\alpha_{\mp}E - \{(A^+ - A^-)\alpha_{\mp}\bar{E} \mp (P^+ - P^-)\alpha_{\mp}\bar{E}\} . \quad (50)$$

For the polarization term we must include the effects due to β-ray scatterings and β-decay branches. So we must replace $\alpha_{\mp}$ by $\delta_{\mp}(E)$ which include these effects for polarization terms. Then $R_D(E)$ is

$$R_D(E) = 1 + (A^+ - A^-)\alpha_{\mp}E \mp (P^+ - P^-)\delta_{\mp}(E) - \{(A^+ - A^-)\alpha_{\mp}\bar{E} \mp (P^+ - P^-)\bar{\delta}_{\mp}\} , \quad (51)$$

$$\bar{\delta}_{\mp} = \int_{E_\ell}^{E_h} \delta_{\mp}(E) f(E) dE / \int_{E_\ell}^{E_h} f(E) dE . \quad (52)$$

By the same way the ratio $R_U(E)$ at $\theta=\pi$ can be obtained as

$$R_U(E) = 1 + (A^+ - A^-)\alpha_{\mp}E \pm (P^+ - P^-)\delta_{\mp}(E) - \{(A^+ - A^-)\alpha_{\mp}\bar{E} \pm (P^+ - P^-)\bar{\delta}_{\mp}\} . \quad (53)$$

The value of $\delta_{\mp}(E)$ was estimated from the measurement with a sizable polarization and a negligibly small alignment, and it turned out to be less than 5% variation in the energy range used for the analyses. In our present measurements of the alignment terms the next relation was established,

$$| P^+ - P^- | < \frac{1}{25} | A^+ - A^- | . \quad (54)$$

Thus the disturbing effects due to the residual polarization was small.

Furthermore we can cancel the disturbing effect by averaging the both ratioes, R_D and R_U, with the same weight as

$$\frac{1}{2}\,(R_U(E) + R_D(E)) = 1 + (A^+ - A^-)\alpha_{\mp}(E - \bar{E}). \qquad (55)$$

Finally we obtained the value of $(A^+ - A^-)\alpha_{\mp}$ from the slope of $\frac{1}{2}(R_U(E) + R_D(E))$. The energy ranges which are indicated with arrows in Fig. 8, were used for the analyses in order to avoid the effects due to the β-ray scatterings, β-decay branches and finite counter resolution. The energy ranges were $5 \sim 12$ MeV for ^{12}B and $7 \sim 14$ MeV for ^{12}N.

Typical examples of the deviation (R(E) - 1) are shown in Fig. 15, where the solid lines are results of the least squares fitting, the dotted line (—·—·—·—) is the theoretical prediction given by M. Morita et al.[41], and the broken line (---------) is the theoretical result given by H. Behrens[42]. Both of the theoretical values were calculated with no SCC. The coefficients $\alpha_{\mp}$ determined from the slope of (R(E) - 1) and the alignment for individual run are shown in Fig. 16. By averaging these results the coefficients $\alpha_{\mp}$ were determined as

$$\alpha_- = + (0.006 \pm 0.018)\ \%/\text{MeV},$$

$$\alpha_+ = - (0.273 \pm 0.037)\ \%/\text{MeV}.$$

The uncertainty includes only the statistical error. The various contributions in the uncertainties of the coefficients $\alpha_{\mp}$ are explained in the following sections.

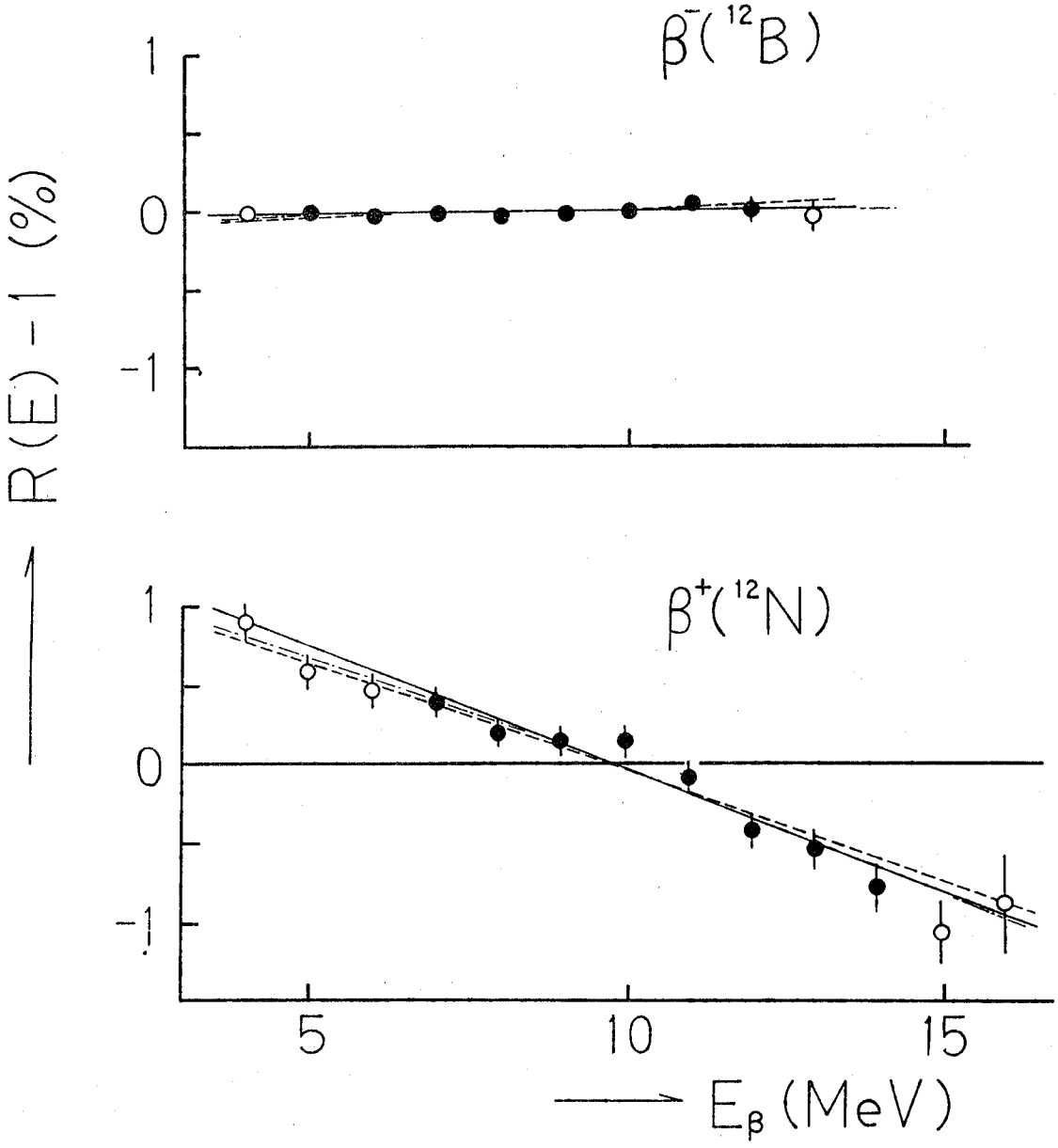

Fig. 15 Typical examples of (R(E)-1). The solid lines are the results of the least squares fitting. The data indicated by closed circles were used for the present analyses to derive $\alpha_{\mp}$ values. The two lines indicated by a dotted and a broken lines show the theoretical predictions given by M. Morita[41] et al. and H. Behrens[42], respectively with no SCC.

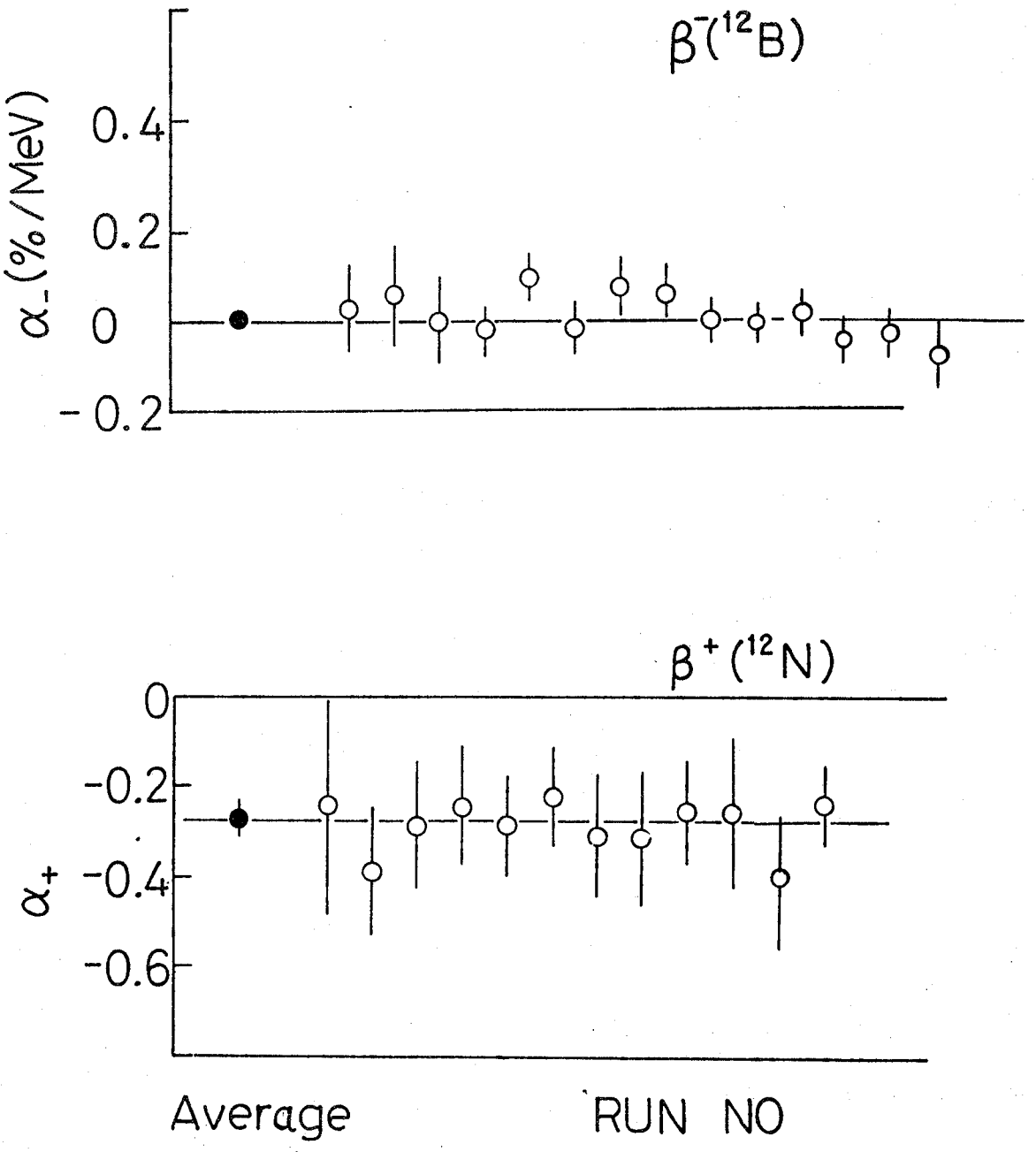

Fig. 16 $\alpha_-(^{12}B)$ and $\alpha_+(^{12}N)$ obtained in individual runs and the final averaged values.

b) Calibration of the energy scale

Energy calibration was performed by examining the pulse height spectra observed by the energy counter. The reliability of this calibration was checked by comparing the results with the end-point energies observed for the β-decay branches to the ground and first excited states of ^{12}C.

The observed pulse height N was related to the β-ray energy E as

$$E = E_o \times \frac{N - N_{zero}}{N_{end} - N_{zero}} , \qquad (56)$$

where the parameters N_{end}, N_{zero} are the end-point and zero-point-pulse heights, respectively, and E_o is the end-point energy. The three free parameters N_{end}, N_{zero} and normalization constant were determined by the chi-squares fitting of the statistical shape $pE(E-E_o)^2$ to the observed pulse-height spectrum. Typical examples of these fittings are shown in Fig. 17. The solid lines in Fig. 17 are the results of the best fitting. A typical ratio of the observed spectrum to the result of chi-squares fitting indicates the goodness of the fitting as shown in Fig. 18. The deviation in the high energy side comes from finite detector resolution and the one in the low energy side comes from finite detector resolution, β-ray scatterings and β-decay branches. The corrections due to these problems are discussed in the section (3)-c). In the case of transitions to the ground state (the first excited state) the energy ranges of 6~12 (3.5~7.5) and 7~14 (4~11) MeV were used for these fittings for ^{12}B and ^{12}N, respectively. As the results parameters used in the best fitting for these examples are summarized in Table I.

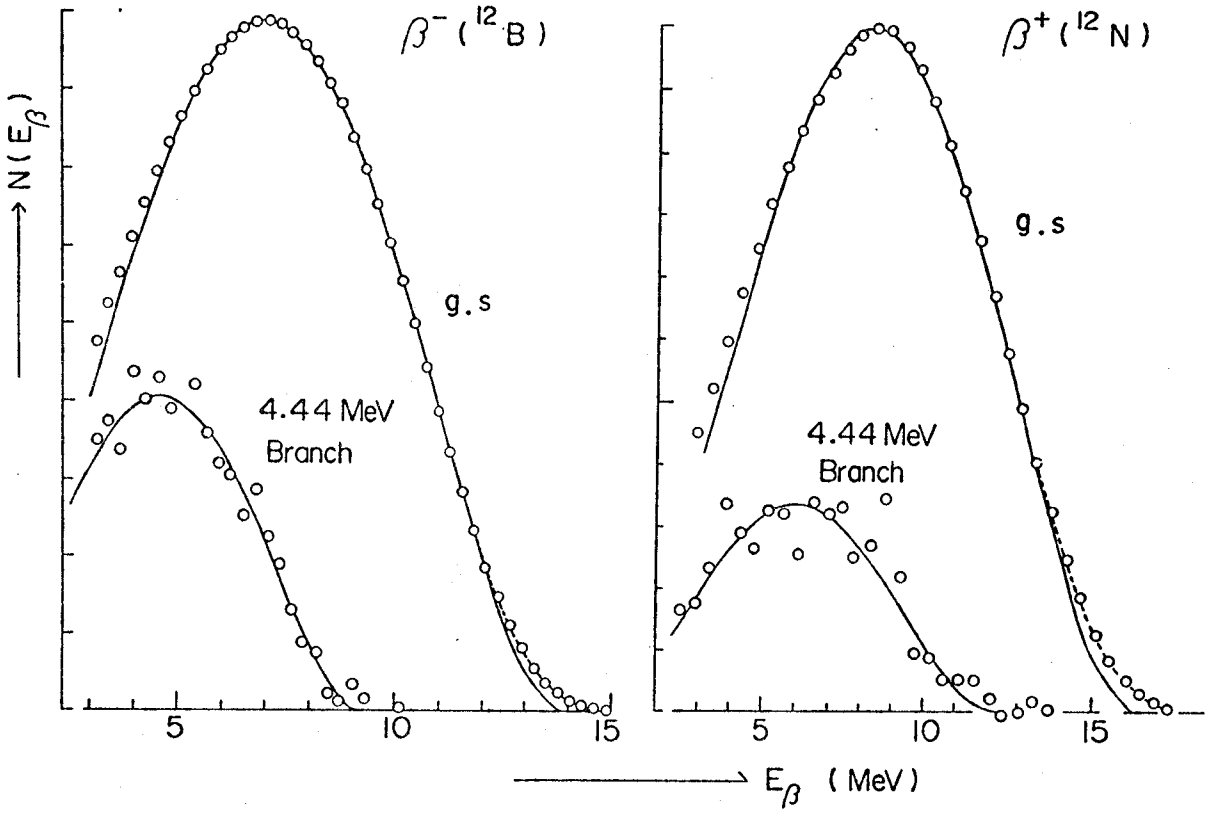

Fig. 17 β-ray-energy spectra in the β-decay branches of ^{12}B and ^{12}N. The end-point-pulse heights for the transitions to the ground and first excited states of ^{12}C were observed in order to confirm the energy scale of the pulse-height spectra. The solid lines are the results of the best fit of the theoretical spectral shape to the experimental shape. The broken lines are the results which include the effect of finite counter resolution. The uncertainties of the energy scales were determined to be ~4 % for the both spectra of ^{12}B and ^{12}N.

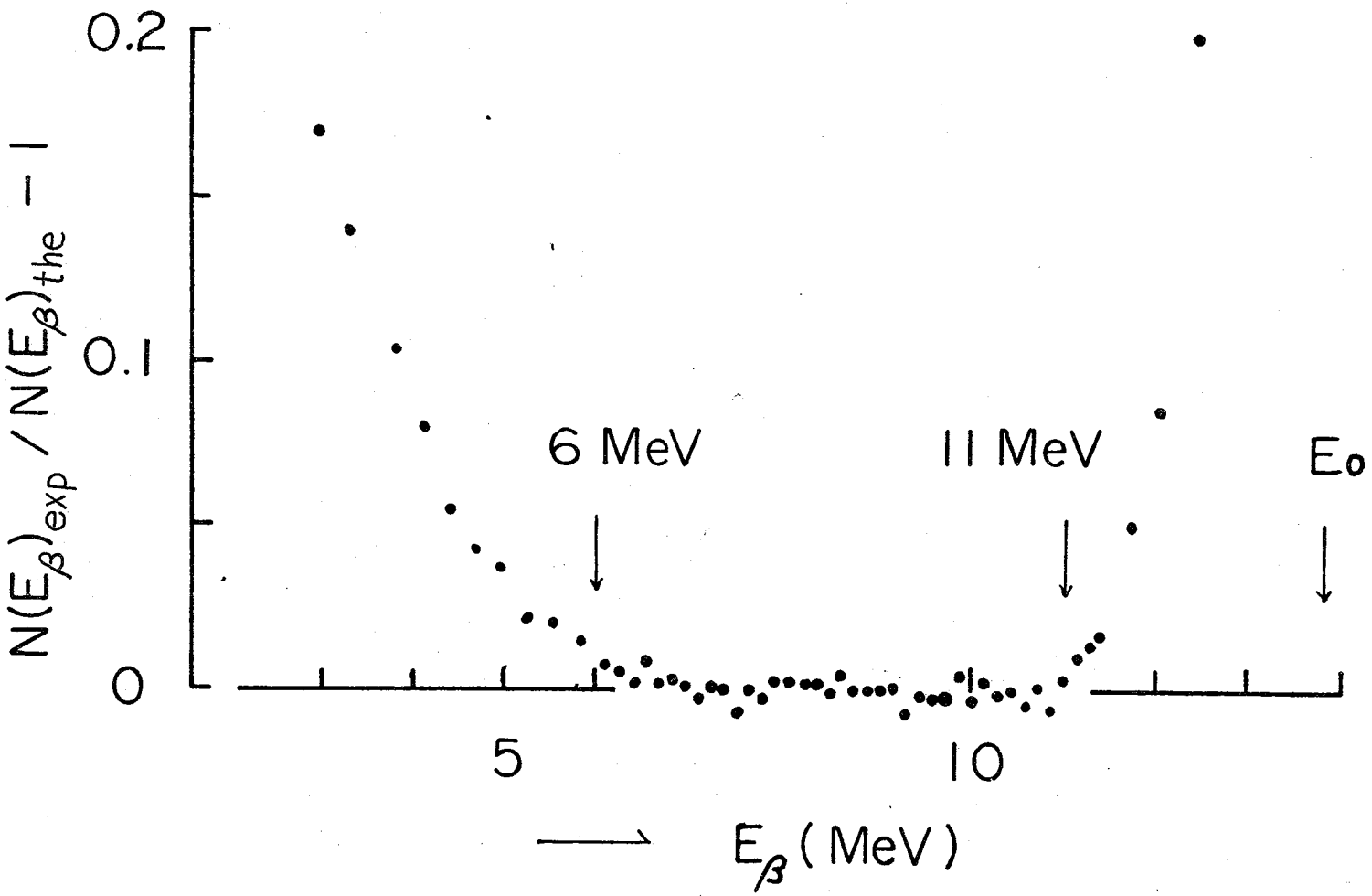

Fig. 18 Deviation of the observed pulse height spectrum from the theoretical one.

Table I. End-Point and Zero-Point Pulse Heights

	a) ^{12}B (β^-) g.s.	4.44 MeV branch
N_{zero}	-17.01 ± 0.06 channel	-17.72 ± 3.46 channel
N_{end}	82.44 ± 0.02	49.14 ± 1.48
		(50.6*)
	b) ^{12}N (β^+)	
N_{zero}	-7.55 ± 0.13	-7.47 ± 3.99
N_{end}	64.97 ± 0.03	46.48 ± 1.56
		(45.8*)

(* These values were predicted by use of the parameters obtained from the transition to the ground state.)

Zero-point channels and end-point channels for the transitions to the ground and first excited states were consistent within the fitting errors. The values of the end-point channels were more reliable than those of the zero-point channels because the effects due to the β-ray scatterings and the β-decay branches are small at higher energy side. Thus, the energy scale was tested by use of the end-point channels. The error of the energy scale (δ_{energy}) was determined as

$$\delta_{energy} = \frac{\sqrt{(\delta N_{end}(g.s))^2 + (\delta N_{end}(branch))^2}}{N_{end}(g.s.) - N_{end}(branch)} , \quad (53)$$

where $N_{end}(g.s.)$ and $N_{end}(branch)$ are the parameters for the transitions to the ground and first excited states, respectively. $\delta N_{end}(g.s.)$ and δN_{end} (branch) are the errors of relevant end-point energies. Thus the errors of the energy scale were

δ_{energy} = 4.3% for ^{12}B,

= 4.3% for ^{12}N.

Counter resolutions were determined for the positron and the negatron from the energy spectra, e.g., the region near the end-point channels of the pulse height spectra, assuming the response function $\theta(E_\beta)$ as,

$$\theta(E_\beta) = \frac{1}{\sqrt{2}} e^{-\frac{1}{2}\left(\frac{E-E_\beta}{\sigma}\right)^2}$$

$$\sigma = W\sqrt{E_\beta} \qquad (E : \beta\text{-ray energy})$$

where the end-point channels and zero-point channels were fixed. The results are also shown in Fig. 9. The resolutions were

$W=0.414\pm0.002\ (\mathrm{MeV})^{\frac{1}{2}}$ $(11<E<18\ \mathrm{MeV})$ for $^{12}N(\beta^+)$,

$W=0.296\pm0.001$ $(8<E<15.5\ \mathrm{MeV})$ for $^{12}B(\beta^-)$.

c) Corrections

The coefficients $\alpha_{\mp}$ obtained in the present experiment were less sensitive to the effects due to β-decay branches, β-ray scatterings and some other effects. Estimation of the corrections due to these disturbances was made with care. The summary of the corrections is given in this section.

(i) Effect of β-decay branches

The β-ray angular distributions[17] of relevant transitions are

$$W_0(\theta,E)=C\cdot f_0(E)\{1\mp P(p/E)(1+\alpha_{\mp}E)P_1(\cos\theta)+A\alpha_{\mp}EP_2(\cos\theta)\} \quad (60)$$

for the transitions to the ground state $(1^+ \to 0^+)$,

$$W_1(\theta,E)=C\cdot f_1(E)\{1\pm\tfrac{1}{2}P(p/E)(1+\alpha_{\mp}E)P_1(\cos\theta)+\tfrac{1}{10}A\alpha_{\mp}EP_2(\cos\theta)\} \quad (61)$$

for the transitions to the first excited state $(1^+ \to 2^+)$,

$$W_2(\theta,E)=C\cdot f_2(E)\{1\mp P(p/E)(1+\alpha_{\mp}E)P_1(\cos\theta)+A\alpha_{\mp}EP_2(\cos\theta)\} \quad (62)$$

for the transitions to the second excited state $(1^+ \to 0^+)$.

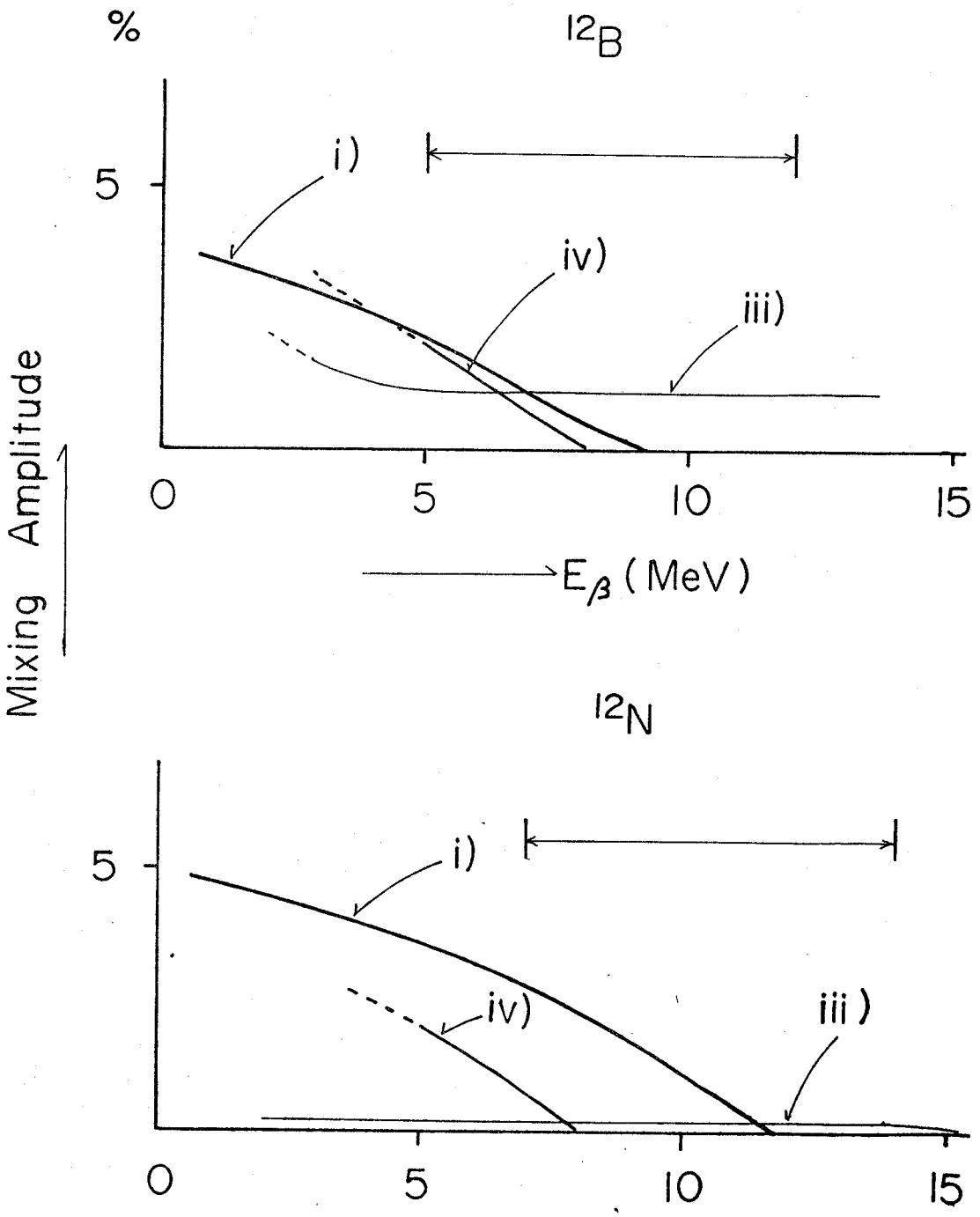

Fig. 19 Intensities (mixing amplitudes) of i) β rays in the branch to the first excited state ($0.9\varepsilon_1(E)$), iii) background β rays ($\omega_B(E)$) and iv) backscattering β rays relative to the β rays in the branch to the ground state. The energy regions indicated by arrows were used in the actual data analyses.

Here $f_0(E)$, $f_1(E)$ and $f_2(E)$ are the β-ray-energy spectra of the transitions to the ground, first and second excited states of ^{12}C. Those f_i's include the branching ratioes. The main disturbing contribution to the energy dependence of alignment and polarization terms comes from the mixing of β rays associated to the β-decay branches.

The angular distribution $W_{ob}(\theta,E)$, which is given from Eqs. (60), (61) and (62) as,

$$W_{ob}(\theta,E) \simeq C\, f_0(E)\ (1+\varepsilon_1(E)+\varepsilon_2(E)) \times\{1 \mp P(p/E)(1-\tfrac{3}{2}\varepsilon_1(E))(1+\alpha_{\mp}E)P_1(\cos\theta) + A(1-\tfrac{9}{10}\varepsilon_1(E))\alpha_{\mp}EP_2(\cos\theta)\}\ , \qquad (64)$$

is observed. Here $\varepsilon_1(E)$ and $\varepsilon_2(E)$ are the mixing amplitudes of β rays of the transitions to the excited states, which are defined as

$$\varepsilon_1(E) \equiv \frac{f_1(E)}{f_0(E)}\ , \quad \varepsilon_2(E) \equiv \frac{f_2(E)}{f_0(E)}\ . \qquad (65)$$

In order to obtain the coefficients $\alpha_{\mp}$, we must correct the effect due to the transition to the first excited state. The shape of the function $\varepsilon_1(E)$ is shown in Fig. 19. The amounts of $\varepsilon_1(E)$ for ^{12}B and ^{12}N are the same order of the nucleon-recoil terms $\alpha_{\mp}E$. As shown in Eq. (64), the effect due to the β-decay branch is small in the measurements of the alignment terms. The effect is enhanced in the measurements of the polarization terms.

The β-decay branches affect the up-down counting ratio, $W(\theta=0)/W(\theta=\pi)$, and so we must correct the value of the alignment accordingly, since it was determined from the polarizations P_I, P_{II} and P_{III}. The correction factor is defined as

$$A = C_{br}^{P}\ A_{obs} \qquad (66)$$

where C^{p}_{br} is the correction factor for this effect, A is the nuclear alignment and A_{obs} is the alignment determined from the polarizations P_{I}, P_{II} and P_{III}. The correction to the gradient of the alignment term as to the β-ray energy can be defined as

$$G = C^{a}_{br}\, G_{obs}\ , \qquad (67)$$

where C^{a}_{br} is the correction factor, G and G_{obs} are the ideal and observed gradients, respectively. The correction factor C_{br} to the coefficients $\alpha_{\mp}$ for the effect of a β-decay branch is obtained from the following relations.

$$G_{obs}/A_{obs} = (C^{p}_{br}/C^{a}_{br})\ (G/A), \qquad (68)$$

$$\alpha_{\mp} = C_{br}(\alpha_{\mp})_{obs}, \qquad (69)$$

$$C_{br} = C^{a}_{br}/C^{p}_{br}. \qquad (70)$$

This correction factor was calculated as

$$C_{br} = 0.995 \pm 0.001 \quad \text{for } {}^{12}B,$$

$$C_{br} = 0.981 \pm 0.003 \quad \text{for } {}^{12}N.$$

(ii) Effect of background β rays

We can not control the spin-ensemble of the recoil nuclei ^{12}B and ^{12}N which landed outside the recoil stopper. The effect due to the background β rays emitted from the outside of the recoil stopper can be treated as a mixing effect such as the one due to the β-decay branch. The mixing amplitude of the background β ray was examined by comparing the β-ray-energy sepctrum in the regular measurement, to the one observed without the recoil stopper (see Fig. 19b). In the actual condition almost all recoil nuclei were stopped in the recoil stopper, therefore, the mixing amplitude determined by the above method gives us the upper limit.

The correction factor C_B for the effect of background β rays was also defined in the same way as the case of (i). The amount of the C_B was

$$C_B = 0.989 \quad \text{for } {}^{12}B,$$
$$C_B = 0.998 \quad \text{for } {}^{12}N.$$

(iii) Effect of β-ray scattering

The β rays which were scattered by the chamber wall, electromagnet and the Mg sample, lose their initial information of the β-ray energy and the angular distribution considerably. The effect of the scattering on the measurements of the alignment terms might be the largest for the β rays which was backscattered by the wall and the Mg sample. The order of the magnitude of the backscattering was examined by comparing the β-ray-energy spectrum observed in the regular measurement to the one with far less backscattering source, e.g., chamber wall of lucite and recoil stopper of the thin Al foil whose thickness was 5μm. The result is shown in Fig. 19. The correction factor C_s estimated from this curve by the same method as described in the section (i) was

$$C_s = 0.998 \quad \text{for } {}^{12}B,$$
$$= 0.995 \quad \text{for } {}^{12}N.$$

This estimation was tested by the following method. The effects of the β-ray scatterings and the β-decay branches are large in the polarization terms as already mentioned. Thus the measurement of the energy dependence of the polarization terms, $\delta_{\pm}(E)$, was performed in the normalization cycle of the regular measurement in order to estimate the order of β-ray

scattering. The order of the difference of the energy dependence of $\delta_{\mp}(E)$ and the coefficients $\alpha_{\mp}$ was obtained from the curves in Fig. 19.

(iv) Effect of finite solid angle of β-ray counter telescope

The β ray was observed by the counters of finite size, which is described in the section IV-(1) c). The angular distribution near $\theta=0$ or $\theta=\pi$ was averaged in the solid angle of the counter telescope accordingly. This affects also both measurements of the polarization and the alignment terms. The correction factor for the finite solid angle can be determined in the same way as in the case of (i)

$$\alpha_{\mp} = C_{\Omega} \, (\alpha_{\mp})_{obs.} \qquad (72)$$

C_{Ω} was calculated as

$$C_{\Omega} = 1.04 \pm 0.01 \quad \text{for } {}^{12}B,$$
$$C_{\Omega} = 1.04 \pm 0.01 \quad \text{for } {}^{12}N.$$

The total correction C_t to the coefficients $\alpha_{\mp}$ was obtained from the product of the all correction factors mentioned in the above sections (i), (ii), (iii) and (iv) as

$$C_t = C_{br} \, C_B \, C_s \, C_{\Omega} = 1.02 \pm 0.01 \quad \text{for } {}^{12}B,$$
$$= 1.02 \pm 0.01 \quad \text{for } {}^{12}N.$$

The values of C_{br}, C_B, C_s, C_{Ω} and C_t were negligibly small compared with the statistical error of the coefficients $\alpha_{\mp}$. Therefore we did not make any correction on the $\alpha_{\mp}$, however included the $(C_t - 1)$ value into the uncertainties of final values of $\alpha_{\mp}$.

(4) Table of the experimental results

The present experimental results are summarized in Table III, IV and V. The relevant physical quantities of ^{12}B and ^{12}N are listed in Table II.

Table II. Decay Properties

	^{12}B	^{12}N
$T_{1/2}$ a)	20.41 ± 0.06 msec	10.97 ± 0.04 msec
Transition to the g.s.		
(I^{π}, T, T_z)	$(1^+,1,-1) \rightarrow (0^+,0,0)$	$(1^+,1,+1) \rightarrow (0^+,0,0)$
End-point energy (including rest mass)	13.88 MeV	16.83 MeV
Branching ratio(%)	97.13 ± 0.31%	94.45 ± 0.48%
Transition to		
the 4.44-MeV level(2^+)	1.29 ± 0.05%	2.10 ± 0.16%
the 7.65-MeV level(0^+)	1.5 ± 0.3 %	2.7 ± 0.4 %

a) F. Ajenberg-Selove, Nucl. Phys. A248 (1975) 1.

Table III. Production of the Polarized ^{12}B and ^{12}N

	^{12}B	^{12}N
Reaction	$^{12}B(d,p)^{12}B$	$^{10}B(^{3}He,n)^{12}N$
Energy of the incident particle	1.5 MeV	3.0 MeV
Beam current	5 μA	10 μA
Recoil angle (θ_r)	40 ~ 75°	25 ~ 45°
P_o (initial polarization)	11.05 ± 0.03 %	20.04 ± 0.13 %
A_o (initial alignment)	~+6%	~+6%

Table IV. Spin-Ensemble Control

	^{12}B	^{12}N
$A^+ - A^-$ (average)	26.7 ± 0.3 %	57.8 ± 0.4 %
$P^+_{II} - P^-_{II}$ (average)	0.61 ± 0.03 %	0.01 ± 0.16 %
Spin-lattice relaxation time		
for A	35.5 ± 0.8 msec	62.2 ± 6.4 msec
for P	100.1 ± 0.2 msec	267 ± 4 msec
Degree of achievement		
η_{DQ} (D.Q.T)	0.954 ± 0.004	0.958 ± 0.006
η^- (S.Q.T)	0.955 ± 0.008	0.963 ± 0.013
η^+	0.957 ± 0.007	0.960 ± 0.014
Magnetic moment μ [b] (n.m)	+1.003 ± 0.001	+0.4571 ± 0.0005
Sign of egQ in Mg	negative	negative
Crystal orientation of Mg (c-axis as to H_0)	0°	90°

b) K. Sugimoto, K. Nakai, K. Matsuda and T. Minamisono, J. Phys. Soc. Japan 25 (1968) 1258.

Table V. Coefficients $\alpha_{\pm}$ (%/MeV)

	α_- (^{12}B)	α_+ (^{12}N)
Run I*	+0.025 ± 0.034	-0.277 ± 0.048
Run II*	-0.001 ± 0.021	-0.267 ± 0.056
Average*	+0.006 ± 0.018	-0.273 ± 0.037
Result	+0.006 ± 0.018	-0.273 ± 0.041
Uncertainties		
energy scale (4.3%)	0.0003	0.012
β-decay branch correction	0.0001	0.006
β-scattering	0.0001	0.002
background	0.0001	0.001
solid angle	0.0003	0.011
counting statistics	0.018	0.037
Total	0.018	0.041

* Uncertainties are due to counting statistics only.

V. Result and Discussion

The coefficients α_- and α_+ for ^{12}B and ^{12}N were determined in the present experiment as

$$\alpha_-(\text{exp}) = +(0.006 \pm 0.018) \quad \%/\text{MeV},$$

$$\alpha_+(\text{exp}) = -(0.273 \pm 0.041) \quad \%/\text{MeV}.$$

The present results, $\alpha_-(\text{exp})$ and $\alpha_+(\text{exp})$, are consistent with the theoretical values given by M. Morita et al.[43] without SCC,

$$\alpha_-(\text{theory}) = +(0.001 \pm 0.003) \quad \%/\text{MeV},$$

$$\alpha_+(\text{theory}) = -(0.269 \pm 0.006) \quad \%/\text{MeV}.$$

(1) The difference, $(\alpha_- - \alpha_+)$, and second class current

The difference, $(\alpha_- - \alpha_+)$, gives us the information on the second class induced tensor term in a nuclear model independent way.

Experimental and theoretical values for the difference, $(\alpha_- - \alpha_+)$, are

$$(\alpha_- - \alpha_+)_{\text{exp}} = +(0.279 \pm 0.045) \ \%/\text{MeV},$$

$$(\alpha_- - \alpha_+)_{\text{theory}} = +(0.270 \pm 0.007) \ \%/\text{MeV}.$$

The theoretical value was obtained in the impulse approximation without SCC. So this agreement is consistent with no appreciable amount of SCC, and with small effects of the off-mass-shell effect and the exchange current. The nuclear form factor for SCC was obtained in the nuclear model independent way, namely elementary particle treatment as,

$$F_T^{(2)}/F_A^{(1)} = -(0.03 \pm 0.06) \ \%/\text{MeV},$$

using the experimental result of the weak magnetism form factor

given by Wu et al.[12],

$$F_M/F_A^{(1)} = (0.18 \pm 0.05)\ \%/\mathrm{MeV}.$$

The fundamental coupling constant for SCC can be determined from the present $(\alpha_- - \alpha_+)$ as

$$f_T = -(0.21 \pm 0.63)\ f_A/2M,$$

assuming the impulse approximation and using the following weak magnetism of a free nucleon,

$$f_W = -3.7\ f_V/2M. \qquad (73)$$

Thus we can conclude that there is no appreciable G-parity irregular SCC in the nuclear β decay.

Allowing no SCC, the present $(\alpha_- - \alpha_+)$ can be directly compared with the results of CVC test in A = 12 system. They are the coefficients $a_\mp$ in the spectral shape factor[12),13)] and the gamma width Γ_γ[44)] of $^{12}C^*$ $(T=1,\ T_z=0,\ I=1^+)$. These three values are related to the value of "a" as follows,

$$\alpha_- - \alpha_+ = \frac{4}{3}\, a\,, \qquad (74)$$

$$a_- - a_+ = \frac{16}{3}\, a^*, \qquad (75)$$

$$\Gamma_\gamma = \frac{4}{3\times 137}\, E_\gamma^3\, \frac{ft(0^+ \to 0^+)}{ft}\, a^2. \qquad (76)$$

Here E_γ is γ-ray energy, ft is ft-values of the β decay of ^{12}B or ^{12}N[45)], ft $(0^+ \to 0^+)$ is ft-value of the $0^+ \to 0^+$ transition[46)] (pure Fermi transition) and $\Gamma_\gamma = 37.0 \pm 1.0$ MeV[47)].

---

* In extracting the value of "a" from the spectral shape factor the Coulmb correction was made[12)].

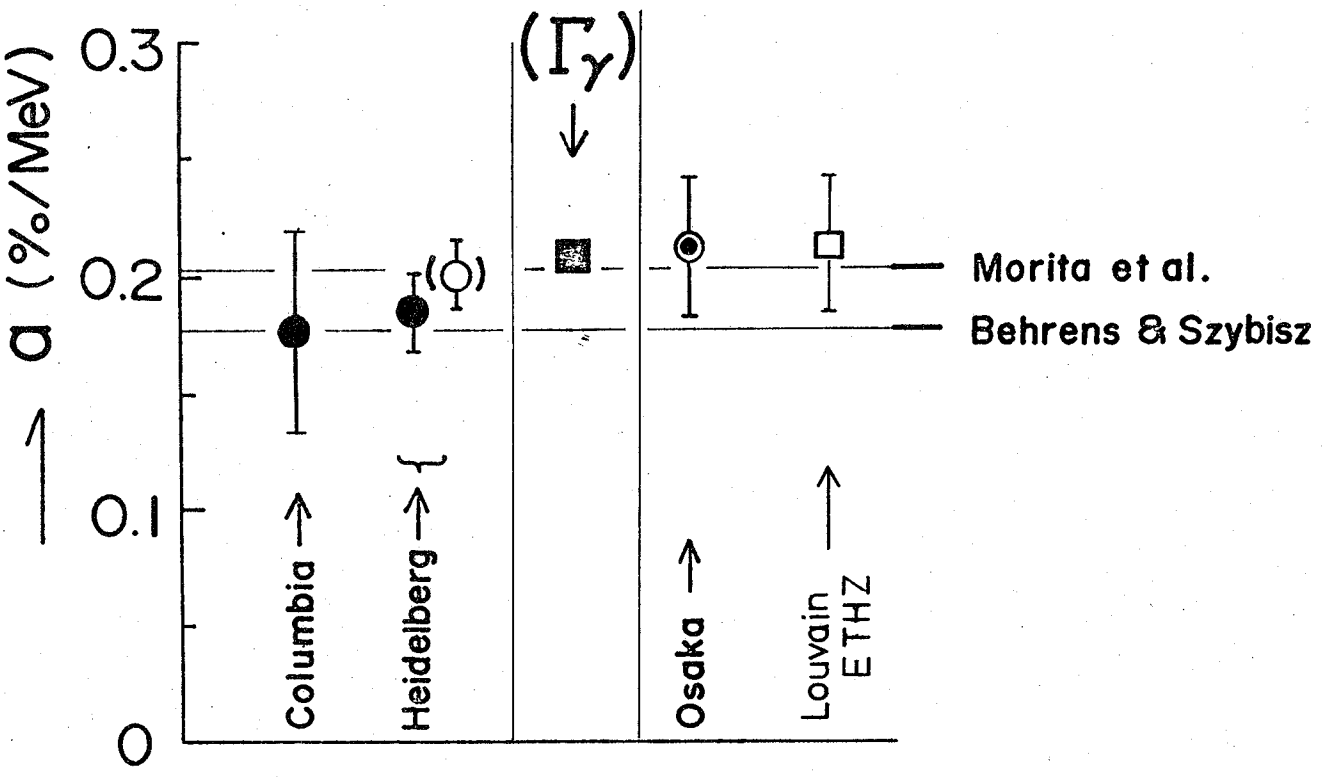

Fig. 20 Comparison of the present result with data for CVC test in A = 12 system referring to the quantity $a = g_W/g_A$; $a = -\frac{\mu+1}{2M} f_V/f_A \simeq 0.2$ %/MeV for the free nucleon. The closed circles represent the values extracted from the spectral shape-factor by the Columbia group[12] and by the Heidelberg group[13], the open circle is the value from linear E fittings, the closed square is from the analogue M1 γ transition[47], the double circle is from the present result and open square is from the $(\alpha_- - \alpha_+)$ by Lonvain and ETHZ groups[48]. Two recent theoretical prediction by M. Morita et al.[15] and H. Behrens and L. Szybisz are[49] also shown.

where "a" is expressed with form factors as

$$a = g_w/g_A$$
$$= -\frac{\mu+1}{2M} \quad (f_V/f_A) (\simeq 0.2 \text{ \%/MeV for a free uncleon}).$$

The "a" values obtained from these three experiments are shown in Fig. 20. The mutual agreement in the various "a" values is fairly good. Thus the present result is consistent with the prediction of the CVC theory and with absence of SCC.

(2) The sum, $(\alpha_- + \alpha_+)$, and meson-exchange current

The meson-exchange effect in the axial vector current can be investigated from the time component.
We extracted the time component from the sum, $(\alpha_- + \alpha_+)$, in the A = 12 system. The present result, $(\alpha_- + \alpha_+)_{exp} = -(0.267 \pm 0.044)$ %/MeV, is consistent with the theoretical prediction, $(\alpha_- + \alpha_+)_{theory} = -(0.268 \pm 0.007)$ %/MeV, given by M. Motita et al.[43] assuming no meson-exchange effects with the nuclear model of Cohen-Kurath[16]. This fact suggests that meson-exchange effect is small.

(3) Other topics in the mass-12 system

Experiments in the A=12 system were reported by the Louvain and ETHZ groups[48] using $A \simeq \frac{3}{4} P_0$ and $P \simeq \frac{3}{4} P_0$, which were produced by only population equalization by use of NMR or level crossing technique[50]. Their results agreed with our results, however, their analyses have an ambiguity in the treatment of the intensity difference of ^{12}B or ^{12}N between the positive and negative alignment cycles. In order to extract the coefficients

$A\alpha_{\mp}$ as a function of E purely from the ratio,

$(W(\theta,A^{+},P^{+})-W(\theta,A^{-},P^{-}))/(W(\theta,A^{+},P^{+})+W(\theta,A^{-},P^{-}))$,

we need a precise production monitor which is independent of the nuclear alignment and the polarization. For example, if we use the β-ray energy spectra for this purpose the term $A\alpha_{\mp}\bar{E}$ and $P\alpha_{\mp}\bar{E}$ remain in the above ratio. Here $\bar{E}$ is the center of gravity for the energy region used for the production monitor. Although the reliability of the monitor and the dependence on the relevant alignment and polarization have a crucial role in the determination of the coefficients $\alpha_{\mp}$ from the above ratio, the details of the monitor are not discussed in their report at all. Thus we used only our $\alpha_{\mp}$ values in our discussions on SCC and the time component.

VI. Summary

The nuclear alignments, $A(^{12}B) \simeq \pm 0.14$ and $A(^{12}N) \simeq \pm 0.29$, were produced with negligibly small polarizations for the experiment by which we obtained reliable values of $\alpha_{\mp}$ to draw a definite conclusion on SCC problem in the A=12 system. The coefficients α_- and α_+ were determined from the alignment terms. The present results of α_- and α_+ were insensitive to the effects due to the β-decay branches and the β-ray scatterings. The amount of the correction for the effects was less than $\sim 5\%$ of the $\alpha_{\mp}$ value.

The difference, $(\alpha_- - \alpha_+)$, provided us a clear conclusion on SCC, e.g., the present $(\alpha_- - \alpha_+)$ was consistent with no appreciable second class induced tensor term and was consistent with the CVC theory. The effect due to the isospin symmetry breaking by the Coulomb interaction on $(\alpha_- - \alpha_+)$ was neglected in the above discussion, however, the amount of the effect was estimated to be about 10% of the $(\alpha_- - \alpha_+)$, but not more than that[15].

The sum, $(\alpha_- + \alpha_+)$, which singles out the time component of the axial vector current, gives us information of the meson-exchange current. The present $(\alpha_- + \alpha_+)$ was consistent with the prediction of the impulse approximation using the Cohen-Kurath-type nuclear wave function. It suggests a rather small effect of the meson-exchange currents in this particular nuclear system.

Acknowledgement

I wish to extend my thanks to all those who have helped to make this work fruitful:

Professor K. Sugimoto for his proposal of the present experiment, earnest guidance in this work, and for discussing this thesis.

Dr. T. Minamisono for his constant collaboration, discussion of idea and results, and for reading and discussing this thesis.

Dr. Y. Nojiri for his constant collaboration, discussion, and encouragement.

Dr. I. Tanihata for his collaboration in the early stage of the present work.

Professor M. Morita for his illuminating discussions on the theory of β decay, and for reding this thesis.

Professor H. Ohtsubo for his illuminating discussions on the theory of beta decay.

Professor S. Yamabe, the Director of the Research Center for Nuclear Physics (Osaka University) for his kind offer of the computer TOSBAC 5600 to the present data analyses, and for reading this thesis.

Professor H. Ejiri for his encouragement, and for reading this thesis.

Professor I. Miura for his encouragement, and for reading this thesis.

Mr. Y. Takahashi for his technical support in the present experiment.

Appendix

A-1. NMR Technique: Dynamic conversion of a polarization to an alignment

We can produce a nuclear alignment from a polarization by interchanging magnetic substate populations.[14] This method is explained in the following sections.

(1) Electric quadrupole interaction in a strong magnetic field

Because of the presence of an electric field gradient(q) which was superimposed to the static magnetic field, the energy gaps between relevant magnetic substates are different with each other. This difference enables us to interchange the magnetic substate populations by inducing selective rf transitions (NMR). We used the internal-electric-field gradient of a Mg single crystal for the present purpose. The direction of q was set parallel to the static magnetic field for the ^{12}B experiment and was set perpendicular for the ^{12}N experiment. The Hamiltonian for this electromagnetic field is given as

$$H = H_M + H_Q \ . \qquad \text{(A-1)}$$

Here

$$H_M = -\gamma\hbar H_o I_z \ , \qquad \text{(A-2)}$$

$$H_Q = \frac{eqQ}{4I(2I-1)} \left[\frac{1}{2}(3\cos^2\theta-1)(3I_z^2-I(I+1))+ \right.$$
$$\left. (\frac{3}{2}\sin\theta\cos\theta)\ \{I_z(I_+ + I_-)+(I_+ + I_-)I_z\}+\frac{3}{4}\sin^2\theta(I_+^2+I_-^2)\right] . \qquad \text{(A-3)}$$

Here

H_o is the strong magnetic field,

γ is the nuclear gyromagnetic ratio,

q is the field gradient,

Q is the nuclear electric quadrupole moment,

θ is the polar angle between H_o and q

and I is the nuclear spin.

Here the field gradient is assumed to be axially symmetric. If the condition, $\mu H_o >> eqQ$, is satisfied, then the first order perturbation theory gives the energy of the magnetic substate for $I_z=m$ as

$$E_m = -m\hbar\omega_L + \frac{\hbar\omega_Q}{12}\{ 3m^2 - I(I+1)\} (3\cos^2\theta - 1). \quad \text{(A-4)}$$

Here

$$\omega_Q = 3eqQ/2I(2I-1)\hbar \quad \text{and} \quad \text{(A-5)}$$

$$\omega_L = \gamma H_o. \quad \text{(A-6)}$$

The energy level is schematically shown in Fig. 21 for $^{12}B(\theta=0)$ and $^{12}N(\theta=\frac{\pi}{2})$ with $eqQ<0$ and $\gamma>0$.

For simplicity, we define the two transition frequencies as ν_H for high frequency and ν_L for low frequency.

(2) Interaction of nuclear spin with rf

Here we discuss the motion of a nuclear spin interacting with an rf magnetic field. If the frequency of rf satisfy the relation, $\omega_0=(E_a-E_b)/\hbar$, where E_a and E_b are the energies of the substates a and b, then we can neglect the presence of other levels in good approximation if $|\omega'-\omega_0|/D>>1$, where 2D is FWHM of the resonance spectrum for NMR and ω' is for other resonance. In the adiabatic fast passage (AFP), the frequency of rf is swept across the resonance ω_0, and approaches the neighbouring resonance ω'. We can, however, suppress the effect of the neighbouring resonance by modulating the amplitude sinusoidally as a function of time. Therefore, the motion of nuclear spin can be treated as a two-level system.

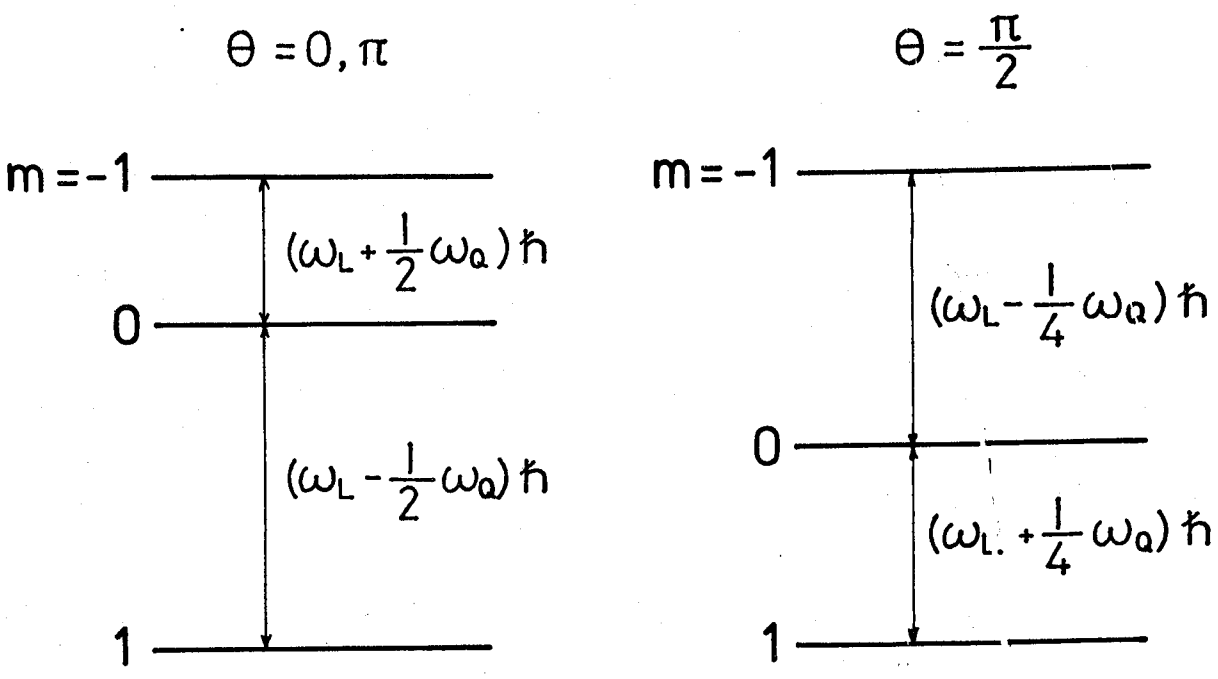

Fig. 21 Energy levels of magnetic substates of $^{12}B(\theta=0)$ and $^{12}N(\theta=\frac{\pi}{2})$ in Mg.

In the two-level system an arbitraly operator $\mathbb{L}$ can be expressed as $\mathbb{L}=\frac{1}{2}\ell_0 + \boldsymbol{\ell}\cdot\mathbb{S}$, using Pauli spin matrix, where $\ell_0=\mathrm{tr}\{\mathbb{L}\}$, $\mathbb{S}=\frac{1}{2}\sigma$ and σ is Pauli spin matrix. The total Hamiltonian,

$$\begin{aligned}\mathcal{H} = -\gamma\hbar H_o I_z + \frac{eqQ}{4I(2I-1)} &[\frac{1}{2}(3\cos^2\theta-1)(3I_z^2-I(I+1)) \\ &+\frac{3}{2}\sin\theta\cos\theta\{I_z(I_+ + I_-)+(I_+ + I_-)I_z\} \\ &+\frac{3}{2}\sin^2\theta(I_+^2+I_-^2)] \\ &-\gamma\hbar H_1\cdot I, \qquad \text{(A-7)}\end{aligned}$$

can be transformed as

$$\mathcal{H} = \frac{1}{2}E_o - \gamma'\hbar(\mathbf{H}'\cdot\mathbb{S}). \qquad \text{(A-8)}$$

Here E_0, γ' and $\mathbf{H}'$ can be determined from the matrix element. $\mathbf{H}'$ and γ' are the virtual magnetic field and gyromagnetic ratio. In our system these parameters are

$$E_o = \gamma\hbar H_o + \frac{eqQ}{4I(2I-1)}(3\cos^2\theta-1)\{\frac{3}{2}-I(I+1)\}, \qquad \text{(A-9)}$$

$$\mathbf{H}' = \mathbf{H}_o' + \mathbf{H}_1', \qquad \text{(A-10)}$$

$$H_{ox}' = H_{oy}' = 0, \qquad \text{(A-11)}$$

$$H_{oz}' = H_o + \frac{1}{\gamma\hbar}\frac{eqQ}{4I(2I-1)}\frac{3}{2}(3\cos^2\theta-1), \qquad \text{(A-12)}$$

$$\mathbf{H}_1' = \sqrt{I(I-1)}\mathbf{H}_1, \qquad \text{(A-13)}$$

$$\gamma' = \gamma. \qquad \text{(A-14)}$$

The density matrix ρ of this two-level system can also be expressed as $\rho = \frac{1}{2} + \mathbf{m}\cdot\mathbb{S}$. The equation of motion for the nuclear spin is given as

$$\hbar/i\,(d\rho/dt) = -[\mathcal{H},\rho]. \qquad \text{(A-15)}$$

From above two Eqs. (A-8) and (A-15), it turns out to be

$$\frac{d\mathbf{m}}{dt} = \gamma\mathbf{m}\times\mathbf{H}'. \qquad \text{(A-16)}$$

This equation is the same as the classical equation of motion for the magnetic moment $\mathbf{m}$ in the magnetic field $\mathbf{H}'$. Thus the motion of nuclear spin can be explained classically.

(3) Adiabatic fast passage

If we sweep the frequency of the rf field across a resonance $\omega_0=(E_m-E_{m'})/\hbar$ with an adequate sweep velocity, then the populations in the magnetic substates, a_m and $a_{m'}$, can be interchanged.

In the rotating coordinate system whose rotation frequency and direction are the same as the one of the rf field and the one of the static field, respectively, the magnetic moment precesses around the effective field $\mathbf{H}_{eff}$,

$$\mathbf{H}_{eff} = \mathbf{k}(H_0 - \frac{\omega}{\gamma}) + \mathbf{i}H_1. \qquad \text{(A-17)}$$

Here

$\mathbf{k}$ is the unit vector of z-axis,

$\mathbf{i}$ is the unit vector of x-axis

in the rotating frame and

ω is the frequency of the rf field.

The effective field $\mathbf{H}_{eff}$ turns around as the rf frequency is swept across the resonance frequency ($\omega_0=\gamma H_0$). The nuclear spin follows the effective field, if the angular velocity is slow enough compared with the Larmor frequency γH_{eff}. This condition is most severe at the resonance frequency ω_0, and is expressed as

$$\frac{1}{\gamma H_1}\frac{d\omega}{dt} << \gamma H_1 \qquad \text{(A-18)}$$

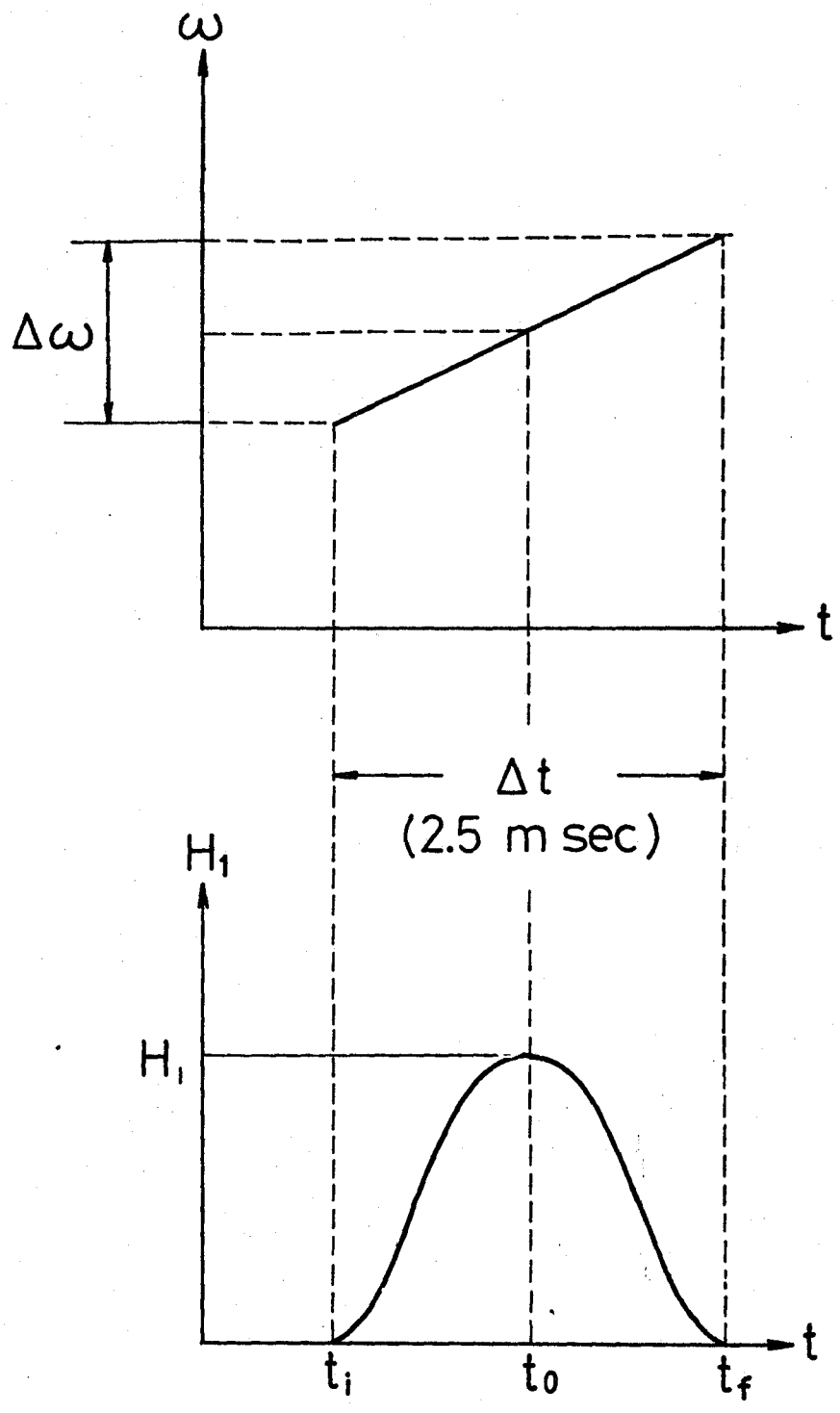

Fig. 22 Frequency and amplitude modulation of rf.

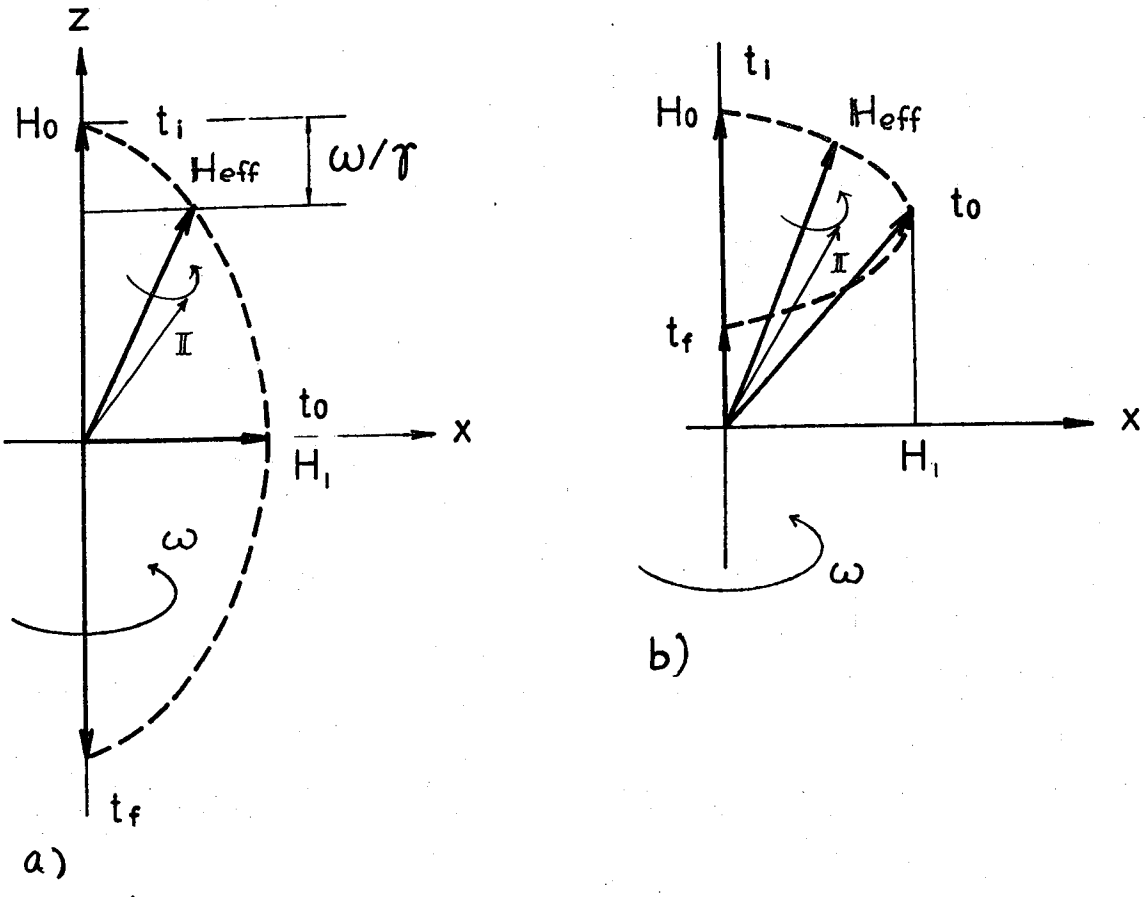

Fig. 23 Effective magnetic field as a function of rf sweep The direction of an effective field in a rotating frame with the angular velocity of ω is inverted as the frequency is swept across a resonance frequency ω_0. As the result, the nuclear spin follows H_{eff} if the adiabatic condition is satisfied, and is simultaneously inverted. The direction of the effective field is recovered to the initial direction after the rf modulation when the sweep does not cover the resonance frequency.

In the actual experiment the rf amplitude was also modulated sinusoidally as a function of time as shown in Fig. 22. The motion of effective field direction is explained schematically in Fig. 23.

If the frequency modulation passes the resonance frequency, the effective field is inverted as Fig. 23a, and the nuclear spin is also inverted as far as the adiabatic condition (A-18) is satisfied. When the frequency modulation does not cover the resonance, then the field direction is not changed after the frequency modulation as shown in Fig. 23b and the direction of nuclear spin which follows H_{eff} is also preserved. The effective field is the smallest at the resonance, namely H_1, then the nuclear spin can be easily perturbed by the field of environment such as nuclear dipole field. The amount of H_1 to hold the nuclear spin to the direction of H_{eff} was empillically known as $\gamma H_1 > 2\pi D$, where 2D is FWHM of resonance curve for NMR spectrum.

The actual conditions for the rf were as follows:

Duration of rf = 2.5ms.

Modulation width = ~20kHz.

rf amplitude = ~7 Gauss for the transition($m=0 \rightarrow m=\pm 1$),

= ~20 Gauss for the transition($m=1 \rightarrow m=-1$).

(4) Equalization method

When the rf is on resonance, the nuclear spin precesses around H_1 with the frequency of γH_1 as the nuclear spin is observed in the rotating frame. Generally the precession frequency is distributed around γH_1 because of the existence of the dipolar field and inhomogeneities of H_1 and H_0. After the time which satisfies the inequality $\gamma H_1 t > 1$, the transverse polarization P_z vanishes by the phase dispersion of this Larmor precession. In the actual experiment we need to modulate the rf frequencies repeatedly to cover the resonance width due to the inhomogeneity of H_o and the dipolar field in order to destroy the polarization completely. Here, this modulation speed need not to satisfy the adiabatic condition.

The typical rf field conditions were as follows:

Duration of rf = 2.5ms.

Modulation width = ~13kHz.

Modulation repetition = ~6 times.

rf amplitude = ~7 Gauss.

We can also equalize the magnetic substate populations by the AFP technique. If the frequency modulation stops at the resonance frequency, the nuclear spins which follow the effective field are left at the transverse position, and the z component of the polarization vanishes.

(5) rf coil and electromagnet

The homogeneities of the static magnetic field and the amplitude of the rf field are essential to control successfully the spin ensemble by use of the NMR.

The NMR spectra of ^{12}B and ^{12}N in a Mg single crystal in a strong magnetic field were observed previously in our group.[7] The results are shown in Fig. 24. In this experiment the rf frequencies were about 1MHz. The width of the resonance curve must be narrow enough to induce selective rf transitions: They are two single quantum transitions with $\nu=\nu_L$ and ν_H, and one double-quantum transition with $\nu = \frac{1}{2}(\nu_L+\nu_H)$. The inhomogeneity of our static magnetic field was less than 1% in the effective area of the recoil stopper. As the rf frequency was about 1MHz, therefore the width from this inhomogeneity was about 10kHz. This condition was narrow enough to achieve AFP. The map of the field strength together with the pole piece of the electromagnet is shown in Fig. 25.

We developped a new type of rf coil whose shape is shown in Fig. 2 to insert the rf coil into the chamber of rotating target and to produce a relatively strong and homogeneious H_1.

The homogeneity of H_1 in this coil was ~10%. The inductance was 33 μH (70 μH) for ^{12}B (^{12}N), and H_1 field of ~30 Gauss was easily produced. The rf magnetic field of ~20 Gauss was enough for DQT, and the field of ~7 Gauss was enough for SQT.

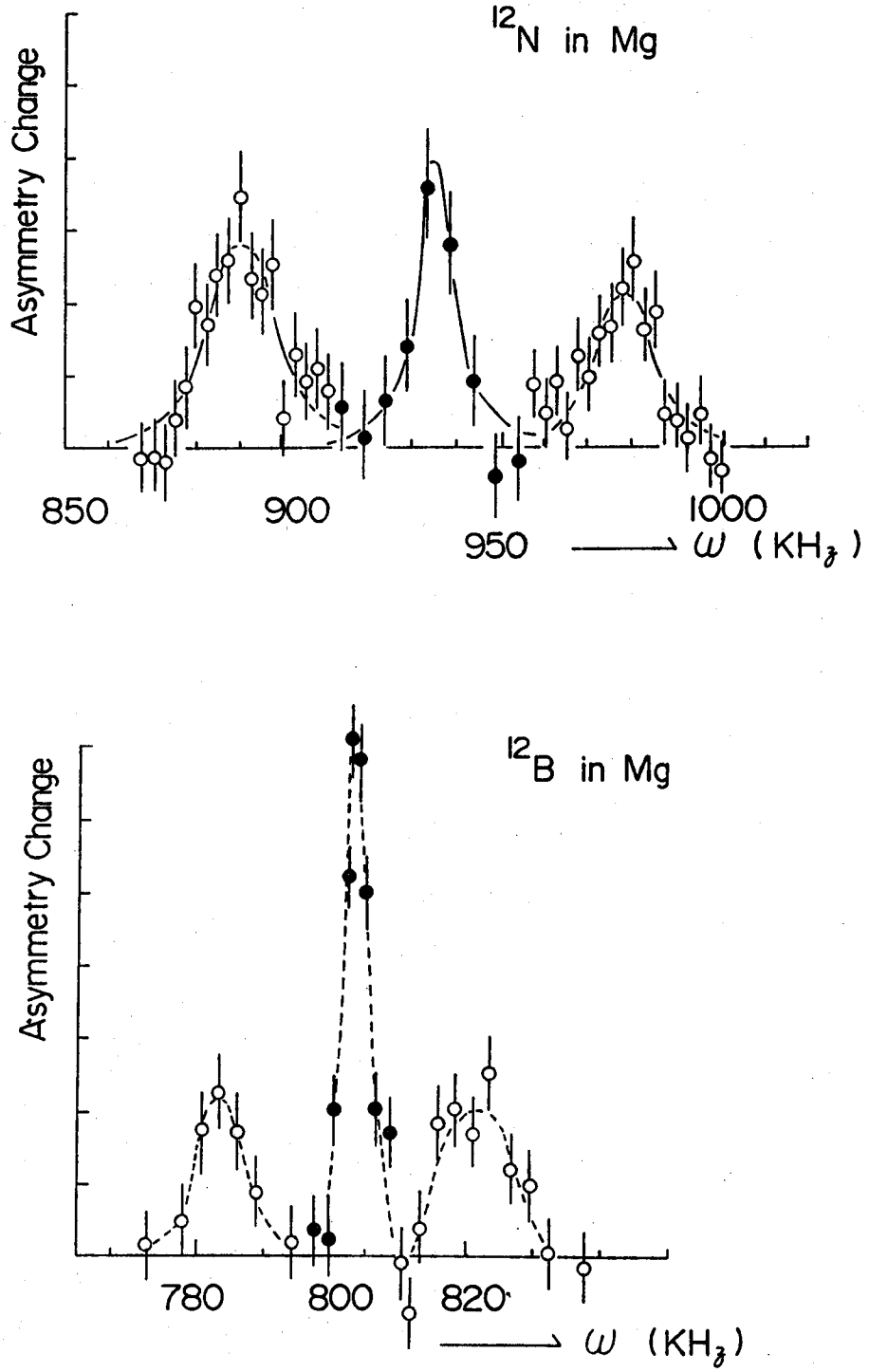

Fig. 24 NMR spectra of ^{12}B and ^{12}N in Mg. The closed circles for ^{12}B are the resonance spectra for DQT, and the open circles are the one for SQT. The closed and open circles for ^{12}N are the resonance spectra for SQT at $\theta=54.7°$ and $\theta=0°$, respectively.

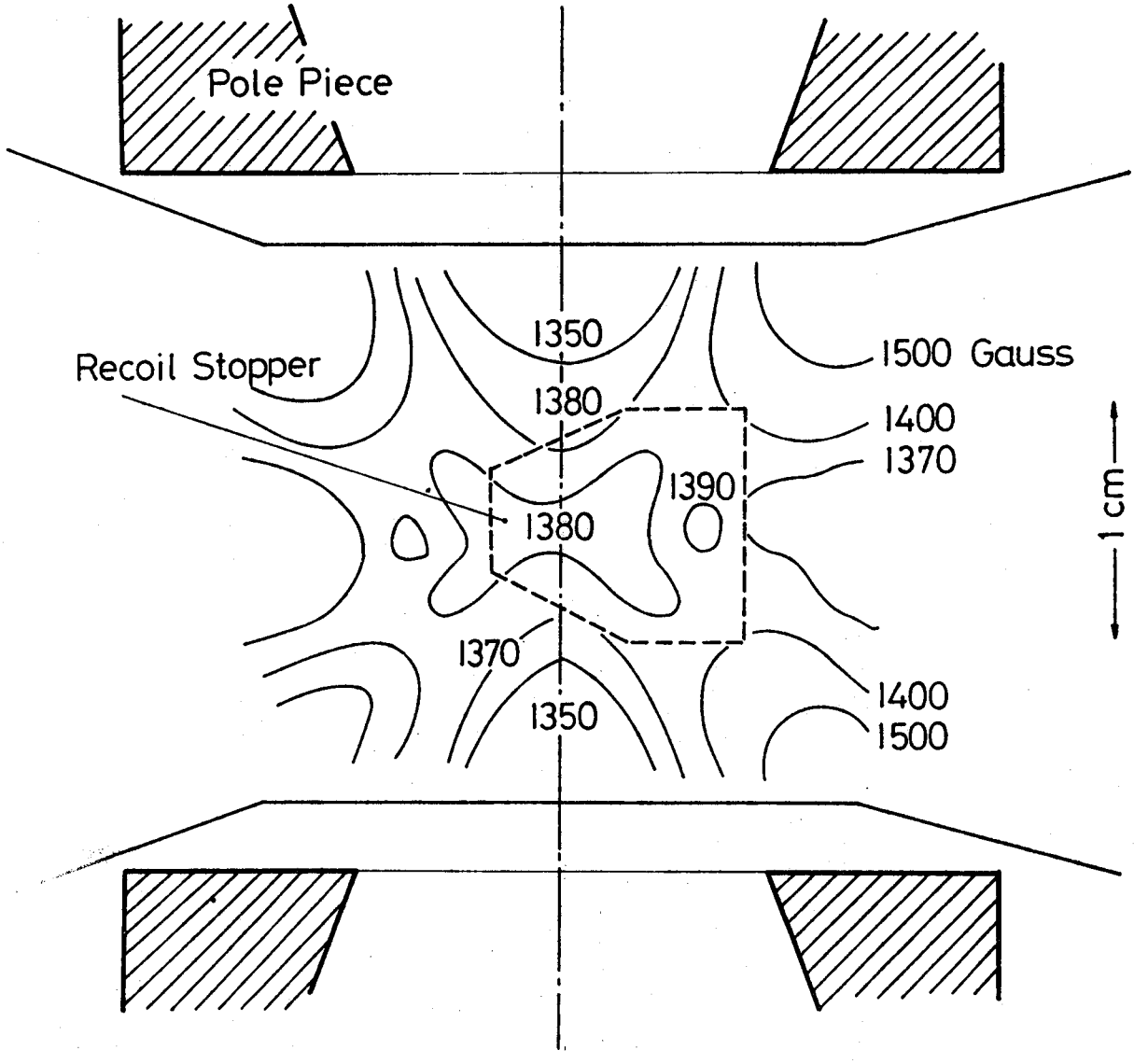

Fig. 25 Distribution of the static magnetic field. The homogeneity of H_o was better than 1 % in the effective area where the recoil stopper was placed.

A-II. Nuclear alignment converted from the polarization

(1) Amounts of the polarization and the alignment

The β-ray angular distribution from polarized nuclei can be expressed as the following equation neglecting higher order terms.

$$W(\theta) = 1 + AP\cos\theta . \qquad \text{(A-19)}$$

Here A is the asymmetry parameter, which is +1(-1) for $^{12}N(^{12}B)$ decay. In this experiment we observed up-down counting ratio, $W(0)/W(\pi)$, from the two counter telescopes set at $\theta=0$ and $\theta=\pi$ in order to measure the polarization and to deduce the alignment.

The ratio is expressed as

$$\frac{W(0)}{W(\pi)} = \frac{C(1+AP)}{C(1-AP)} \frac{\varepsilon_0}{\varepsilon_\pi} = \frac{1+AP}{1-AP} \frac{\varepsilon_0}{\varepsilon_\pi} , \qquad \text{(A-20)}$$

where C is proportional to the production rate, and ε_0 and ε_π are the efficiencies of the counters at $\theta=0$ and $\theta=\pi$, respectively. For the polarization $-P$ reversed by AFP the ratio is expressed as

$$\left(\frac{W(0)}{W(\pi)}\right)^R = \frac{1-AP}{1+AP} \frac{\varepsilon_0}{\varepsilon_\pi} . \qquad \text{(A-21)}$$

We can obtain the efficiency ratio $\varepsilon_0/\varepsilon_\pi$ from Eqs. (A-20) and (A-21) as

$$\varepsilon_0/\varepsilon_\pi = \sqrt{W(0)/W(\pi)) \times (W(0)/W(\pi))^R} . \qquad \text{(A-22)}$$

If we know the efficiency ratio, then we can obtain the polarization from the equation (A-20),

$$A P = \frac{y - 1}{y + 1} ,$$

$$y = \frac{W(0)/W(\pi)}{\varepsilon_0/\varepsilon_\pi} . \qquad \text{(A-23)}$$

The amount of the alignment can be determined from the polarizations P_I, P_{II} and P_{III} and the degree of achievement for NMR technique. The magnetic substate populations for counting sections I and II are schematically shown in Fig. 26. In the counting section I, $a_1 \cong a_o$ was achieved by the preceding equalization rf.

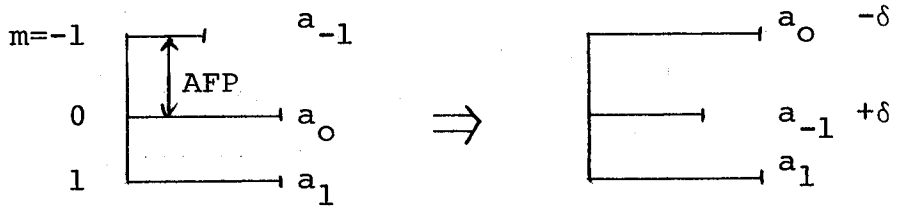

Fig. 26 Control of the substate populations in the main routine.

The polarizations P_I and P_{II} can be expressed using these populations a_m's as,

$$P_I = a_1 - a_{-1} , \qquad \text{(A-24)}$$

$$P_{II} = a_1 - a_o + \delta . \qquad \text{(A-25)}$$

Here δ is defined using the degree of achievement η for AFP for single quantum transition as

$$\delta \equiv (1 - \eta)(a_o - a_{-1}), \qquad \text{(A-26)}$$

where a_m's are normalized as,

$$1 = a_1 + a_o + a_{-1} . \qquad \text{(A-27)}$$

From Eqs. (A-24), (A-25) and (A-27) the alignment value is obtained as,

$$P = 1 - 3(a_{-1} + \delta)$$

$$= 2P_I - P_{II} - 2\delta. \qquad \text{(A-28)}$$

δ is expressed with the polarization P_I as

$$\delta = (1 - \eta)(a_1 - a_{-1}) + (1 - \eta)\delta_e$$

$$\simeq (1 - \eta) P_I. \qquad \text{(A-29)}$$

Here $\delta_e = a_1 - a_0 \cong 0$, and thus $(1-\eta)\delta_e$ is the higher order term.*

Then A is

$$A = 2\eta P_I - P_{II}. \qquad \text{(A-30)}$$

From Eq. (A-30) we can obtain Eq. (24), and also obtain Eq.(25) by the same way.

$$[A^+ - A^-]_{t_1} = 2[P_I^{(+)}\eta^{(+)} + P_I^{(-)}\eta^{(-)}]_{t_1} - [P_{II}^{(+)} + P_{II}^{(-)}]_{t_1}, \quad (24)$$

$$[A^+ - A^-]_{t_2} = 2[P_{III}^{(+)}/\eta^{(+)} + P_{III}^{(-)}/\eta^{(-)}]_{t_2} - [P_{II}^{(+)} + P_{II}^{(-)}]_{t_2}, \quad (25)$$

where plus and minus signs refer to positive and negative alignment production cycles, respectively.

---

* The difference of a_1 and a_0 depends on the degree of achievement for the equalization of the populations of the relevant substates. If the equalization is perfect, then $P_I^{(+)} + P_I^{(-)} = \frac{3}{2}P_0$. The typical values for these polarizations in the present experiment were

$$P_I^{(+)} + P_I^{(-)} = 16.1\%, \quad \tfrac{3}{2}P_0 = 16.9\% \quad \text{for } {}^{12}B,$$

$$P_I^{(+)} + P_I^{(-)} = 29.9\%, \quad \tfrac{3}{2}P_0 = 30.9\% \quad \text{for } {}^{12}N.$$

The good agreement of experimental values of $(P_I^{(+)} + P_I^{(-)})$ and $\frac{3}{2}P_0$ indicates that the equalization was well achieved. This was also shown in Fig. 6. So we can neglect the difference of $a_1(a_0)$ and $a_0(a_{-1})$ in calculating the value of δ.

(2) Degree of achievement for AFP

The substate populations of the test routine are schematically shown in Fig. 27.

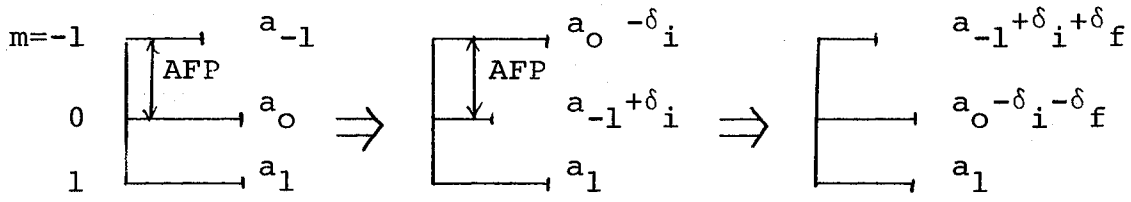

Fig. 27 Spin-ensemble control in the test routine

Here δ_i and δ_f are defined as

$$\delta_i = (1-\eta)\ (a_o - a_{-1})\ , \qquad \text{(A-31)}$$

$$\delta_f = (1-\eta)\ (a_o - \delta_i - a_{-1} - \delta_i)\ ,$$

$$= (1-\eta)\ (a_o - a_{-1}) - 2\delta_i(1-\eta) \simeq \delta_i . \qquad \text{(A-32)}$$

The δ_i is also expressed with the polarization P_I

$$\delta_i = (1-\eta) P_I + (1-\eta)\delta_e ,$$

$$\simeq (1-\eta) P_I . \qquad \text{(A-33)}$$

From the magnetic substate populations the next relation is obtained,

$$P_I - P_{III} = \delta_i + \delta_f$$

$$\simeq 2\delta_i . \qquad \text{(A-34)}$$

The degree of achievement η_{SQ} is determined from the Eqs. (A-33) and (A-34) as

$$(1 - \eta_{SQ}) = (P_I - P_{III})/2P_I . \qquad \text{(A-35)}$$

By the same method the degree of achievement η_{DQ} for double quantum transition can be obtained as

$$\delta_i = (1 - \eta_{DQ})(a_1 - a_{-1})$$
$$= (1 - \eta_{DQ})\ P_I \qquad \text{(A-36)}$$

$$\delta_f = (1 - \eta_{DQ})\ P_I - 2\delta_i(1 - \eta_{DQ})$$
$$\simeq \delta_i \qquad \text{(A-37)}$$

$$P_I - P_{III} = 2\ (\delta_i + \delta_f) \simeq 4(1-\eta_{DQ})P_I \qquad \text{(A-38)}$$

$$(1 - \eta_{DQ}) = (P_I - P_{III})/4P_I\ . \qquad \text{(A-39)}$$

We must consider the effect due to the nuclear lifetime τ and the spin-lattice relaxation time T_1 in deducing the degree of achievement. The diagram of count section and rf section in the test routine is shown in Fig. 28.

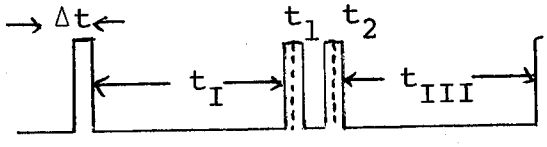

Fig. 28 Time-sequence program for the test routine

From a simple calculation the values of polarization at $t=t_1$ and $t=t_2$ are obtained as

$$P(t_1) = P_I \frac{\tau}{T} \frac{1 - e^{t_I/T}}{1 - e^{-t_I/T}} e^{-(t_I + \Delta t)/T_1}, \qquad \text{(A-40)}$$

$$P(t_2) = P_{III} \frac{\tau}{T} \frac{1 - e^{t_{III}/T}}{1 - e^{-t_{III}/T}} e^{\Delta t/T_1}. \qquad \text{(A-41)}$$

Here T is defined by $\frac{1}{T} = \frac{1}{T_1} + \frac{1}{\tau}$. (A-42)

Using Eqs. (A-35), (A-39), (A-40) and (A-41) the degree of achievement are obtained as

$$1 - \eta_{SQ} = \frac{P(t_1) - P(t_2)}{2P(t_1)} , \qquad \text{(A-43)}$$

$$1 - \eta_{DQ} = \frac{P(t_1) - P(t_2)}{4P(t_1)} . \qquad \text{(A-44)}$$

III. Electronics and diagram of the system control

(1) Counter system

The diagram of counting circuit is schematically shown in Fig. 29. The counter telescope consisted of A, B, C nad E. We used Hamamatsu R329 phototubes for δE counters A, B, C and an RCA4522 phototube for an energy counter E. The two kinds of signals, fast and slow signals were separated from the signal produced in the energy counter. The fast signal of 5 nsec width was used for four-counter coincidence ($A \cap B \cap \bar{C} \cap E$) and pile-up rejection. At the high counting rate as the case of ^{12}B experiment, the pulse hight psectrum was distorted in the high energy region due to the pile-up effect, if the pile-up signal was not rejected. The slow signal included the information of β-ray energy was gated at the linear gate. The gate was opened by the coincidence signal. If more than two pulses entered in a gate time, the fast signals were rejected at the pile-up rejector.

The typical counting rate of the energy signal which passed the linear gate was 2000 cps for ^{12}B and 50 cps for ^{12}N, respectively, in this experiment. The rate of the pile-up was reduced to ~0.05% of the counting rate for the ^{12}B in the actual data taking.

We used the only one PHA memory for the two ADC's which were used to analyze the energy signals from the two energy counters, namely UP ($\theta=\pi$) and DOWN ($\theta=0$) counters. Residual parts of the system were used for the prevention of the two counter system from interfering with each other at the input stage of the PHA memory. Accidental coincidence signals between UP and DOWN counters were removed at the pile-up rejector and at the input stage of ADC's and OR gates.

The counter system was blocked during the production time by a common gate system to save the counters from the after effect due to the intense beam burst. Especially for a energy counter, the signal was blocked at the second dinode of the phototube.

The same counter system as the one used in the $A\alpha\frac{-}{+}E$ measurement was used at $\theta=0$ for the β-ray detection in the measurement of β-γ correlation. The 4.44-MeV γ ray was detected by the 5"ϕ × 5" NaI(Tl). Using the β-γ coincidence signal, β-ray spectrum of the β-decay branch to the first excited state of ^{12}C was obtained. The β-ray-energy spectra for the transitions to the ground and the first excited state of ^{12}C were simultaneously stored in the PHA memory.

Fig. 29a

Counting System

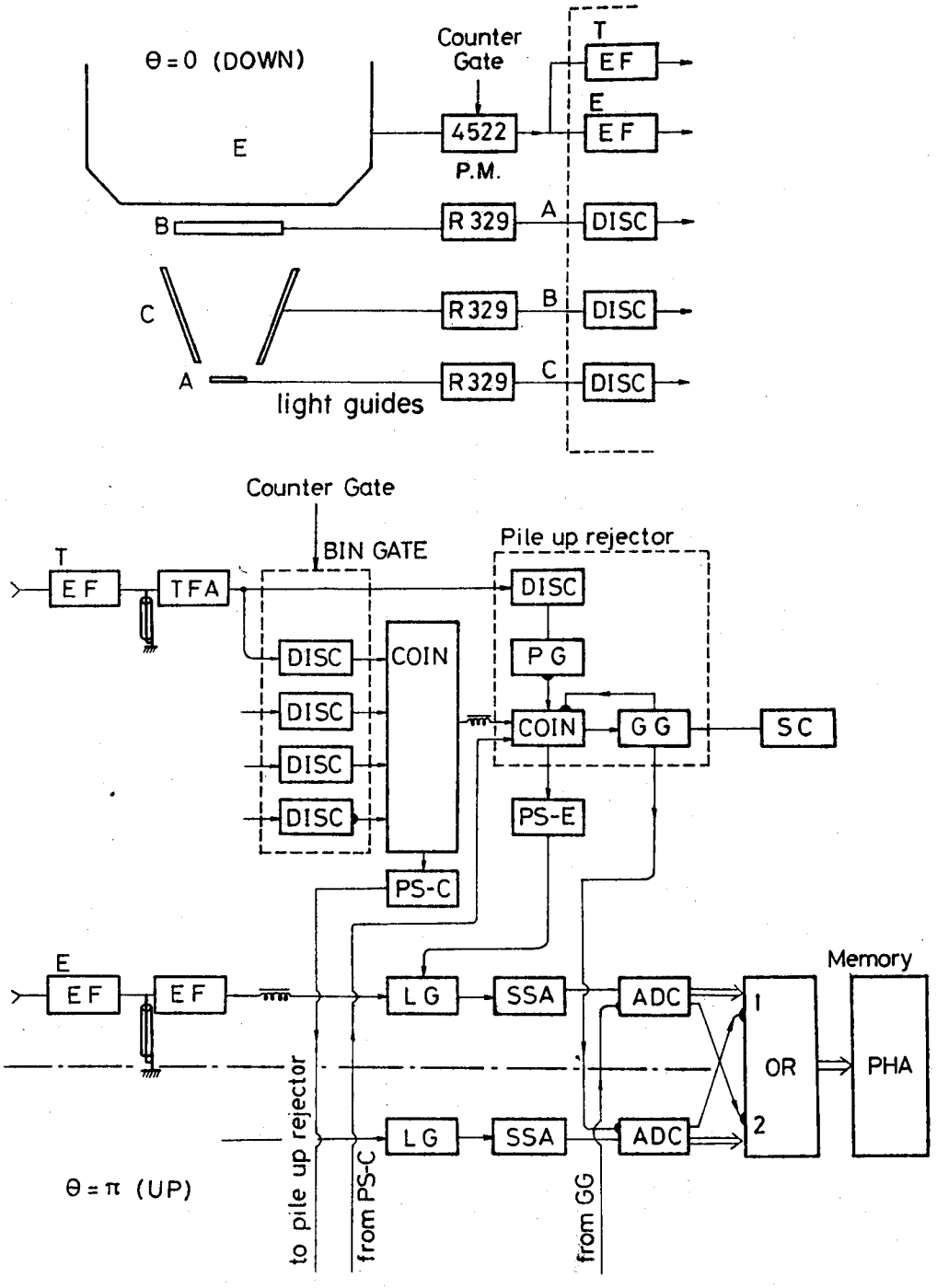

Fig. 29a Counting system for the observation of β-ray energy spectra. The output signal from the energy-counter E was killed at the second dynode of the RCA 4522 phototube during the beam burst and rf time. For δE counters, the signals were gated at the input stage of discriminators. The gate of energy signal was opened by the coincidence signal ($A \cap B \wedge \bar{C} \cap E$) which passed the pile-up rejector. The energy signal from the linear gate was transferred to the PHA after the accidentally mixed signals from the UP ($\theta=\pi$) and DOWN ($\theta=0$) counters was removed at the input stage of the PHA.

(EF: emitter follower, DISC: discriminator, TFA: timing filter amplifier, COIN: coincidence unit, PG: pile up gate, GG: gate generator, SC: scalor, PS-E and PS-S: pulse shaper, LG: linear gate, SSA: spectra scopy amplifier, ADC: anolog to digital converter, OR: or gate, PHA: pulse height analyzer.)

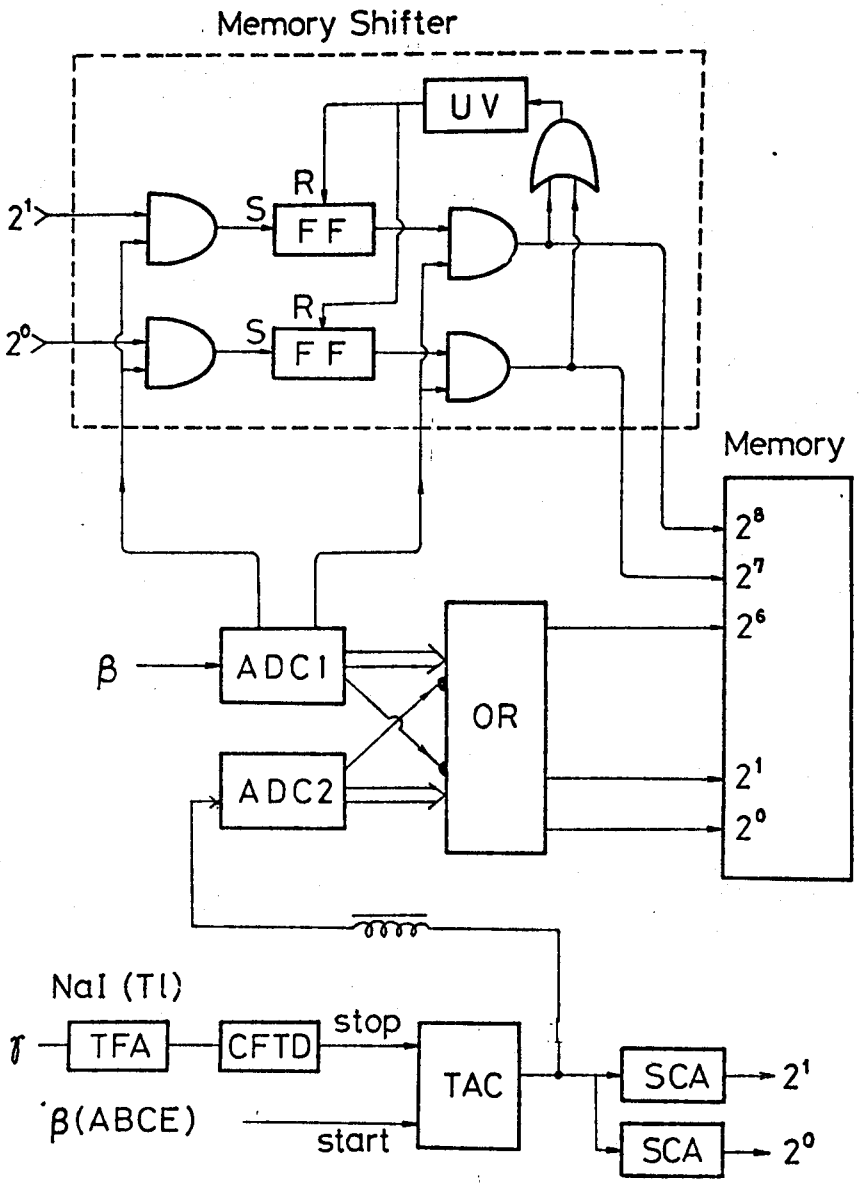

Fig. 29b Counting system for β-γ correlation. The coincidence rate of β ray and 4.44-MeV γ ray was measured. Simultaneously β-ray-energy spectra of the transitions to the ground state and the first excited state of ^{12}C were accumulated in the different area of PHA memory. The selection of the β rays was performed by use of the β-γ coincidence system.

(FF: flip flop, UV: univibrator, SCA: single channel analyzer, CFTD: constant fraction timing discriminator, TAC: time to amplitude converter.)

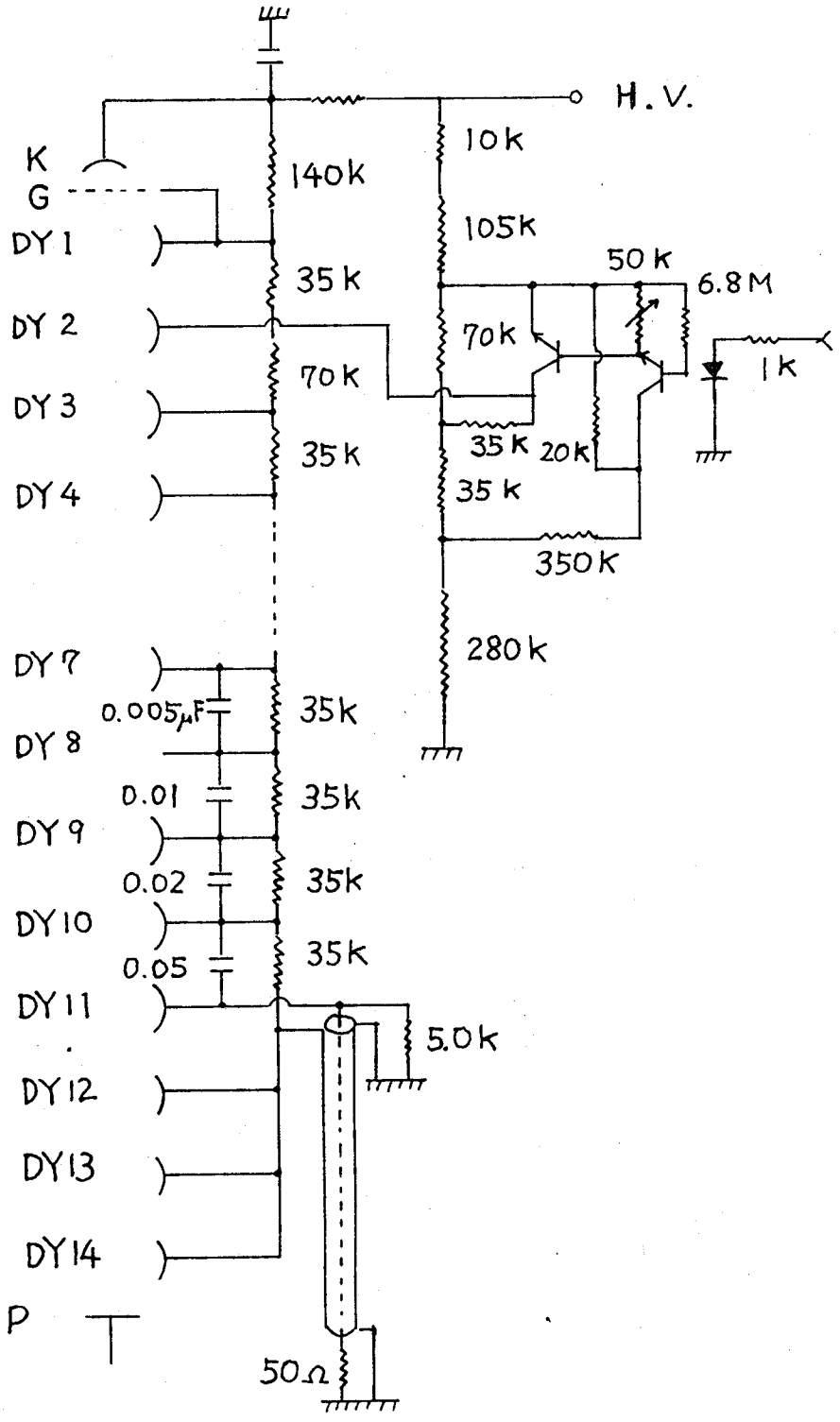

Fig. 30 H.V. bleeder for RAC 4522 (for the E counter).

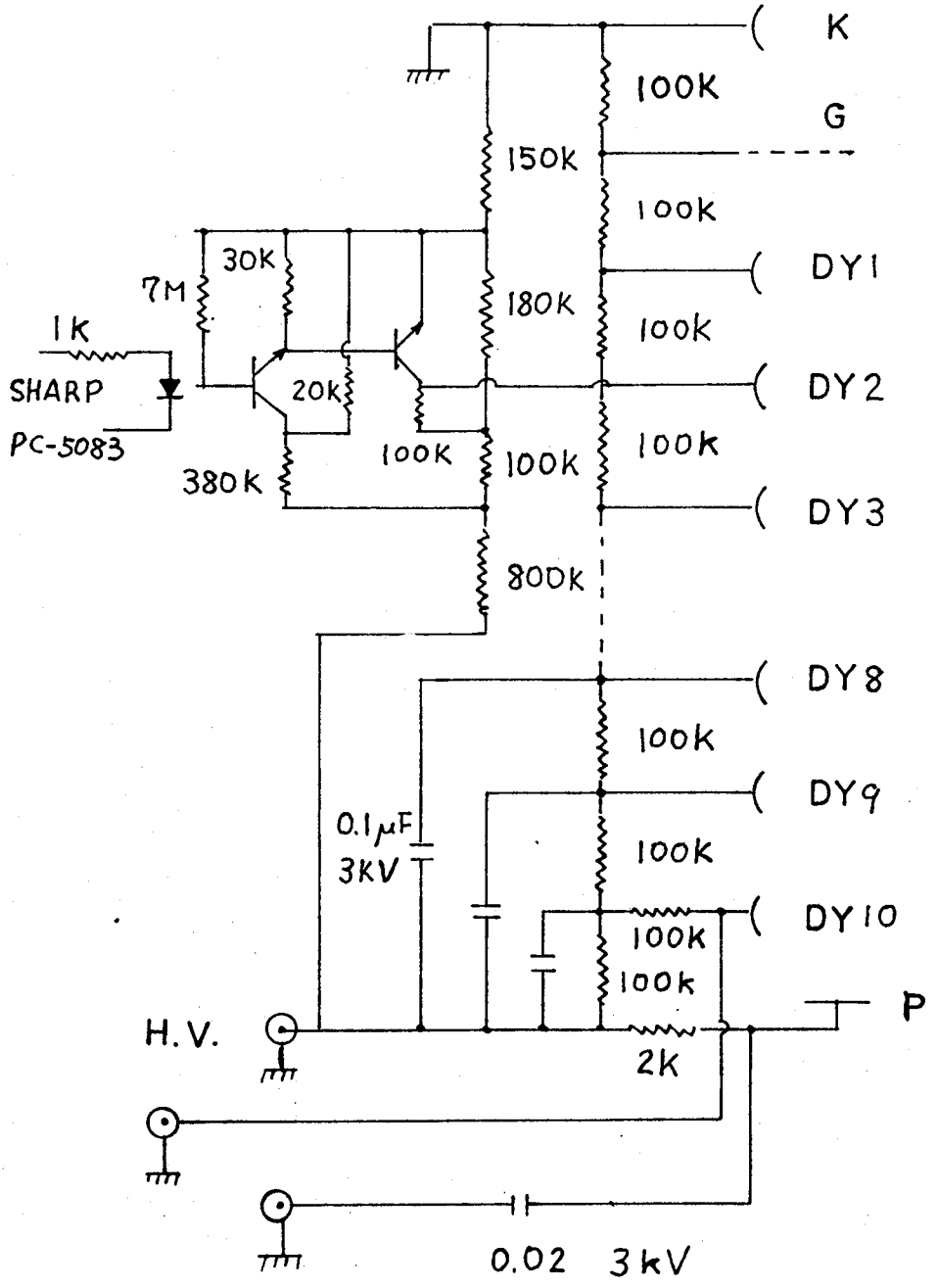

Fig. 31 H.V. bleeder for RCA 8055 (for the NaI(Tl) counter; γ-ray detection).

(2) rf system

The rf system is schematically shown in Fig. 32. The rf processor was used to produce electric voltage levels which were fed to the rf synthesizer in order to select the rf frequency. The typical example of this frequency modulation is shown in Fig. 9. The rf from the synthesizer was also modulated in its amplitude sinusoidally as a function of time at an rf gate. The amplitude modulation is shown in Fig. 33. The power amplifier drived the rf coil to produce H_1 enough to control the spin ensemble by the NMR technique. The level of the output power of this amplifier was controlled properly by selecting voltage levels which was fed into the screen grid of 5F20RA in the power amplifier. This was necessary to produce suitable rf amplitude for the spin ensemble control. The whole system was supervised by a mini-computer (OKI-MINITAC 7000).

(3) Control system

The total system of this experiment was synchronized with the rotation of the target holder. The control signal was produced by a pair of photo-couplers which picked up the position of the rotating target. Using this control signal the beam was pulsed, e.g., the beam bombarded the target when the target was in the right position in the beam line. An off-beam signal triggered the clock signal. Referring to this clock the computer controlled the rf and the PHA system, and the whole detection systems in every cycles. The counter system was blocked by the busy signals of the rf processor and the beam control system. The diagram of the control system is shown in Fig. 9.

The six kinds of energy spectra from UP ($\theta=\pi$) and DOWN ($\theta=0$) counters were time-sequentially stored in the PHA memory. These were the energy spectra in the counting sections I, II and III with the positive and negative alignments. The data accumulation system including the PHA system was also supervised by the computer.

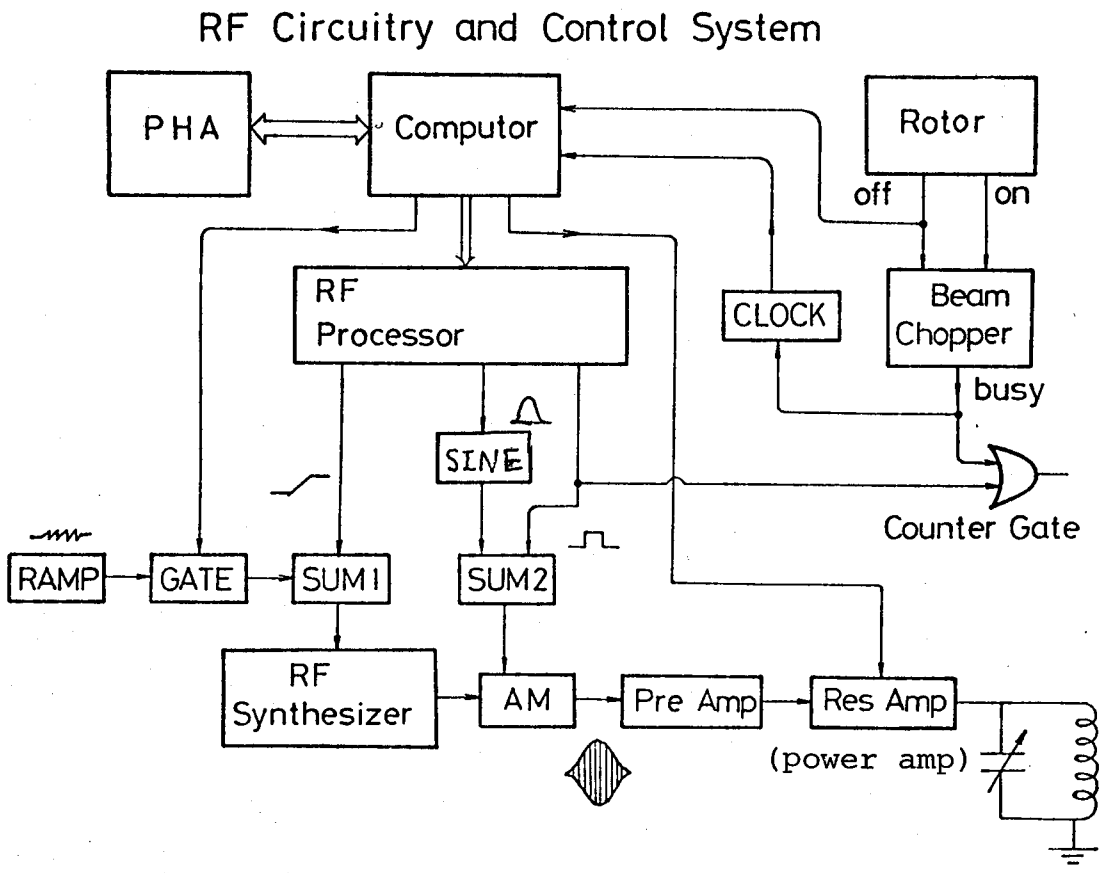

Fig. 32 rf control system. The experimental system was synchronized with the rotation of the target holder. The beam chopper was switched on following the signal of the rotor in the beam path. During the off-beam time the rf processor produced signal for the frequency and the amplitude modulations following the commands from the computer. The rf synthesizer produced the rf which was modulated in the frequency. The rf was transmitted to the power amplifier, and also was modualted in the amplitude at the gate AM. The amplitude of the rf was also suitably selected for the SQT and DQT, respectively, by selecting suitable voltages for the screen-grid of 5F20RA in the power amplifier.

(CLOCK: clock pulser, SINE: sine wave generator SUM: summing amplifier, AM: gate for amplitude modulation, RAMP: ramp generator, Res Amp: resonance amplifier.)

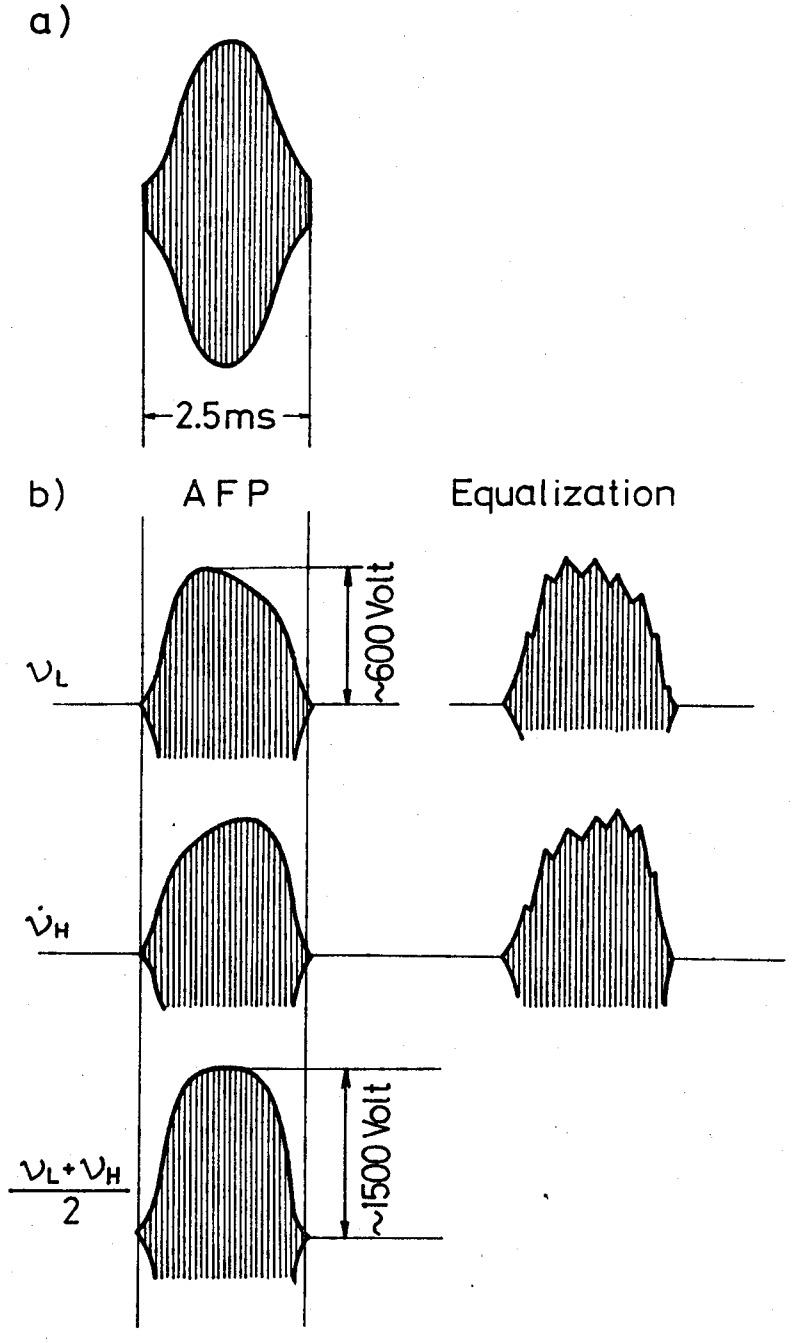

Fig. 33 Schematic view of rf amplitude modulation

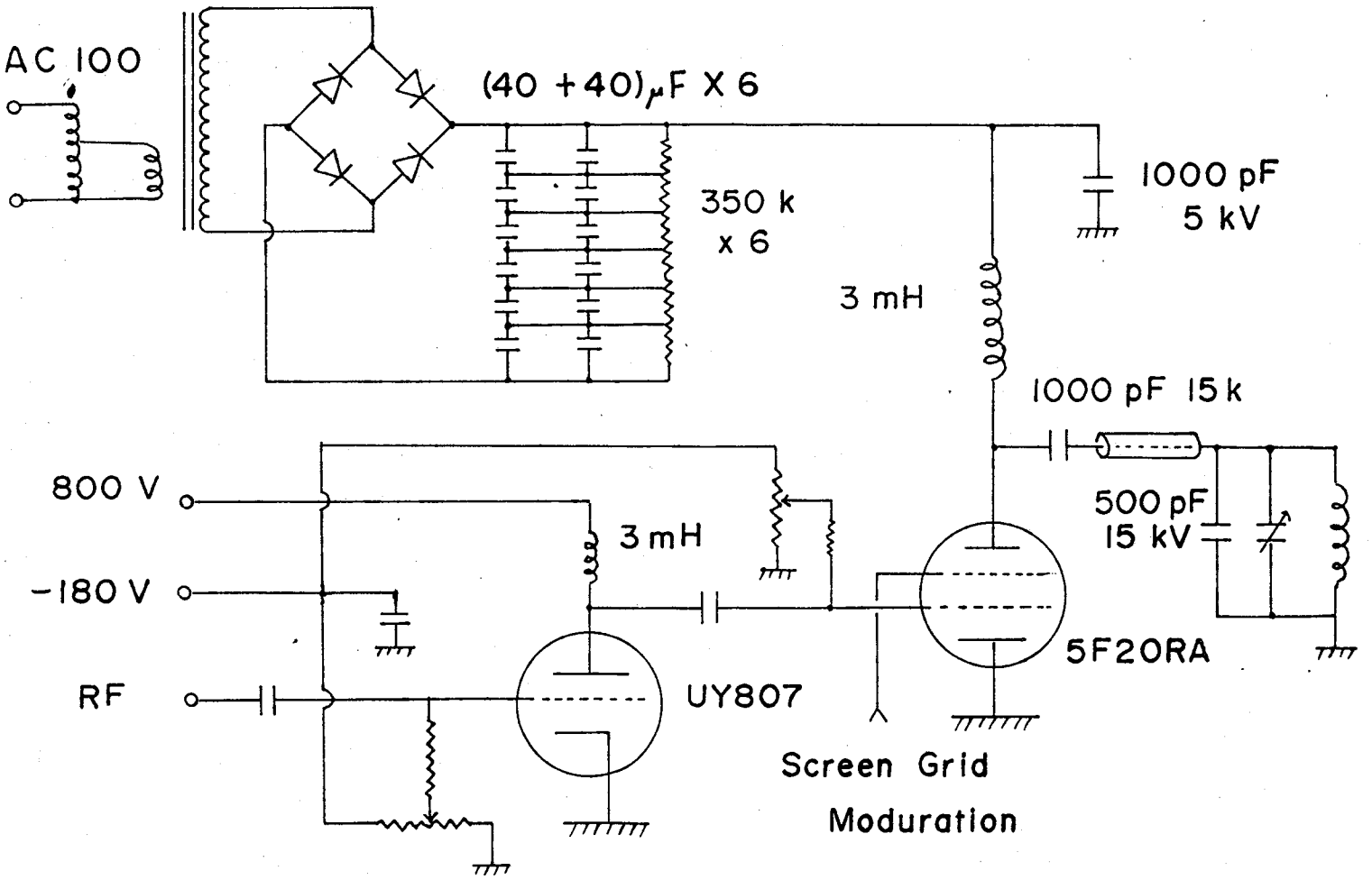

Fig. 34 rf power amplifier.

Reference

1) S. Weinberg, Phys. Rev. 112 (1958) 1375.

2) D.H. Wilkinson, Phys. Letters 31B (1970) 447.

3) M. Morita, Phys. Rev. 113 (1959) 1584

4) M. Morita, Bull. Amer. Phys. Soc. Ser. II 4 (1959)407; Nucl. Phys. 14 (1959) 106; Phys. Rev. 114 (1959) 1080; and private communication.

5) B.R. Holstein and S.B. Treiman, Phys. Rev. C3 (1971) 1921. B.R. Holstein, Phys. Rev. C4 (1971) 740, 764.

6) C.W. Kim, Phys. Letters 34B (1971) 383.

7) K. Sugimoto, I. Tanihata, and J. Göring, Phys. Rev. Letters 34 (1975) 1533.

8) F.P. Calaprice, S.J. Freedman, W.C. Mead and H.C. Vantine, Phys. Rev. Letters 35 (1975) 1566.

9) R.E. Tribble and G.T. Garvey, Phys. Rev. C12 (1975) 967.

10) N.D. Rolin, J.P. Deutch, D. Fovert and R. Pricels, Phys. Letters 79B (1978) 359.

11) R.E. Tribble and D.P. May, Phys. Rev. C13 (1978) 2704.

12) Y.K. Lee, L.W. Mo and C.S. Wu, Phys. Rev. Letters 10 (1963) 253. C.S. Wu, Y.K. Lee and L.W. Mo, Phys. Rev. Letters 39 (1977) 72.

13) W. Kaina, V. Soergel, H. Thies and W. Trost, Phys. Letters 70B (1977) 411.

14) T. Minamisono, J. Phys. Soc. Japan 34 (1973) Suppl. 324.

15) M. Motita, M. Nishimura, A. Shimizu, H. Ohtsubo and K. Kubodera, Prog. Theor. Phys. 60 (1976) Suppl. 1.

16) S. Coehn and D. Kurath, Nucl. Phys. 73 (1965) 1.

17) M. Morita, M. Nishimura, H. Ohtsubo and J. Yamane, J. Phys. Soc. Japan 44 (1978) Suppl. 470.

18) K. Kubodera, J. Delorme and M. Rho, Phys. Rev. Letters 40 (1978) 755.

19) M. Morita, Beta Decay and Muon Capture, W.A. Benjamine (1973).

20) E.C.G. Sudarshan and R.E. Marshak, Phys. Rev. 114 (1958) 1329.

21) R.P. Feynman and M. Gell-Mann, Phys. Rev. 109 (1958) 193.

22) J.J. Sakurai, Nuova Cimento 7 (1958) 649.

23) T.D. Lee and C.N. Yang, Phys. Rev. 104 (1956) 254.

24) C.S. Wu, E. Ambler, R.W. Hayward, D.D. Hoppers and R.P. Hudson, Phys. Rev. 165 (1957) 1413.

25) J.N. Huffaker and E. Greuling, Phys. Rev. 132 (1963) 738.

26) R.J. Blin-Stoyl and M. Rosina, Nucl. Phys. 70 (1965) 321.

27) D.H. Wilkinson and D.E. Alburger, Phys. Rev. Letters 26 (1971) 1127.

28) K. Kubodera and A. Arima, Prog. Theor. Phys. 57 (1977) 1599.

29) B.R. Holstein, Rev. Mod. Phys. 46 (1974) 789.

30) A.M. Nathan, G.T. Garvey, P. Paul and E.K. Warburton, Phys. Rev. Letters 35 (1975) 1137.

31) K. Kubodera, J. Delorme and M. Rho, Nucl. Phys. B66 (1973) 252.

32) D.H. Wilkinson, unpublished.

33) K. Kubodera, H. Ohtsubo and Y. Horikawa, Phys. Lett. 58B (1975) 402.

34) T. Sato and H. Ohtsubo, Prog. Theor. Phys. 59 (1978) 141.

35) R.O. Riska and G.E. Brown, Phys. Letters 38B (1972) 193.

36) K. Kubodera, J. Delorme and M. Rho, Phys. Rev. Letters 40 (1978) 755.

37) A. Fujii, M. Morita and H. Ohtsubo, Prog. Theor. Phys. (1968) Suppl. 303.

P.A.M. Guichon, M. Giffor and C. Samour, Phys. Letters 74B (1978) 15.

K. Koshigiri, H. Ohtsubo and M. Morita to be published.

38) K. Sugimoto, K. Nakai, K. Matsuda and T. Minamisono, J. Phys. Soc. Japan 25 (1968) 1258.

39) M. Hori, S. Ochi, T. Minamisono, A. Mizobuchi and K. Sugimoto, J. Phys. Soc. Japan 34 (1973) Suppl. 161. M. Tanaka, S. Ochi, T. Minamisono, A. Mizobuchi and K. Sugimoto, Nucl. Phys. A206 (1976) 1.

40) H. Ohtsubo, private communication. See also, M. Morita and R.S. Morita, Phys. Rev. 110 (1958) 461.

41) M. Morita et al., to be published, private communication.

42) H. Behrense, to be published.

43) M. Morita, M. Nishimura and H. Ohtsubo, Phys. Letters 73B (1978) 17.

44) M. Gell-Mann, Phys. Rev. 111 (1958) 362.

45) R.E. McDonald, J.A. Becker, R.A. Chalmers and D.H. Wilkinson, Phys. Rev. C10 (1974) 333.

46) J.M. Freeman, J.G. Jenkin, D.C. Robinson, J.S. Ryder, W.E. Burcham, Phys. Letters 27B (1968) 156. G.J. Clark, J.M. Freeman, D.C. Robinson, J.S. Ryder, W.E. Burcham and G.T.A. Squire, Phys. Letters 35B (1971) 563.

47) B.T. Chertok, S. Sheffield, J. Lightbody, S. Penner and D. Blum, Phys. Rev. C8 (1973) 23.

48) P. Lebrun, Ph. Deschepper, L. Grenacs, J. Lehmann, C. Leroy, L. Dalffy, A. Passoz and A. Mrio, Phys. Rev. Letters 40 (1978) 302; H. Biändle, G. Miklos, L. Ph. Doesch, V.L. Telegdi, P. Trutlman and A. Zehnder, Phys. Rev. Letters 41 (1978) 299.

49) H. Behrens and L. Szybisz, Z. Phys. A273 (1975) 177.

50) I. Tanihata, S. Kogo and K. Sugimoto, Phys. Lett. 67B (1977) 392.